Chapter I

Introduction and summary

The topic of this PhD thesis is the stability of flattened galaxy models. The first and last words of the title cover the bulk of the research presented in the following chapters. Before we delve into the realms of the construction of galaxy models and the stability analysis thereof, we describe the objects that are studied: flattened, axisymmetric galaxy models. We also give an overview of the contents of the next chapters.

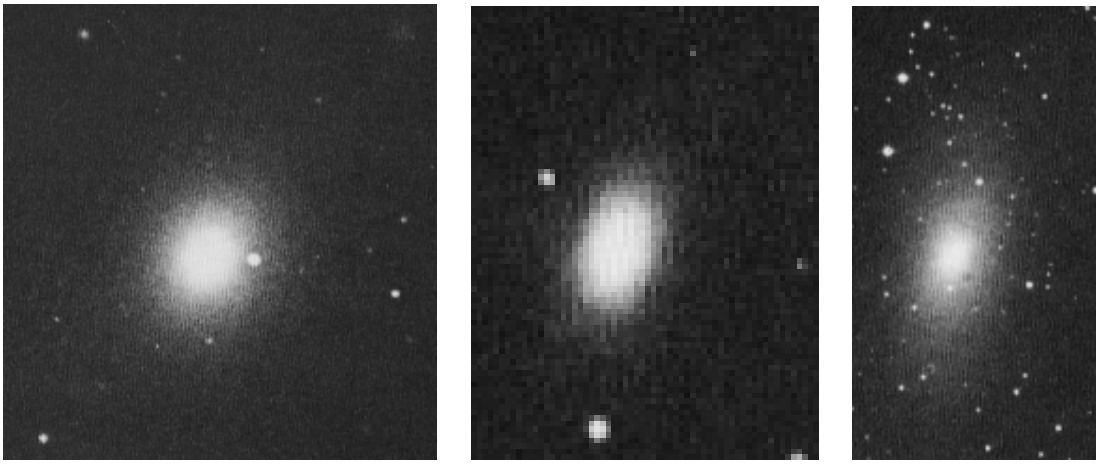

E2 (M49) E5 (M59) E6 (NGC205)

Figure 1. Elliptical galaxies vary from nearly round to strongly flattened.

1 The nature of elliptical galaxies

It became clear in the mid 1920s that galaxies are huge stellar systems. Based on their visual appearance, most galaxies can be classified as disk or elliptical systems. Many disk galaxies look very impressive, showing a spiral pattern and other spectacular features. In contrast, ellipticals look rather boring (Figure 1).

Delineating the dynamical structure of galaxies is one of the major topics of astronomical research. In a galaxy billions of stars move in the combined gravitational field almost without direct encounters. Measurement of the stellar motions is restricted by projection effects. Only the radial velocity distribution, integrated along the line of sight, can be obtained. Instead of measuring the stellar motions, it turned out to be easier to observe the Doppler shift in the emission lines of a gaseous component, such as neutral hydrogen, which is present in most spiral galaxies. The gas and stars do not have the same kinematics, but the motion of both is governed by the galactic potential. Observations showed that the bulk of the stars in spirals have almost circular orbits. In the majority of ellipticals gas is absent, and measurements of the Doppler shift in absorption lines proved to be a more difficult task. Led by the visual appearance of ellipticals, it was generally accepted until the mid 1970s that these galaxies have an oblate spheroidal shape. The luminosity profiles were consistent with truncated isothermal spheroids (Gott 1973, Wilson 1975), in which the rapid rotation is responsible for the flattening.

Twenty years ago new observations changed this picture dramatically. It was the measurement of the rotation of NGC4697 by Bertola & Capaccioli (1975) that started the revolution: the rotation was too low by a factor of three compared to the value predicted by the dynamical models. The significance was soon realized (Binney 1976): the flattening could not be explained by rotation. As data for more galaxies became available, it turned out that NGC4697 in fact is one of the faster rotators. Instead of being more or less isothermal, with a distribution function

(hereafter DF) that depends on the energy E and angular momentum L_z only, a realistic dynamical model for an elliptical galaxy should have a three-integral DF. Measurement of the kinematics in the solar neighbourhood had shown much earlier that our own Galaxy also has a three-integral DF, and approximations for the third integral had been derived (e.g., Contopoulos 1960; Ollongren 1962). Similarly, there is now abundant evidence for the existence of a third integral in theoretical studies of the orbits in elliptical galaxies (Schwarzschild 1979; de Zeeuw 1985).

The view of an elliptical as being an oblate spheroid also had to be adjusted. Three-integral models can be made for prolate spheroidal and triaxial densities as well. From a theoretical point of view there is no compelling reason that the angular momentum L_z should be an integral of motion (Binney 1978). Hence a model where L_z is conserved, i.e., an axisymmetric system, is considered to be a special case of the general class of triaxial models. As galaxies that satisfy special conditions are rare, one expects that most of the ellipticals are triaxial. Indeed the photometric data showed that in many galaxies the ellipticity of the isophotes varies with radius (King 1978; Williams & Schwarzschild 1979; Leach 1981). Since the projection of a spheroidal model does not exhibit this behaviour, isophote twisting forms direct evidence for the triaxial shape of ellipticals. More recently, e.g., Davies & Birkinshaw (1986) found strong minor axis rotation, which is only possible in prolate or triaxial models. In the last two decades new observations and theoretical studies have demonstrated that there is a rather large variation of shapes and dynamical contents within the family of elliptical galaxies (see de Zeeuw & Franx (1991) for a review), but the general view has not changed greatly.

The dynamical structure of ellipticals also provides insight in the process of galaxy formation. From the study of galaxy models we can infer the distribution of shapes and dynamical contents of ellipticals as a class: from a purely dynamical point of view, all stable models are equally likely to occur. If certain models prevail among the galaxies observed in the Universe, that must be due to a selection mechanism at the time the galaxy was formed.

2 Dynamical models for ellipticals

Observations of elliptical galaxies do not provide the dynamical structure directly. Three of the six phase space dimensions are inaccessible: the position along and velocity perpendicular to the line of sight are not measurable. Instead we can only determine which of the vast number of possible phase-space distributions are compatible with the data. However, to understand the nature of ellipticals we do not need to know the exact phase-space structure of individual galaxies. We are more interested in the characteristics of ellipticals as a class. But it is important to know the range of dynamical models that are consistent with the observed properties of a particular galaxy. Hence it is important that we are able to build a fairly complete library of models for a given configuration.

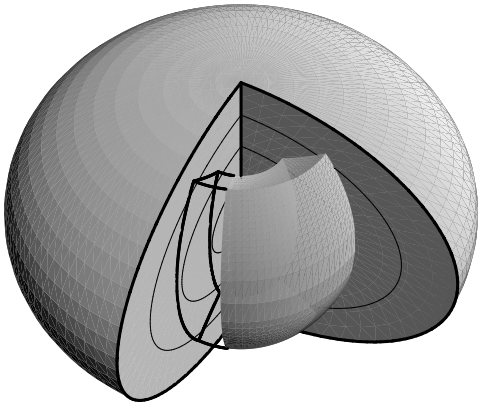

Figure 2. The volume filled by a general (short axis tube) orbit in a Stäckel mass model, truncated at an isodensity surface.

There are few methods available for constructing dynamical models for a given spheroidal or triaxial mass density. For the construction of spheroidal two-integral DFs that depend on E and L_z there are methods (Lynden-Bell 1962, Hunter 1975, Dejonghe 1986) that require analytic knowledge of the density as a function of the potential and radius. Hunter and Qian (1993) found a more general inversion formula that relaxes this condition. There are also numerical methods to solve the two-integral DF from the density; they are based on either Lucy's method (Lucy 1974), maximum entropy (Richstone 1987), series expansion (Dehnen & Gerhard 1994) and linear programming techniques (Schwarzschild 1979, 1982). The latter has also been used to produce triaxial galaxy models.

Construction of three-integral DFs is more difficult. Part of the problem is the fact that only in special cases an explicit expression for the third integral is known. Dynamical models based on other potentials can be built by a linear programming technique (Schwarzschild 1979, 1982; Richstone 1980, 1982, 1984; Levison & Richstone 1985a, b) or by use of an approximate integral (Petrou 1983a, b; Dehnen & Gerhard 1993). There is a large class of models that have so-called Stäckel potentials: the equations of motion separate in a suitable coordinate system. For these models the third integral is known analytically and a complete orbital classification can be made (de Zeeuw 1985). The models investigated in this thesis are all oblate Stäckel models; Figure 2 shows a general orbit in such a galaxy. The volume occupied by an orbit is aligned with prolate spheroidal coordinates.

Even when the third integral is known, it is still difficult to build a three-integral dynamical model. Many orbits with different values for all three integrals can pass through the same point, contributing to the density there (Figure 3). The density is then related to the DF by an integral equation. Solving this equation is feasible only by numerical means. There are special models for which the three-integral DF can be found analytically: models populated only by *thin orbits*. A star on a thin orbit has essentially no radial motion because the orbit lies on a shell. In this case the inversion from density to DF is a one-dimensional problem (Figure 3) which can be solved analytically (Bishop 1987, de Zeeuw & Hunter 1990).

In Chapter 2 we present a new algorithm to derive a three-integral DF from the

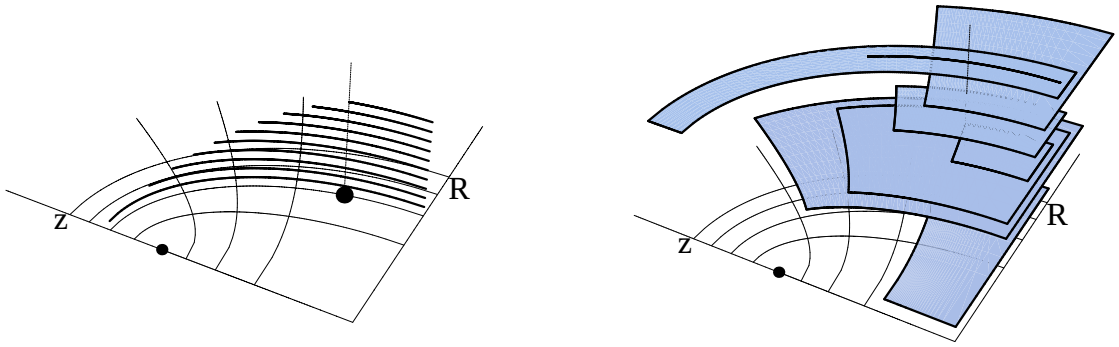

Figure 3. A sample of the orbits that contribute to the density at a given point (big dot) in an oblate galaxy model, where the symmetry axis is aligned with the *z* axis. For *thin-orbit* models (left) the orbits lie on a line in the three-integral space; in general (right) they are drawn from a three-dimensional subspace.

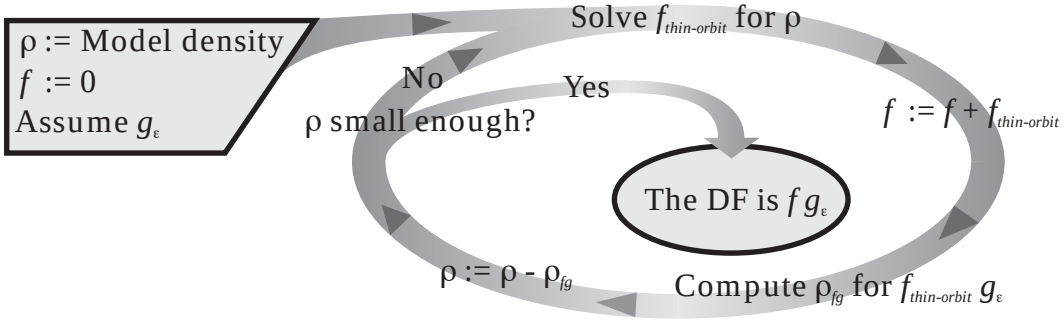

Figure 4. The iterative scheme used to construct dynamical models from a given model density.

density. We do not solve the full 3D problem; instead we assume part of the DF (a one-parameter family of functions g_ε that depend on three integrals) and solve for a two-integral function f so that the DF is fg_ε. The thin-orbit DF is of this form with g_ε a delta function in one of the integrals. The basic idea is that two solutions f will be very similar if the corresponding g-functions are alike. This idea was first employed by Shu (1969). We take it one step further and show that it can be used successfully in an iterative numerical scheme (Figure 4). Since the method uses the analytic thin-orbit solutions, most computer time is spent in computing residual densities from a DF by a simple quadrature.

The algorithm is applied to build several dynamical models for a given mass distribution. It performs quite well as long as orbits with zero angular momentum are excluded. It is shown that the DF does not depend strongly on the shape of the function g_ε: only the first order moments are important (the precise definition of moments is given in Chapter 2; basically it is a weighted integral of g). The same is true for the projected velocity moments. The consequence of this is that we can not hope to determine the shape of the g_ε function unless we have very accurate velocity profiles. On the other hand, it provides us with a useful parametrization of models for ellipticals by means of the moments of g_ε.

3 Stability of dynamical models

It is generally assumed that the elliptical galaxies are in dynamical equilibrium, at least in their inner parts. Hence models of the kind constructed in Chapter 2 can be used to fit observational data. As ellipticals are long-lived systems, with ages of the order of a hundred galactic years, there is an additional requirement that models should satisfy: they must be stable. Most ellipticals are members of galaxy clusters and the distant interaction with its fellow members may be strong enough to cause instabilities to reshape the elliptical. Hence models that are subject to instabilities that grow on time scales much less than a Hubble time are not realistic and should be discarded.

The methods for examining the stability of galaxy models were pioneered for disk and spherical galaxies. These systems are much simpler than spheroidal or triaxial galaxies because they have a higher degree of symmetry. For spherical systems, Antonov (1962) was able to derive analytic stability criteria. He also discovered (Antonov 1973) the radial orbit instability: if the fraction of the stars that move on predominantly radial orbits is too large, the system is subject to the formation of a bar. This instability has been found in non-spherical models as well (Palmer, Papaloizou & Allen 1991). The radial orbit instability appears to be the only result relevant to realistic spherical galaxy models.

Disk galaxies are prone to more instabilities. Apart from warping and other modes that have a three-dimensional nature, many unstable modes have been found for flat disks ranging from cold (all stars move on circular orbits) to hot (stars on radial orbits) models (e.g., Kalnajs 1971; Zang & Hohl 1978; Athanassoula & Sellwood 1986; Araki 1987; Hunter 1992). Oblate spheroidal galaxies connect the disks and spheres: for every mode found in disks there must be a critical flattening of a spheroidal model where the instability sets in. This field is largely unexplored; only a few papers have been devoted to spheroidal models:

(•) oblate homogeneous spheroids (Vandervoort 1991) can be treated analytically. Although homogeneous models are not very realistic, it still is worthwhile to examine these models. Some of the instabilities are an artefact of the constant density, others may also be found in other models.

(•) Palmer, Papaloizou & Allen (1991) examined the radial orbit instability in axisymmetric models. They found that models in which many stars move on predominantly radial orbits are subject to a bar-forming mode. This type of instability is also present in disk and spherical systems. It puts an upper limit on the radial velocity dispersion of a realistic model.

(•) Merritt & Hernquist (1991) tested prolate thin-orbit models using N-body simulations, and found that these models become unstable to bending modes if they are more flattened than E7. A flattening of E7 is a magical boundary: no ellipticals have been found that are more flattened than E7 (Binney & de Vaucouleurs 1981). A possible explanation for the gap between disk and elliptical galaxies was proposed by Fridman & Polyachenko (1984), who suggest that all very flattened galaxies

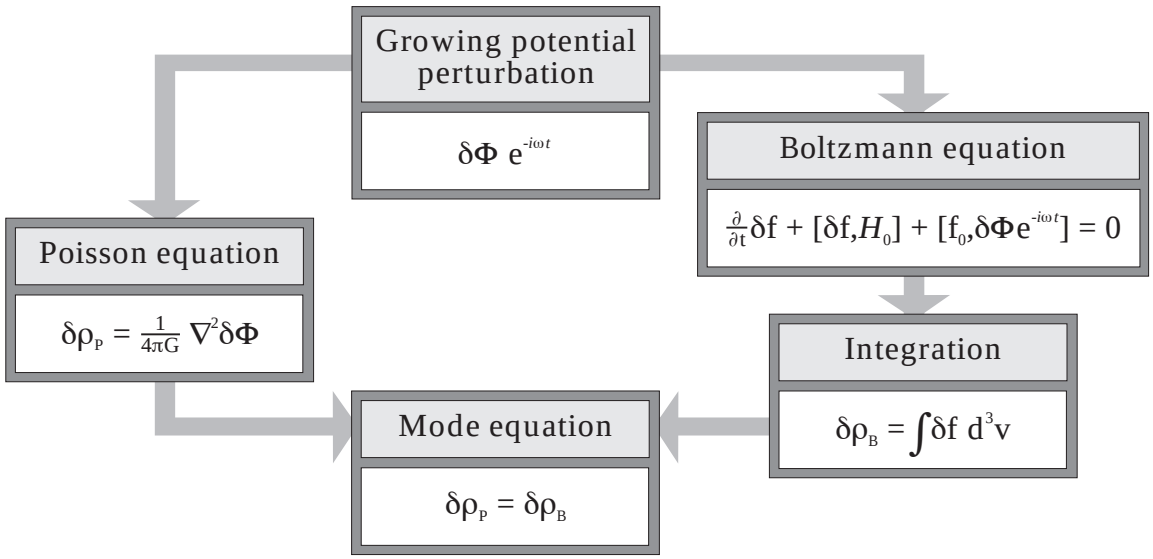

Figure 5. Finding an unstable mode of a system characterized by the Hamiltonian H_0 and initial DF f_0. Expanding the perturbation in a basis of potential-density pairs turns the final equality into a matrix equation.

are unstable. The presence of bending modes in thin-orbit models supports that hypothesis.

(•) Merritt & Stiavelli (1990) used N-body simulations to study modes of thin-orbit oblate spheroids with no net rotation. They found that E6 and more flattened models are unstable to an axisymmetric ring instability. The existence of this mode was confirmed by de Zeeuw & Schwarzschild (1991) using the analytic Goodman (1988) indicator. Merritt & Stiavelli (1990) also found a lopsided ($m = 1$) mode for nearly all flattened systems, which was present in more spherical models as well. They could trace it to models as round as E2, but suggested that the instability also occurred in E1 models.

Although N-body simulations can be used to investigate the stability of galaxy models, they are best suited for relatively strong instabilities. All current N-body techniques suffer from noise in phase space: even in an unperturbed equilibrium model a star which starts out in one orbit will be found in a slightly different orbit after several time steps. For a simulation of a violently unstable model, where the change in a star's orbit due to the perturbation dominates, the numerical noise is not very important. For more subtle modes, the effect on the orbits is of the same magnitude as the noise. In this case it is hard to distinguish between an intrinsic mode of a model and the noise-induced density fluctuations.

In the second part of this thesis we examine nearly spherical oblate models using a semi-analytical method (Figure 5), pioneered by Kalnajs (1977) to study disk models. In this so-called *matrix method* the response of the orbits to a perturbation is determined in analytical terms, although the actual computations are done numerically. An unstable mode is found when the perturbation, which grows in

amplitude with time, induces a response that equals the perturbation. By expanding the perturbation and response density in a basis of potential-density pairs, this equality is turned into a matrix equation. This method has recently been used by Hunter (1992) for disk systems, and by Polyachenko & Shukhman (1981), Palmer & Papaloizou (1987), Weinberg (1989, 1991), Saha (1991) and Bertin et al. (1994) for spherical galaxies.

In the matrix method noise in phase-space is absent: the orbits can be determined to arbitrary precision. The main source of error lies in the choice of basis functions for the perturbation. Acceptable results are only obtained if the response density can be represented accurately in the basis set. Since the errors in the matrix method have a different origin, it complements N-body simulations.

In Chapter 3 we discuss a method to construct a basis of potential-density pairs that is very flexible, and allows the selection of a basis that matches the mode shape, provided, of course, that we know what the mode looks like.

Chapter 4 describes the implementation of the matrix method for moderately flattened, oblate galaxy models with low radial velocity dispersion. As a limiting case, the thin-orbit models studied by Merritt & Stiavelli (1990) are included. We confirm their suspicion that all oblate, non-rotating thin-orbit models are unstable to a lopsided instability, and examine the effect of net rotation. The instability disappears when the dynamical temperature, or the radial velocity dispersion, of the models increases. We give an estimate of the boundary between stable and unstable models.

References

Antonov V.A., 1962, Vestnik Leningrad Univ. **19**, 96; translation in *Structure and dynamics of elliptical galaxies*, IAU symposium 127, ed. P.T. de Zeeuw, p. 531. Reidel, Dordrecht

Antonov V.A., 1973, in *Dynamics of Galaxies and Clusters*, ed. T.B. Omarov, p 139. Alma Ata, Akad. Nauk Kaz. SSR; translation in *Structure and dynamics of elliptical galaxies*, IAU symposium 127, ed. P.T. de Zeeuw, p. 548. Reidel, Dordrecht

Araki S., 1987, Astron. J. **94**, 99

Athanassoula E., Sellwood J.A., 1986, Mon. Not. R. Astr. Soc. **221**, 213

Bertin G., Pegoraro F., Rubini F., Vesperini E., 1994, Astroph. J. **434**, 94

Bertola F., Capaccioli, M., 1975, Astroph. J. **200**, 439

Binney J.J., 1976, Mon. Not. R. Astr. Soc. **177**, 19

Binney J.J., 1978, Comments on Astrophysics **8**, 27

Binney J.J., de Vaucouleurs G., 1981, Mon. Not. R. Astr. Soc. **194**, 697

Contopoulos G., 1960, Zeits. f. Astroph. **49**, 273

Davies R.L., Birkinshaw M., 1986, Astroph. J. Lett. **303**, L45

Dehnen W., Gerhard O.E., 1994, Mon. Not. R. Astr. Soc. **268**, 1019

Dejonghe H., 1986, Phys. Rep. **133**, 217

de Zeeuw P.T., 1985, Mon. Not. R. Astr. Soc. **216**, 273, 599

de Zeeuw P.T., Franx M., 1991, AnnuRevAA 29, 239

de Zeeuw P.T., Hunter C., 1990, Astroph. J. **356**, 365

de Zeeuw P.T., Schwarzschild M., 1991, Astroph. J. **369**, 57

Fridman A.M., Polyachenko V.L., 1984, *Physics of Gravitational Systems.* Springer Verlag, New York

Goodman J., 1988, Astroph. J. **329**,612
Gott J.R., 1973, Astroph. J. **186**, 481
Hunter C., 1975, Astron. J. **80**, 783
Hunter C., 1992, Ann. NY Acad. Sc. **678**, 22
Hunter C., Qian E., 1993, Mon. Not. R. Astr. Soc. **262**, 401
Levison H. F., Richstone D. O., 1985a, Astroph. J. **295**, 340
Levison H. F., Richstone D. O., 1985b, Astroph. J. **295**, 349
Kalnajs, A.J., 1971, Astroph. J. **166**, 275
Kalnajs, A.J., 1977, Astroph. J. **212**, 637
King I.R., 1978, Astroph. J. **222**, 1
Leach R., 1981, Astroph. J. **248**, 485
Lynden-Bell D., 1962, Mon. Not. R. Astr. Soc. **123**, 447
Merritt D.R., Hernquist, L., 1991, Astroph. J. **376**, 439
Merritt D.R., Stiavelli, M., 1990, Astroph. J. **358**, 399
Ollongren A., 1962, Bull. Astr. Inst. Neth. **16**, 241
Palmer P.L., Papaloizou J., 1987, Mon. Not. R. Astr. Soc. **224**, 1043
Palmer, P.L., Papaloizou, J., Allen A.J., 1991, Mon. Not. R. Astr. Soc. **253**, 129
Polyachenko V.L., Shukhman I.G., 1981, Astron. Zh. **58**, 933, English translation in Sov. Astr. **25**, 553
Richstone D. O., 1980, Astroph. J. **238**, 103
Richstone D. O., 1982, Astroph. J. **252**, 496
Richstone D. O., 1984, Astroph. J. **281**, 100
Richstone D.O., 1987, in *Structure and dynamics of elliptical galaxies*, IAU symposium 127, ed. P.T. de Zeeuw, p. 261. Reidel, Dordrecht
Saha P., 1991, Mon. Not. R. Astr. Soc. **248**, 494
Schwarzschild M., 1979, Astroph. J. **232**, 236
Schwarzschild M., 1982, Astroph. J. **263**, 599
Shu F. H., 1969, Astroph. J. **158**, 505
Vandervoort P.O., 1991, Astroph. J. **377**, 49
Weinberg M.D., 1989, Mon. Not. R. Astr. Soc. **239**, 549
Weinberg M.D., 1991, Astroph. J. **368**, 66
Williams T.B., Schwarzschild M., 1979, Astroph. J. **227**, 56
Wilson C.P., 1975, Astron. J. **80**, 175
Zang T.A., Hohl F., 1978, Astroph. J. **226**, 521

Chapter II

Three–integral oblate galaxy models

A simple numerical scheme is presented for the construction of three-integral phase-space distribution functions for oblate galaxy models with a gravitational potential of Stäckel form, and an arbitrary axisymmetric luminous density distribution. The intrinsic velocity moments can be obtained simultaneously with little extra effort. The distribution of the inner and outer turning points of the short-axis tube orbits that are populated can be specified freely, and is chosen in advance. The entire distribution function is then derived from the density by an iterative scheme that starts from the explicitly known distribution function of the thin-orbit (maximum streaming) model, in which only the tubes with equal inner and outer turning points are populated. The versatility and limitations of this scheme are illustrated by the construction of a number of self-consistent three-integral flattened isochrone models of Kuzmin-Kutuzov type, and by investigation of special cases where the scheme is tractable analytically. This includes the behaviour of the distribution functions in the outer regions of the models. The scheme converges rapidly for models containing orbits with ratios of the outer to inner turning point as large as ten, and is particularly suited for the construction of tangentially anisotropic flattened models, self-consistent as well as non-consistent. The algorithm simplifies in the disk and spherical limit, and can be generalized to triaxial models.

Preliminary version of a paper co-authored by P.T. de Zeeuw.

1 Introduction

The observable properties of elliptical galaxies indicate that their internal dynamics is governed by three integrals of motion (Binney 1976, 1978). For oblate systems two of the three are known, the energy E and the angular momentum component L_z along the symmetry axis. An exact third integral I_3 exists only for special classes of potentials, but adequate approximations have been derived for moderately flattened axisymmetric models (e.g., Saaf 1968; Innanen & Papp 1977; Gerhard & Saha 1991).

The construction of the full class of dynamical models for elliptical galaxies is a major undertaking. Progress has been made recently on a number of fronts, in particular for oblate systems. Even though elliptical galaxies as a class have triaxial shapes, the majority may well be nearly oblate (Franx, Illingworth & de Zeeuw 1991), so that oblate models are useful. Various practical methods have been developed for the construction of the special model with phase-space distribution function $f = f(E,L_z)$ (Hunter & Qian 1993; Dehnen & Gerhard 1994; Magorrian 1995; Kuijken 1995; Qian et al. 1995).

An exact third integral is known explicitly for the class of flattened models with a potential of Stäckel form (Kuzmin 1956; de Zeeuw 1985, hereafter dZ), and some self-consistent three-integral dynamical models of this type have been constructed, e.g., by numerical methods (Bishop 1986; 1987) or by series expansions (Dejonghe & de Zeeuw 1988, hereafter DZ). The distribution function for the model with the maximum possible streaming motions can be found by a single quadrature over the density (Bishop 1987; de Zeeuw & Hunter 1990, hereafter ZH). In oblate Stäckel models all orbits are short-axis tubes, but only those with vanishing radial action — which lie on spheroidal shells — are populated in the maximum streaming model. They are often referred to as *thin* (tube) orbits, and the corresponding model is called the *thin-orbit model*. These flattened models connect the sphere made exclusively of circular orbits with the similar axisymmetric disk.

When no exact I_3 is known, dynamical models can be constructed by numerical methods (e.g., Richstone 1980, 1982, 1984; Levison & Richstone 1985a, b) or by use of an approximate integral (Petrou 1983a, b). This approach has been employed recently by Dehnen & Gerhard (1993), who constructed a large family of approximate three-integral distribution functions for a flattened isochrone model, and investigated the relation between the internal dynamics and the observable kinematics. Their method is applicable to a wide variety of mass models with realistic density profiles. The one application that has been published so far is for a mass model that is nearly identical to the Kuzmin-Kutuzov model. This has a Stäckel potential, and its exact third integral has been used to construct a number of distribution functions (DZ, ZH).

Little is known about the stability of flattened galaxy models. Some N-body simulations have been carried out (Merritt 1987; Merritt & Stiavelli 1990), but the paucity of available distribution functions to set up the initial conditions is one of the main reasons for our lack of knowledge. In Chapter 4 we show that the

linear stability analysis pioneered by Kalnajs (1977) for axisymmetric disks, and subsequently used by e.g., Polyachenko & Shukhman (1981), Palmer & Papaloizou (1987), Weinberg (1989, 1991) and Saha (1991, 1992) to study spherical models, also can be carried out for oblate Stäckel models. One of the first applications is a study of the thin orbit models, which have been shown by N-body simulations to be liable to ring- and lopsided instabilities, depending on the flattening of the model. Based on studies of spheres and flat disks, we expect that an increase in the amount of radial support will stabilize the radially 'cold' thin-orbit models. In order to investigate this, we need distribution functions for models in which not only the thin short-axis tubes are populated, but also 'thick' tube orbits with a finite radial extent. It is those models that we construct here.

The thin-orbit model has a distribution function of the form $f = f_{\rm tsm}(J_\phi,J_\nu)\delta(J_\lambda)$, where J_λ is the radial action, $J_\phi = L_z$ is the azimuthal action, and J_ν is the latitudinal action. In this paper we write the distribution function in the (general) form $f = f_{\rm gsm}(J_\phi,J_\nu)g(J_\lambda,J_\phi,J_\nu)$, where g is a preassigned function, and we show how to find $f_{\rm gsm}$, consistent with a given axisymmetric density ρ in an oblate Stäckel potential V, by an iterative method, starting with the thin-orbit function $f_{\rm tsm}$ as a first guess for $f_{\rm gsm}$. We will consider functions g that are peaked in J_λ, so that the models will be fairly close to the thin-orbit model, and few iterations are needed. The stability analysis of these models will be discussed in Chapter 4.

Our method of specifying part of the distribution function, and solving for the remainder, is not new, and was used for flat disks by Shu (1969). Bishop (1986) applied it to oblate Stäckel models, starting from a different initial guess. Gerhard (1991) and Gerhard & Dehnen (1993) have recently popularized this approach for spherical and oblate models.

In Section 2 we define our notation, and present the construction method. A detailed description is given in Section 3, where we also investigate what properties of the assigned function g are important for convergence of the iterative scheme. We illustrate the method by constructing a number of self-consistent Kuzmin-Kutuzov models with thick tubes. In Section 4 we consider special and limiting cases for which the algorithm simplifies, and where further insight in the method can be gained by analytic means. Concluding remarks follow in Section 5.

2 Oblate galaxy models

We first summarize the basic properties of oblate Stäckel models, present the fundamental integral equation for their phase-space distribution functions, and then outline an iterative scheme for its solution. Derivations and further information can be found in dZ85, DZ, and ZH.

2.1 Orbits and integrals of motion

The motion in an oblate galaxy with a gravitational potential of Stäckel form is best described in prolate spheroidal coordinates (λ,ν,ϕ). These are related to standard

cylindrical coordinates (R,z,ϕ) by

$$R^2 = \frac{(\lambda+\alpha)(\nu+\alpha)}{(\alpha-\gamma)}, \qquad z^2 = \frac{(\lambda+\gamma)(\nu+\gamma)}{(\gamma-\alpha)}, \tag{2.1}$$

where α and γ are constants and the coordinates ν and λ lie in the range $-\gamma \leq \nu \leq -\alpha \leq \lambda$. Surfaces of constant λ are prolate spheroids, while those of constant ν are two-sheeted hyperboloids. The foci are located at $z = \pm\sqrt{\gamma-\alpha}$. Each set of (λ,ν,ϕ) corresponds in general to two points $(R, \pm z,\phi)$. In these coordinates the potential $V(\lambda,\nu)$ takes the form:

$$V = -\frac{(\lambda+\gamma)G(\lambda) - (\nu+\gamma)G(\nu)}{(\lambda-\nu)}, \tag{2.2}$$

where $G(\tau)$ is an arbitrary smooth function that determines the shape of the potential, and $\tau = \lambda,\nu$.

The equations of motion separate in the (λ,ϕ,ν) coordinates. Since the potential is axisymmetric, the momentum p_ϕ conjugate to ϕ is constant, and equals $L_z = R^2\dot{\phi}$, the component of the angular momentum parallel to the z–axis. The motion in λ and ν, i.e., in the meridional plane, is described by

$$p_\tau^2 = \frac{B(\tau)}{2(\tau+\alpha)^2(\tau+\gamma)}, \qquad (\tau = \lambda,\nu), \tag{2.3}$$

where

$$B(\tau) = (\tau+\alpha)(\tau+\gamma)E - (\tau+\gamma)I_2 - (\tau+\alpha)I_3 - U(\tau). \tag{2.4}$$

and

$$U(\tau) = -(\tau+\alpha)(\tau+\gamma)G(\tau). \tag{2.5}$$

Here E is the total orbital energy, $I_2 = \frac{1}{2}L_z^2$, and I_3 is the third isolating integral of motion given by (cf. eq. [2.13] of DZ)

$$I_3 = \tfrac{1}{2}(L_x^2 + L_y^2) + (\gamma-\alpha)[\tfrac{1}{2}v_z^2 - z^2\frac{G(\lambda)-G(\nu)}{\lambda-\nu}]. \tag{2.6}$$

Each set of values of E, $I_2 \geq 0$ and I_3 for which $p_\lambda^2 \geq 0$ and $p_\nu^2 \geq 0$ in some range of λ and ν, respectively, corresponds to an orbit. It is bound when $E \leq 0$. In this case the function $B(\tau)$ generally has three zeroes for $\tau = \nu_0,\lambda_1,\lambda_2$, and each orbit fills an area in the meridional plane defined by

$$-\gamma \leq \nu \leq \nu_0, \qquad \lambda_1 \leq \lambda \leq \lambda_2. \tag{2.7}$$

Orbits of this shape are usually referred to as *short-axis tubes*.

The constants $\nu_0,\lambda_1,\lambda_2$ are functions of E,I_2,I_3, and are called the *turning points* of the orbit. ZH have shown that the relations between the standard integrals (E,I_2,I_3)

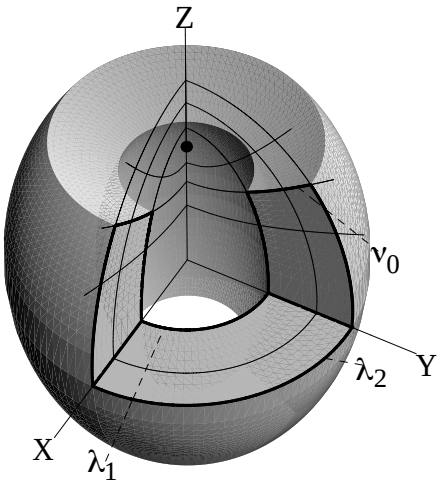

Figure 1. The three-dimensional volume filled by a short-axis tube orbit in an oblate Stäckel model. The thin solid lines are the intersections of the prolate spheroidal coordinates (λ,ϕ,ν) in which the motion separates with the equatorial plane $z = 0$ and with two meridional planes (R,z) at $\phi = 0$ and $\phi = \pi/2$. The dot indicates the location of the focus along the positive z-axis. The orbital volume is bounded by four prolate spheroidal coordinate surfaces: the top and bottom surfaces are parts of hyperboloids of revolution, labelled by the turning point ν_0, while the inner and outer boundaries are spheroids of revolution labelled by the turning points λ_1 and λ_2.

and $(\nu_0,\lambda_1,\lambda_2)$ can be written as

$$\begin{aligned} E &= U[\nu_0,\lambda_1,\lambda_2], \\ I_2 &= \frac{(-\alpha-\nu_0)(\lambda_1+\alpha)(\lambda_2+\alpha)}{\gamma-\alpha}U[-\alpha,\nu_0,\lambda_1,\lambda_2], \\ I_3 &= \frac{(\nu_0+\gamma)(\lambda_1+\gamma)(\lambda_2+\gamma)}{\gamma-\alpha}U[-\gamma,\nu_0,\lambda_1,\lambda_2], \end{aligned} \tag{2.8}$$

where the square brackets indicate *divided differences* of the function $U(\tau)$ defined in equation (2.5). These are defined iteratively by

$$U[\tau_1,\tau_2] = \frac{U(\tau_1)-U(\tau_2)}{\tau_1-\tau_2}, \tag{2.9a}$$

and

$$U[\tau_1,\tau_2,\ldots,\tau_n] = \frac{U[\tau_1,\tau_3,\ldots,\tau_n]-U[\tau_2,\tau_3,\ldots,\tau_n]}{\tau_1-\tau_2}. \tag{2.9b}$$

The ordering of the arguments is not significant. With this notation the function $B(\tau)$ of equation (2.4) becomes

$$B(\tau;\nu_0,\lambda_1,\lambda_2) = (\tau-\nu_0)(\tau-\lambda_1)(\lambda_2-\tau)U[\tau,\nu_0,\lambda_1,\lambda_2]. \tag{2.10}$$

Centrally concentrated models have $U'''(\tau) > 0$ for $\tau \geq -\gamma$. This guarantees that all third order divided differences $U[\tau_1,\tau_2,\tau_3,\tau_4]$ are strictly positive (Hunter & de Zeeuw 1992), so that $B(\tau)$ has no more than three zeroes: all orbits are short–axis tubes.

The three *action integrals* $J_\tau = (2\pi)^{-1} \oint p_\tau d\tau$ can be written as follows:

$$\begin{aligned} J_\lambda &= \frac{\sqrt{2}}{\pi} \int_{\lambda_1}^{\lambda_2} \sqrt{\frac{B(\lambda;\nu_0,\lambda_1,\lambda_2)}{\lambda+\gamma}}\,\frac{d\lambda}{\lambda+\alpha}, \\ J_\phi = L_z &= \sqrt{\frac{-2B(-\alpha;\nu_0,\lambda_1,\lambda_2)}{\gamma-\alpha}}, \\ J_\nu &= \frac{\sqrt{2}}{\pi} \int_{-\gamma}^{\nu_0} \sqrt{\frac{B(\nu;\nu_0,\lambda_1,\lambda_2)}{\nu+\gamma}}\,\frac{d\nu}{(-\alpha-\nu)}. \end{aligned} \tag{2.11}$$

The integrals for J_λ and J_ν generally need to be evaluated numerically.

2.2 Distribution functions

The fundamental integral equation for the phase-space distribution function $f_{\rm sm}(\lambda,\nu,v_\lambda,v_\phi,v_\nu)$ that gives rise to a density $\rho_m(\lambda,\nu)$ in a gravitational potential $V(\lambda,\nu)$ is

$$\rho_m(\lambda,\nu) = \int\int\int f_{\rm sm}(\lambda,\nu,v_\lambda,v_\phi,v_\nu)\,dv_\lambda\,dv_\phi dv_\nu. \tag{2.12}$$

Because V is here of Stäckel form, each orbit has three exact isolating integrals of motion, so that Jeans' theorem is valid: $f_{\rm sm}$ is a function of the three integrals of motion, so we can consider $f_{\rm sm} = f_{\rm sm}(E,I_2,I_3)$, or $f_{\rm sm} = f_{\rm sm}(\nu_0,\lambda_1,\lambda_2)$, or $f_{\rm sm} = f_{\rm sm}(J_\lambda,J_\phi,J_\nu)$. In each case, transformation of $dv_\lambda dv_\phi dv_\nu$ to $dEdI_2dI_3$ etc., with the appropriate Jacobian determinant, gives the relevant form of the fundamental integral equation (2.12). DZ (eq. [3.2]) write (2.12) in terms of E,I_2,I_3), while ZH discuss its forms in terms of the turning points $(\nu_0,\lambda_1,\lambda_2)$ and the actions (J_λ,J_ϕ,J_ν) (their eqs [2.23] and [2.47]).

Since $f_{\rm sm}$ is a function of three arguments, and ρ_m depends on only two variables, many different $f_{\rm sm}$'s will be consistent with the same ρ_m, so that equation (2.12) has many solutions. Two of these are readily available. The first is the special model with $f_{\rm sm} = f_{\rm sm}(E,L_z)$, in which the orbits are populated such that there is no net dependence on the third integral. Its distribution function can be found by application of the Hunter & Qian (1993) method, which requires (numerical) evaluation of a contour integral. The second is the so–called thin-orbit model, in which the stars occupy only the short axis tubes that have no λ–excursion, and hence lie on prolate spheroidal shells. In this case $f_{\rm sm} = f_{\rm tsm}(J_\phi,J_\nu)\delta(J_\lambda)$. Bishop (1987) and ZH have shown that $f_{\rm tsm}$ can be found by a single real quadrature.

We are interested in distribution functions that populate not only the thin orbits, but also those with a finite λ-extent. Instead of the turning points λ_1 and λ_2, we employ the quantities

$$\lambda_m = \tfrac{1}{2}(\lambda_1+\lambda_2), \qquad \varepsilon = \tfrac{1}{2}(\lambda_2-\lambda_1). \tag{2.13}$$

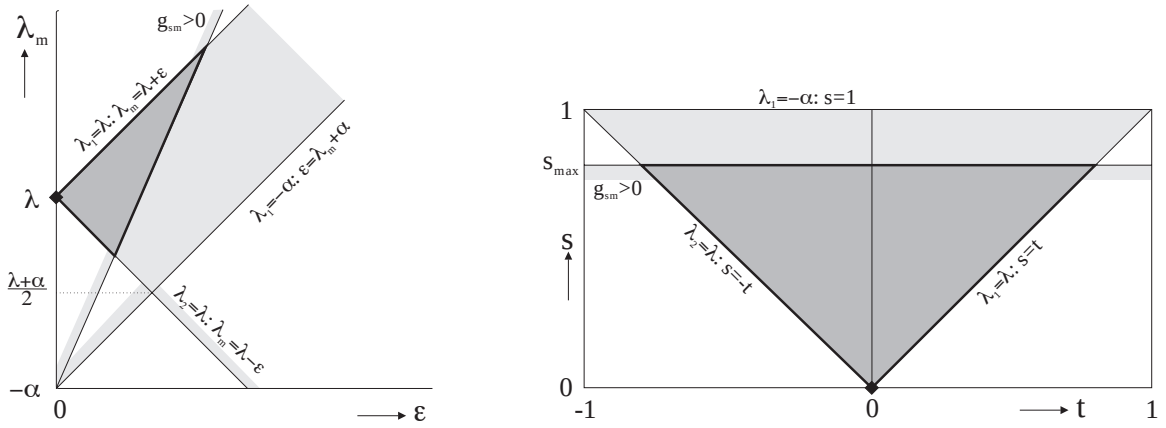

Figure 2. Integration areas for the fundamental integral equation. a) In the (ε,λ_m)-plane, defined in equation (2.13). b) In the (s,t)-plane, defined in equations (3.2) and (3.9). The light shaded regions indicate the full integration areas: all orbits with inner and outer λ-turning points that correspond to values of (ε,λ_m) or (s,t) in these areas contribute density on the spheroidal shell with coordinate λ in configuration space. The specific choice (3.6) for the function $g_{\rm sm}$ only populates orbits up to a maximum relative thickness $s_{\rm max}$, so that the integration over s runs between 0 and $s_{\rm max}$, as indicated by the dark shaded regions. The thin-orbit model has $s_{\rm max} = 0$, so that the integration areas shrink to a point, indicated by the filled squares.

Here $\varepsilon \geq 0$ controls the 'thickness' of the short-axis tube, and λ_m indicates its mean location in the radial direction (Figure 1). When $\varepsilon = 0$ the two radial turning points λ_1 and λ_2 coincide, so that the 'radial' action $J_\lambda = 0$, and the orbit is a thin short-axis tube. The relations between the standard integrals (E,I_2,I_3) and $(\nu_0,\lambda_m,\varepsilon)$ follow from equation (2.8), upon substitution of $\lambda_1 = \lambda_m - \varepsilon$, $\lambda_2 = \lambda_m + \varepsilon$.

With the definitions (2.13), equation (2.23) of ZH can be transformed to the fundamental integral equation in terms of the three integrals $\nu_0,\lambda_m,\varepsilon$:

$$\rho_m(\lambda,\nu) = 4\sqrt{2}\int_{\nu}^{-\alpha} d\nu_0 \int_{\frac{1}{2}(\lambda+\alpha)}^{\infty} d\lambda_m \int_{|\lambda-\lambda_m|}^{\lambda_m+\alpha} d\varepsilon \, \frac{U^*(\lambda,\nu;\nu_0,\lambda_1,\lambda_2)}{\sqrt{(\nu_0-\nu)(-\alpha-\nu_0)(\lambda-\nu_0)}} \times \frac{\varepsilon[(\lambda_m-\nu_0)^2-\varepsilon^2]f_{\rm sm}(\nu_0,\lambda_m,\varepsilon)}{\sqrt{[(\lambda_m-\nu)^2-\varepsilon^2][(\lambda_m+\alpha)^2-\varepsilon^2][\varepsilon^2-(\lambda-\lambda_m)^2]}}, \tag{2.14}$$

where

$$U^* = \frac{U[\nu_0,\lambda_1,\lambda_1,\lambda_2]U[\nu_0,\lambda_1,\lambda_2,\lambda_2]U[\nu_0,\nu_0,\lambda_1,\lambda_2]}{\sqrt{U[\nu_0,\lambda_1,\lambda,\lambda_2]U[\nu,\nu_0,\lambda_1,\lambda_2]U[\nu_0,-\alpha,\lambda_1,\lambda_2]}} \tag{2.15}$$

and we still have to substitute $\lambda_1 = \lambda_m - \varepsilon$, $\lambda_2 = \lambda_m + \varepsilon$. The area of integration in the (λ_m,ε) plane is illustrated in Figure 2a.

2.3 Iterative scheme

Our aim is to construct distribution functions $f_{\rm sm}(\nu_0,\lambda_m,\varepsilon)$ that also populate orbits with non-zero thickness $\varepsilon > 0$. In the spirit of Bishop (1986), we resolve the distribution function $f_{\rm sm}$ as the following product

$$f_{\rm sm}(\nu_0,\lambda_m,\varepsilon) = f_{\rm gsm}(\nu_0,\lambda_m)\tilde{g}_{\rm sm}(\nu_0,\lambda_m,\varepsilon), \tag{2.16}$$

where $\tilde{g}_{\rm sm}$ gives the distribution of the radial excursions ε of the orbits, which may depend on the values of the latitudinal turning points ν_0 and the mean radial positions λ_m. Writing $f_{\rm sm}$ in this way does not imply any restrictions; all distribution functions can be split up as in (2.16). If we specify $\tilde{g}_{\rm sm}$, and substitute the result in equation (2.14), we are left with an integral equation for $f_{\rm gsm}(\nu_0,\lambda_m)$. The choice of $\tilde{g}_{\rm sm}$ determines what function will be found.

We choose to normalize the function $\tilde{g}_{\rm sm}$ such that

$$\int_0^\infty \tilde{g}_{\rm sm}(\nu_0,\lambda_m,\varepsilon)\, dJ_\lambda = 1, \tag{2.17}$$

for fixed (ν_0,λ_m). It then follows that when $\tilde{g}_{\rm sm} = \delta(J_\lambda)$, the function $f_{\rm gsm}$ is identical to $f_{\rm tsm}$, the thin orbit distribution function of Bishop (1987) and ZH. It is given by

$$\begin{aligned} f_{\rm tsm}(\lambda_m,\nu_0) = \frac{1}{8\pi^2\sqrt{\lambda_m+\gamma}(\lambda_m-\nu_0)U[\nu_0,\lambda_m,\lambda_m,\lambda_m]}\Big[&(\lambda_m+\alpha)\rho(\lambda_m,-\alpha)- \\ &\sqrt{(-\alpha-\nu_0)U[\nu_0,-\alpha,\lambda_m,\lambda_m]}\int_{\nu_0}^{-\alpha}\frac{[\partial(\lambda_m-\sigma)\rho(\lambda_m,\sigma)/\partial\sigma]d\sigma}{\sqrt{(\sigma-\nu_0)U[\sigma,\nu_0,\lambda_m,\lambda_m]}}\Big], \end{aligned} \tag{2.18}$$

where ρ equals ρ_m, the model density. The divided differences of U are always derived from the model potential V, but the above expression gives $f_{\rm tsm}$ for any axisymmetric density ρ in the potential $V(\lambda,\nu)$.

When the function $\tilde{g}_{\rm sm}$ is sharply peaked near $\varepsilon = 0$ (i.e., near $J_\lambda = 0$), the solution $f_{\rm gsm}$ of (2.14) should be very similar to the thin orbit function $f_{\rm tsm}$. This suggests the following approach. We start with the zeroth-order distribution function

$$f_0(\nu_0,\lambda_m,\varepsilon) = f_{\rm tsm}\{\rho_m\}\tilde{g}_{\rm sm}(\nu_0,\lambda_m,\varepsilon), \tag{2.19}$$

where $f_{\rm tsm}\{\rho_m\}$ is short-hand for the thin-orbit function $f_{\rm tsm}(\nu_0,\lambda_m)$ that follows from equation (2.18) upon substitution of $\rho = \rho_m$. Since $\tilde{g}_{\rm sm}$ is not the delta function in J_λ that is appropriate for $f_{\rm tsm}\{\rho_m\}$, the residual density

$$\rho_1 = \rho_m - \int\int\int f_{\rm tsm}\{\rho_m\}\tilde{g}_{\rm sm}(\nu_0,\lambda_m,\varepsilon)\, d^3\nu, \tag{2.20}$$

does not vanish everywhere, although we expect it to be much smaller than ρ_m. We have $f_{\rm gsm} = f_0 + f_c$, where f_c is the solution of

$$\rho_1 = \int\int\int f_c(\nu_0,\lambda_m)\tilde{g}_{\rm sm}(\nu_0,\lambda_m,\varepsilon)\, d^3\nu. \tag{2.21}$$

This is the same integral equation as (2.14), but now for the density ρ_1 in the potential $V(\lambda,\nu)$. For sharply-peaked $\tilde{g}_{\rm sm}$ we approximate f_c by $f_1 = f_{\rm tsm}\{\rho_1\}$. Taking as first order approximation $f_{\rm gsm} = f_{\rm tsm}\{\rho_m\} + f_{\rm tsm}\{\rho_1\}$ then leads to a residual density ρ_2, which should be smaller than ρ_1. We can repeat this process as many times as we want, which leads to the following algorithm:

$$f_{\rm gsm}(\nu_0,\lambda_m) = \sum_{i=0}^{n} f_{\rm tsm}\{\rho_i\}, \tag{2.22}$$

where

$$\begin{aligned} \rho_0 &= \rho_m(\lambda,\nu), \\ \rho_{i+1} &= \rho_i - \int\int\int f_{\rm tsm}\{\rho_i\}\tilde{g}_{\rm sm}\, d^3\nu, \quad (i = 1,\ldots,n). \end{aligned} \tag{2.23}$$

If the residual densities ρ_i decrease with increasing i, the series (2.22) will provide an increasingly better approximation to the actual distribution function. If this process converges, we still have to check that the resulting $f_{\rm gsm}$ is non-negative everywhere. If it is not, it is not a physical distribution function, and another choice needs to be made for $\tilde{g}_{\rm sm}$.

When $\tilde{g}_{\rm sm}$ is sharply peaked, the zeroth order approximation (2.19) may already be adequate. Shu (1969) used it to construct self-consistent flat circular disks with nearly circular orbits. For less sharply peaked functions the iterative scheme (2.22)–(2.23) should work very well. However, as the thickness of the populated orbits increases, the density residuals ρ_i will become larger and it is not clear *a priori* whether the algorithm will converge. We have implemented the algorithm, and have constructed a number of models. It turns out that convergence is reached easily for models with quite 'fat' orbits $\varepsilon \sim 0.7(\lambda_m + \alpha)$, but that the number of required iterations increases strongly for broad $\tilde{g}_{\rm sm}$ functions. The algorithm is described in detail in Section 3.

2.4 Kuzmin-Kutuzov mass models

We illustrate our method by applying it to the construction of self-consistent models with potential

$$V(\lambda,\nu) = -\frac{GM}{\sqrt{\lambda} + \sqrt{\nu}}, \tag{2.24}$$

and associated density

$$\rho_m(\lambda,\nu) = \frac{M\gamma}{4\pi}\,\frac{\alpha(\lambda + 3\sqrt{\lambda\nu} + \nu) - \lambda\nu}{(\lambda\nu)^{3/2}(\sqrt{\lambda} + \sqrt{\nu})^3}. \tag{2.25}$$

This mass model was introduced by Kuzmin (1956) and connects Kuzmin's (1953) flat circular disk ($\gamma = 0$) with Hénon's (1959) spherical isochrone ($\gamma = \alpha$). The surfaces of constant density are smooth and nearly oblate spheroidal with an axis

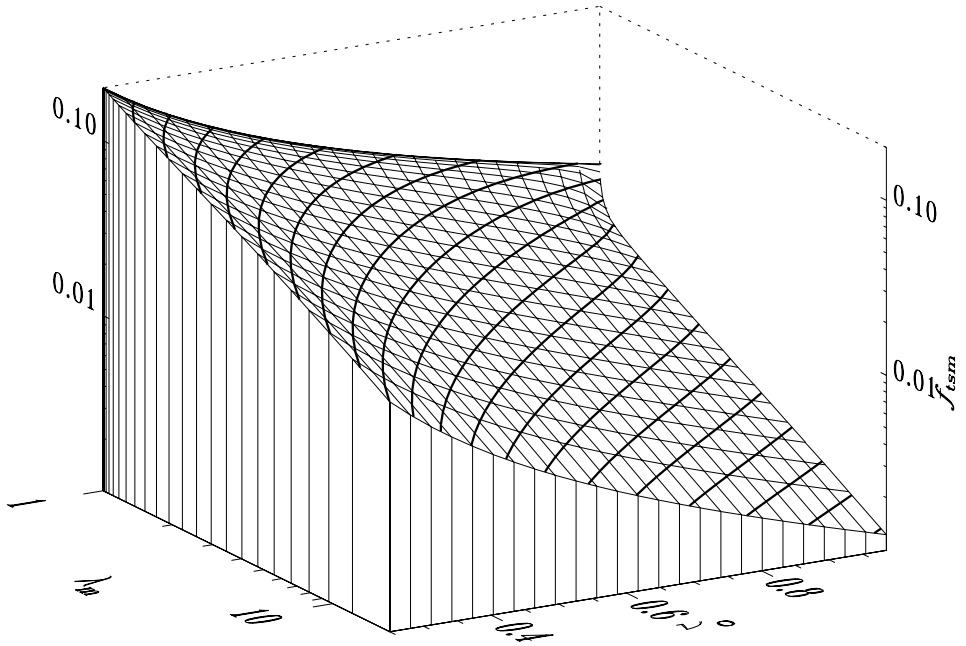

Figure 3. The distribution function $f_{\rm tsm}(\lambda_m,\nu_0)$ for an E5 Kuzmin-Kutuzov model with $\alpha = -1$ and $\gamma = -0.25$. The thick solid curves are contours spaced logarithmically at intervals of 2. The focal corner lies at $\lambda_m = \nu_0 = 1$. See also Figure 2 of ZH.

ratio $\sim \sqrt{\gamma/\alpha}$, and become slightly less flattened at large radii. Kuzmin & Kutuzov (1962) showed that the distribution function $f_{\rm sm}(E,L_z)$ could be found as a series expansion in powers of E and L_z. Many properties of these Kuzmin-Kutuzov models were described by DZ, who also derived a closed form for $f_{\rm sm}(E,L_z)$, albeit with a typographical error (see Batsleer & Dejonghe 1993). ZH showed that the thin-orbit distribution function $f_{\rm sm} = f_{\rm tsm}(\nu_0,\lambda_m)\delta(J_\lambda)$ (Figure 3) can be given in terms of elementary functions, and discussed its properties in detail.

3 Description of the method

We first discuss a practical way to choose the function $\tilde{g}_{\rm sm}$, introduce more convenient variables, and show that the convergence of the iterative scheme depends mostly on the moments of $\tilde{g}_{\rm sm}$. Then we show how kinematic properties of the models can be calculated with little extra effort, and we briefly describe the numerical implementation.

3.1 Normalization of $\tilde{g}_{\rm sm}$: the function $g_{\rm sm}$

The normalization of $\tilde{g}_{\rm sm}$ is to some extent arbitrary, as is the factorization (2.16) of the distribution function. All we require is that $\tilde{g}_{\rm sm}$ is normalized such that in the limit of thin orbits only, we recover $f_{\rm tsm}$. The most natural normalization is to take the

condition (2.17), but at constant values of the actions (J_ϕ,J_ν) rather than at constant values of the integrals (ν_0,λ_m). However, the transformation $(\nu_0,\lambda_m,\varepsilon) \leftrightarrow (J_\lambda,J_\phi,J_\nu)$ generally requires numerical inversion, so that in fact both these normalizations are not very practical. We therefore work with a function $g_{\rm sm}(\nu_0,\lambda_m,s)$ defined by

$$\tilde{g}_{\rm sm}(\nu_0,\lambda_m,\varepsilon) = \frac{c_g(\nu_0,\lambda_m)}{(\lambda_m+\alpha)\sqrt{\lambda_m-\nu_0}}\, g_{\rm sm}(\nu_0,\lambda_m,s), \tag{3.1}$$

where

$$s = \frac{\varepsilon}{\lambda_m+\alpha}, \tag{3.2}$$

so that s is an integral of motion which gives the *relative thickness* of the orbit, and $0 \le s \le 1$. We require that

$$\int_0^1 g_{\rm sm}(\nu_0,\lambda_m,s)\, ds^2 = 1, \tag{3.3}$$

at fixed ν_0 and λ_m. By comparison of equations (3.3) and (2.17) it then follows that

$$c_g(\nu_0,\lambda_m) = \frac{(\lambda_m+\alpha)\sqrt{\lambda_m-\nu_0}}{\displaystyle\int_0^1 ds^2\, g_{\rm sm}(\nu_0,\lambda_m,s)\left|\partial J_\lambda/\partial s^2\right|_{(\nu_0,\lambda_m)}}, \tag{3.4}$$

which therefore depends on the choice of $g_{\rm sm}$. The partial derivative of J_λ can be written as a single quadrature, and is given in Appendix A. It is even in s, and hence a function of s^2.

We have not incorporated the factor $(\lambda_m+\alpha)\sqrt{\lambda_m-\nu_0}$ in the definition of c_g, because it diverges on orbits with $\lambda_m = \nu_0 = -\alpha$, i.e., on the oscillations along the z-axis that just reach the foci of the spheroidal coordinates. We will come back to the behaviour of the algorithm near the foci in Section 4.2. In the limit $\tilde{g}_{\rm sm} = \delta(J_\lambda)$, so that only thin orbits are populated, we have $s = 0$, $g_{\rm sm}(s) = \delta(s^2)$, and

$$c_g(\nu_0,\lambda_m) = \frac{\sqrt{2(\lambda_m+\gamma)}}{\sqrt{U[\nu_0,\lambda_m,\lambda_m,\lambda_m]}}. \tag{3.5}$$

This is well-behaved for all physical values of $-\gamma \le \nu_0 \le -\alpha \le \lambda_m$.

3.2 Choice of $g_{\rm sm}$; moments

Any distribution function $f_{\rm sm}$ can be written as $f_{\rm gsm}c_g g_{\rm sm}$. As an example, Figure 4 shows both the factor $f_{\rm gsm}c_g$ and the factor $g_{\rm sm}$ for the two-integral Kuzmin-Kutuzov model with $f_{\rm sm}(E,L_z)$. Both factors vary smoothly, but the function $g_{\rm sm}$

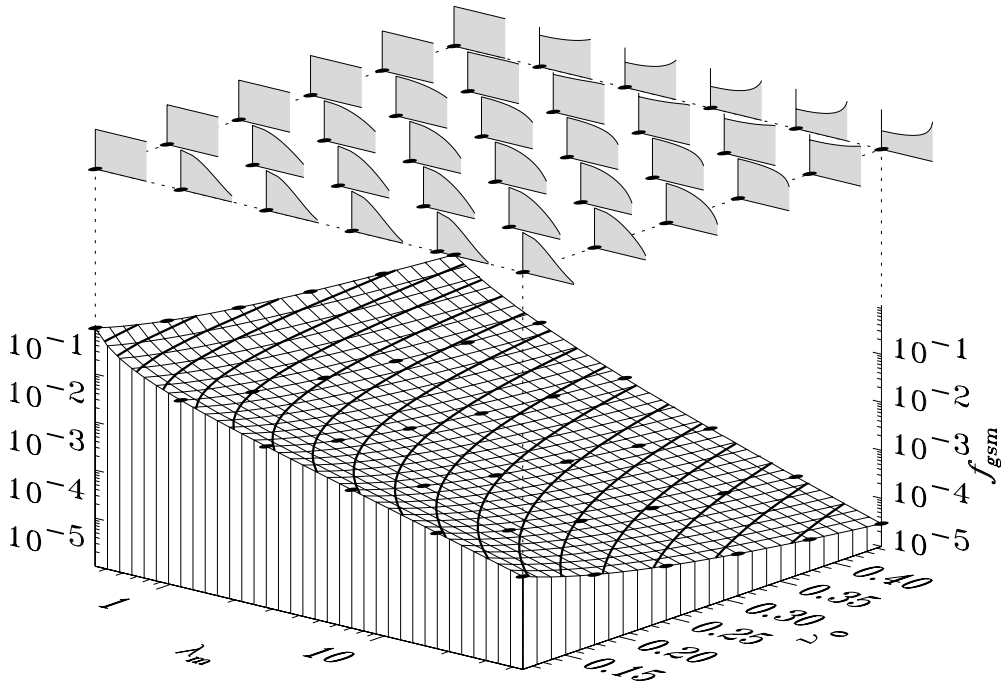

Figure 4. The distribution function $f_{\rm sm}(E,L_z^2)$ for an E5 Kuzmin-Kutuzov model with $\alpha = -4/9$ and $\gamma = -1/9$. The surface is the $f_{\rm gsm}$ part, which includes the normalizations factor c_g. The thick solid curves are contours spaced logarithmically at intervals of 2. The focal corner lies at $\lambda_m = \nu_0 = 4/9$. The small diagrams in the upper half show the behaviour of $g_{\rm sm}$ as a function of s, on the interval [0,1].

shows a range of behaviour as a function of s^2, depending on the values of λ_m,ν_0. In this chapter we consider functions $g_{\rm sm}$ that are even in s, and are of the form

$$g_{\rm sm}(s) = \begin{cases} \frac{q+1}{s_{\rm max}^2}\left(1 - \frac{s^2}{s_{\rm max}^2}\right)^q & \text{for } 0 \le s \le s_{\rm max}, \\ 0 & \text{for } s \ge s_{\rm max}, \end{cases} \tag{3.6}$$

with $q > -1$ and $0 \le s_{\rm max} \le 1$. These functions are all normalized as in equation (3.3), and show a similar range of shapes as seen in Figure 4. In principle, we can choose the maximum relative thickness $s_{\rm max}$ to be a function of ν_0 and λ_m, but we do not do so here, and from now on we suppress the dependence of $g_{\rm sm}$ on ν_0 and λ_m in the expressions that follow. Figure 5 illustrates the cases $q = 0,1,2$.

We define the moments $\langle s^{2n} g_{\rm sm}\rangle$ of $g_{\rm sm}$ by

$$\langle s^{2n} g_{\rm sm}\rangle = \frac{1}{n!}\int_0^1 s^{2n} g_{\rm sm}(s)\, ds^2, \tag{3.7}$$

for $n = 0,1,\ldots$. It follows that $\langle g_{\rm sm}\rangle = \langle s^0 g_{\rm sm}\rangle = 1$, by the normalization (3.3). The higher moments can be given explicitly for the choice (3.6):

$$\langle s^{2n} g_{\rm sm}\rangle = \frac{\Gamma(q+2)}{\Gamma(n+q+2)}\, s_{\rm max}^{2n}. \tag{3.8}$$

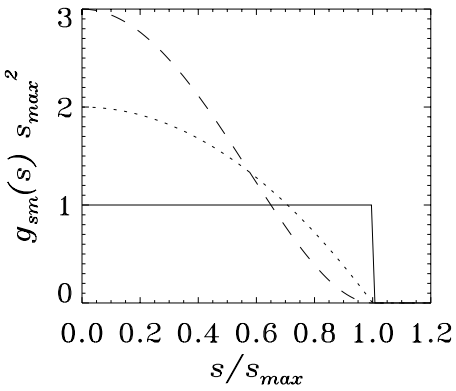

Figure 5. Three different functions $g_{\rm sm}$ of the form (3.6) with $q = 0$ (solid line), $q = 1$ (dotted line), $q = 2$ (dashed line). They are normalized with respect to s^2 (see eq. [3.3]).

When $s_{\rm max} \to 0$, we have $g_{\rm sm}(s) = \delta(s^2)$, and all higher order moments vanish. When $0 < s_{\rm max} \ll 1$, the higher moments decrease very rapidly with increasing n.

3.3 New variables

The fundamental integral equation appears in our iterative scheme in the form (2.23). We transform it to a more useful form by means of an alternative set of variables. In addition to the relative orbital thickness s, defined in equation (3.2), we introduce

$$t = \frac{\lambda - \lambda_m}{\lambda_m + \alpha}, \qquad u = \frac{-\alpha - \nu_0}{-\alpha - \nu}, \qquad x = \frac{-\alpha - \nu}{\lambda - \nu}, \tag{3.9}$$

so that $0 \le t, 0 \le u$, and $0 \le x \le 1$. These definitions mix the turning point variables (ν_0,λ_m) with the coordinates (λ,ν), but they facilitate the analysis of the fundamental integral equation. Carrying out the substitutions (3.9), and rearranging various terms results in

$$\rho_{i+1} = \rho_i - \int_0^1 du\, w_1(u) \int_0^{s^2_{\rm max}} ds^2 g_{\rm sm}(s) \int_{-s}^{s} dt\, \frac{w_2(s,t,u)}{\sqrt{s^2 - t^2}} f_{\rm tsm}\{\rho_i\}, \tag{3.10}$$

where we have written

$$\begin{aligned} w_1 &= \frac{4\sqrt{2}}{\sqrt{u(1-u)(1-x+xu)}}, \\ w_2 &= \frac{[[1-x+xu(1+t)]^2 - (1-x)^2 s^2]}{\sqrt{(1+tx)^2 - (1-x)^2 s^2}\sqrt{1-x+xu(1+t)}} \frac{U^*(s,t,u) c_g(t,u)}{(1+t)^{3/2}\sqrt{1-s^2}}, \end{aligned} \tag{3.11}$$

and c_g and U^* are defined in equations (3.4) and (2.15), respectively. The thin orbit function $f_{\rm tsm}\{\rho_i\}$ is defined in equation (2.18), and is independent of s. Both w_1 and w_2 depend also on the coordinates λ and ν, but we suppress them as arguments because they are not integration variables. The square root of $s^2 - t^2$ vanishes at $s = t = 0$, which lies in the area of integration (Figure 2b). For this reason we have not incorporated it in the definition of w_2. Finally we remark that w_2 is an even function of s, and hence depends on s^2.

3.4 Convergence

When $s_{\max} \ll 1$, the function $g_{\rm sm}$ is sharply peaked, and it is useful to expand it in a series of derivatives of delta functions (e.g., Fridman & Polyachenko 1984, p. 150):

$$g_{\rm sm}(s) = \sum_{n=0}^{\infty} (-1)^n \langle s^{2n} g_{\rm sm} \rangle \delta^{(n)}(s^2), \tag{3.12}$$

where the $\langle s^{2n} g_{\rm sm} \rangle \propto s_{\max}^{2n}$ are the moments of $g_{\rm sm}$ defined in equation (3.7), and $\delta^{(n)}$ is the n^{th} derivative of the delta function, which satisfies the relation

$$\int_{-}^{+} \delta^{(n)}(x) h(x)\, dx = (-1)^n h^{(n)}(0). \tag{3.13}$$

We use this expansion to show that the convergence of our iterative scheme depends mostly on the moments of $g_{\rm sm}$, and less on its detailed functional behaviour.

Substitution of (3.12) in equation (3.10) gives

$$\rho_{i+1} = \rho_i - \int_0^1 du\, w_1(u) \sum_{n=0}^{\infty} \langle s^{2n} g_{\rm sm} \rangle \frac{d^n W_2(0,u)}{d(s^2)^n}, \tag{3.14}$$

where we have written the t-integral as

$$W_2(s,u) = \int_{-s}^{s} dt\, \frac{w_2(s,t,u)}{\sqrt{s^2 - t^2}} f_{\rm tsm}\{\rho_i\}, \tag{3.15}$$

and we have used the definition (3.13) to carry out the s-integration. The first term in the series expansion for $g_{\rm sm}$ is $\delta(s^2)$. Its contribution to the right hand side of equation (3.14) equals $-\rho_i$. Upon substitution of the specific form (3.8) for the moments, we are therefore left with

$$\rho_{i+1} = -\sum_{n=1}^{\infty} \frac{\Gamma(q+2)}{\Gamma(n+q+2)} s_{\max}^{2n} \int_0^1 du\, w_1(u) \frac{d^n W_2(0,u)}{d(s^2)^n}. \tag{3.16}$$

This is valid for all functions $g_{\rm sm}$ of the form (3.6) with $s_{\max} < 1$.

Since $0 \le t \le s \le s_{\max}$, it follows that both s and t are small when $g_{\rm sm}$ is sharply peaked. The functions $w_2(s,t,u)$ and $f_{\rm tsm}\{\rho_i\}$ then vary little over the integration area, and so does $W_2(s,u)$. Its derivatives with respect to s^2 are finite at $s = 0$. Since W_2 contains the thin orbit function $f_{\rm tsm}\{\rho_i\}$ as a factor, and since this is independent of s and proportional to ρ_i, it follows that all the derivatives of W_2 are similarly proportional to ρ_i.

For small $s_{\max}$, the first term in the series on the right hand side of equation (3.16) dominates. This means that the residual density ρ_{i+1} is roughly proportional to the

residual ρ_i times the first moment of the function $g_{\rm sm}$. Since this is proportional to $s^2_{\rm max}$, this shows why even for moderately peaked functions our iterative scheme converges rapidly. It furthermore shows that the shape of $g_{\rm sm}$ is less important than its moments. We can vary the shape of $g_{\rm sm}$ without significantly affecting the residual density, as long as we do not dramatically change the lowest order moments of $g_{\rm sm}$. Since $f_{\rm tsm}\{\rho_i\}$ is derived from these residuals, the solutions $f_{\rm gsm}(\lambda_m,\nu_0)$ that correspond to different $g_{\rm sm}$ will be rather similar as long as the first moments of these $g_{\rm sm}$ functions are the same.

We found that even for very broad $g_{\rm sm}$ functions the iterative scheme performed well. Figure 6 shows the density residuals in the construction of an E5 Kuzmin-Kutuzov model with $q = 2$ and $s^2_{\rm max} = 0.9$. The computation was continued until $|\rho_i/\rho_{\rm m}| < 10^{-3}$, which occurred after five iterative steps. Even for this 'fat' model the residuals decrease rapidly. The resulting $f_{\rm gsm}$ is also shown, compared to the thin-orbit distribution function $f_{\rm tsm}$.

3.5 Velocity moments

When a distribution function $f_{\rm sm} = f_{\rm gsm} c_g g_{\rm sm}$ for a given density ρ_m in a potential V has been found, we are most often also interested in the observable kinematical properties of the resulting dynamical model. These follow by taking the appropriate velocity moments of $f_{\rm sm}$, followed by a line-of-sight integration. It turns out that the intrinsic velocity moments can be found easily by a slight extension of our algorithm.

The intrinsic velocity moments are defined as

$$\rho_m \langle v_\lambda^i v_\phi^j v_\nu^k \rangle = \int\int\int v_\lambda^i v_\phi^j v_\nu^k f_{\rm sm}\, dv_\lambda dv_\phi dv_\nu, \tag{3.17}$$

The expressions for the velocity components at a point (λ,ν) along an orbit with turning points $(\nu_0,\lambda_1,\lambda_2)$ are given in equation (3.2) of ZH. Upon transformation to our variables (s,t,u,x) we find

$$\begin{aligned} v_\lambda^2 &= 2(\lambda+\alpha)\frac{(1-x+xu)}{(1+t)^2}(s^2-t^2)U[\lambda,\lambda_1,\lambda_2,\nu_0], \\ v_\phi^2 &= 2(\lambda+\alpha)\frac{u(1-s^2)}{(1+t)^2}U[-\alpha,\lambda_1,\lambda_2,\nu_0], \\ v_\nu^2 &= 2(\lambda-\nu)\frac{(1+xt)^2-(1-x)^2s^2}{(1+t)^2}(1-u)U[\nu,\lambda_1,\lambda_2,\nu_0]. \end{aligned} \tag{3.18}$$

Hence, if we insert $v_\lambda^i v_\phi^j v_\nu^k$ in our equation (3.10), after use of the transformation (3.18), we find the contribution to the required moment. Since the U-functions occur in U^*, they have already been evaluated, so calculating the velocity moments in parallel with carrying out the iteration to get $f_{\rm sm}$ adds very little to the required CPU time.

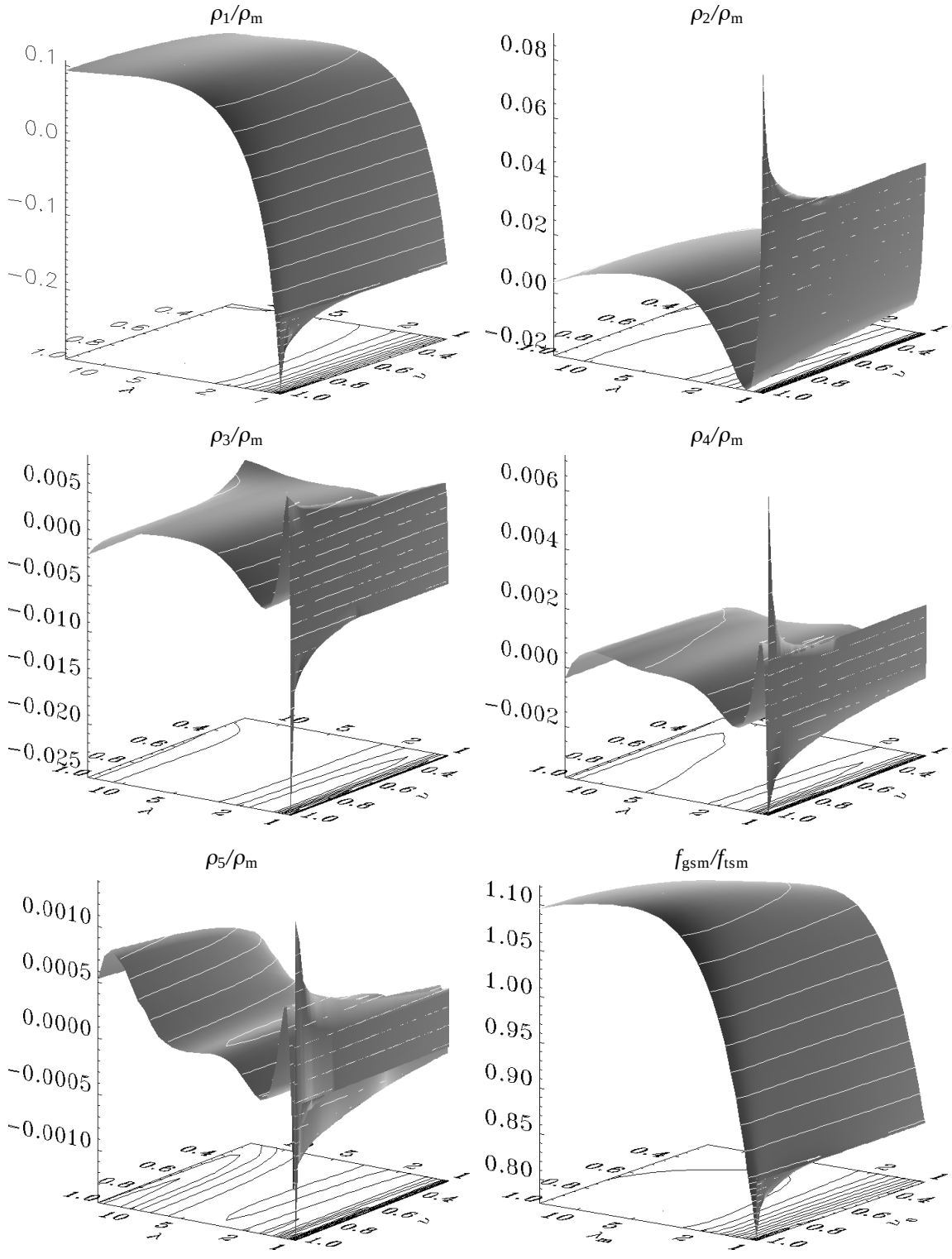

Figure 6. Successive steps of the iterative scheme to obtain f_{gsm} for an E5 Kuzmin-Kutuzov model with $\alpha = -1, \gamma = -0.25$, and a function g_{sm} with parameters $q = 2$ and $s^2_{max} = 0.9$. Shown is the residual density ρ_i/ρ_m for each step. The bottom right plot shows the ratio of the resulting f_{gsm} (after five iterations) and f_{tsm}.

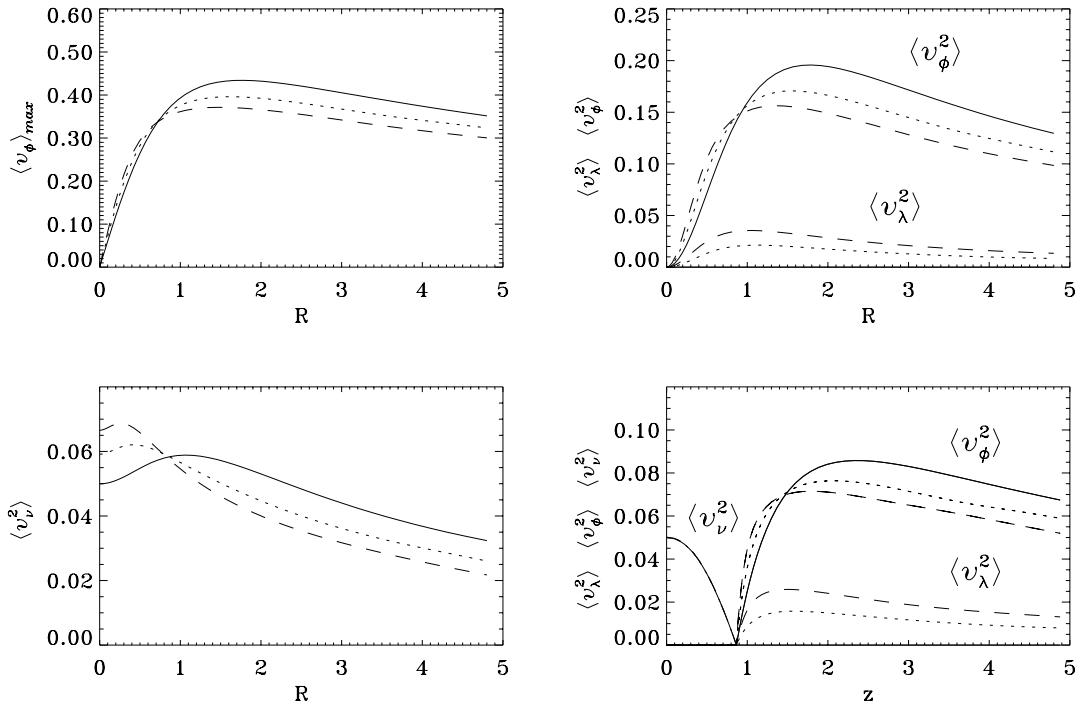

Figure 7. The intrinsic velocity moments for the E5 Kuzmin-Kutuzov thin-orbit model (solid) and $q = 0$ models with $s_{\max} = 0.5$ (dotted) and 0.7 (dashed lines).

As an example, we have constructed two E5 Kuzmin-Kutuzov model with $q = 0$ and $s^2_{\max} = 0.5$ and 0.7, respectively. In five iterations the residual density is less than $10^{-3}\rho_{\rm m}$. The velocity moments are shown in Figure 7 (cf. Figures 5 and 7 in ZH). As expected, the dispersion in the ν- and ϕ-directions decrease while the 'radial' dispersion increases. The $s^2_{\max} = 0.7$ model has the largest ratio of $\langle v^2_\lambda \rangle / \langle v^2_\phi \rangle$, which is of the order of 0.25.

3.6 Numerical implementation

We have written a code to implement the iterative scheme defined in equations (2.22) and (2.23). The density residuals and the terms in the series for $f_{\rm gsm}$ are calculated on a (λ,ν) grid that doubles as a (λ_m,ν_0) grid. The quantities are interpolated using splines as their values are also needed in between mesh points to evaluate the s– and t–integrals. The actual integrations are carried out using Romberg integration after switching to more appropriate integration variables instead of s and u to remove the square roots from the denominators.

The (λ,ν) grid points have to be chosen with some care. We need to cover the full λ domain in order to prevent boundary errors in the determination of the residual density. This is accomplished by using a grid that is linear in the variable t_λ defined by

$$\lambda(t_\lambda) + \alpha = (\lambda_H + \alpha)\frac{(2t_\lambda)^p}{(2 - 2t_\lambda)^q}, \qquad 0 < t_\lambda < 1, \tag{3.19}$$

where λ_H is the value of λ in the middle of the grid, p determines the resolution near $\lambda = -\alpha$ and q is chosen to match the large-radii behaviour of the distribution function. Most of the computations in this paper were done using $p = 3$, $q = 0.25$ and $\lambda_H = 4$.

When the model is very flattened towards the equatorial plane, its associated prolate spheroidal coordinate system is very elongated along the z-axis. The net effect of this opposite elongation is that the density and distribution function are sharply peaked near $\nu = -\gamma$. We therefore use a ν–grid that is linear in the variable u_ν, where

$$\nu(u_\nu) + \gamma = A\Big[\frac{(1+u_\nu)^p}{B + (1+u_\nu)^{p-1}} - \frac{1}{B+1}\Big]. \tag{3.20}$$

for some $p \geq 1$; B is set to $(\frac{7}{4})^{p-1}$. The parameter A is determined so that $\nu(1) = -\alpha$. We have found this substitution to be adequate for models as flattened as E7.

The thin-orbit distribution function is computed from the density residuals using (2.18). A straightforward implementation of (3.10) is feasible, but a single iteration step on a (λ,ν) grid of 50x50 would take about 100 minutes CPU time on an HP735. There is a faster way to implement the algorithm. The only part of the integral in (3.10) that changes in successive iterations is the $f_{\rm tsm}\{\rho_i\}$ factor, which does not depend on s. We therefore exchange the order of integration, and carry out the s-integral first. It is

$$T_g(t,u,x) = \int_{t^2}^{s^2_{\rm max}} ds^2 \, \frac{w_2(s,t,u) g_{\rm sm}(s)}{\sqrt{s^2 - t^2}}, \tag{3.21}$$

and can be tabulated before the first iteration. Using a 81x27x100 grid for (t,u,x), the initialization stage takes 5 minutes CPU time, or 10 minutes if the velocity moments have to be computed as well. Each iteration step then simplifies to

$$\rho_{i+1} = \rho_i - \int_0^1 du\, w_1(u) \int_{-s_{\rm max}}^{s_{\rm max}} dt\; T_g(t,u,x) f_{\rm tsm}\{\rho_i\}, \tag{3.22}$$

which takes about 1 CPU minute to complete. The program is written in Fortran. The number of iteration steps to reach a relative accuracy better than 10^{-3} is 1 for $s_{\rm max} = 0.1$, 3 for $s_{\rm max} = 0.5$ and 5 for $s_{\rm max} = 0.7$ in the case of $q = 0$ models. It is smaller when $q > 0$.

There is a further reduction possible in the limiting cases of a spherical or a disk galaxy. These are described in Sections 4.4 and 4.5, respectively.

4 Special cases

Approximate solutions of the fundamental integral equation (3.10) can be found by analytic means at large radii, and near the foci of the spheroidal coordinates. We consider them in turn, and then show how the scheme simplifies for models with sharply peaked $g_{\rm sm}$ functions, and in the spherical and disk limits.

4.1 Large radii

The relation (3.10) for the density residuals simplifies considerably in the limit of large radii, i.e., $\lambda \to \infty$ so that $x \to 0$. The functions w_1 and w_2 then reduce to

$$\begin{aligned} w_1(u) &= \frac{4\sqrt{2}}{\sqrt{u(1-u)}}, \\ w_2(s,t,u) &= \frac{U^*(s,t,u)c_g(t,u)}{(1+t)^{3/2}}. \end{aligned} \tag{4.1}$$

In order to evaluate the various third-order divided differences that appear in the definitions (2.15) and (3.4) for U^* and c_g, respectively, we assume that $s_{\max} < 1$, so that the orbits that contribute to the density at (λ,ν) have $\lambda_2 \geq \lambda \geq \lambda_1 = \lambda_m(1-s) \geq \lambda_m(1-s_{\max}) \gg -\alpha$. The details of the calculations are given in Appendix B. We find that in this case neither U^* nor c_g depend on u at large λ, and that

$$U^* c_g \simeq \frac{GM}{2^{5/2}C_g}\frac{(1+t)}{\lambda}L(s,t), \tag{4.2}$$

where $L(s,t)$ is the elementary function given in equation (B4), and the constant $C_g \geq 1$ is defined in equation (B10). $C_g = 1$ in the thin orbit limit $g_{\rm sm} = \delta(s^2)$.

We consider a flattened density ρ_i that falls off as a power of λ at large radii:

$$\rho_i(\lambda,\nu) \simeq \frac{\rho_i^\nu(\nu)}{\lambda^p}, \tag{4.3}$$

for some (positive) value of p. Selfconsistent models with finite total mass must have $p > 3/2$. By Kuzmin's formula, such models must also have $p \leq 2$ (e.g., de Zeeuw, Peletier & Franx 1986). Non-consistent densities ρ_m may fall off steeper than this. Substitution of the form (4.3) in expression (2.18) for $f_{\rm tsm}\{\rho_i\}$ and use of the approximations (B1) then shows that $f_{\rm tsm} \propto \lambda_m^{1-p}$ times a function of ν_0 (cf ZH, eq. [2.56]). Transformation to the variables (s,t,u) gives

$$f_{\rm tsm}\{\rho_i\} \simeq \frac{(1+t)^{p-1}}{\lambda^{p-1}}\frac{f_{\rm tsm}^\nu(u)}{\pi^2 GM}, \tag{4.4}$$

where

$$f_{\rm tsm}^\nu = \Big[\rho_i^\nu(-\alpha) + \sqrt{u}\int_0^u \frac{[d\rho_i^\nu(u')/du']du'}{\sqrt{u-u'}}\Big]. \tag{4.5}$$

Thus, at large radii the thin orbit distribution function becomes a product of a function of t and a function of u.

Substitution of all the above approximations in the basic relation (3.10) shows that for $\lambda \gg -\alpha$ the triple integration over s,t and u reduces to the product of an integral over u times a double integral over s and t:

$$\rho_{i+1} \simeq \rho_i - \frac{L_g(p)}{\pi C_g}\frac{1}{\lambda^p}\int_0^1 \frac{du\, f_{\rm tsm}^\nu(u)}{\sqrt{u(1-u)}}, \tag{4.6}$$

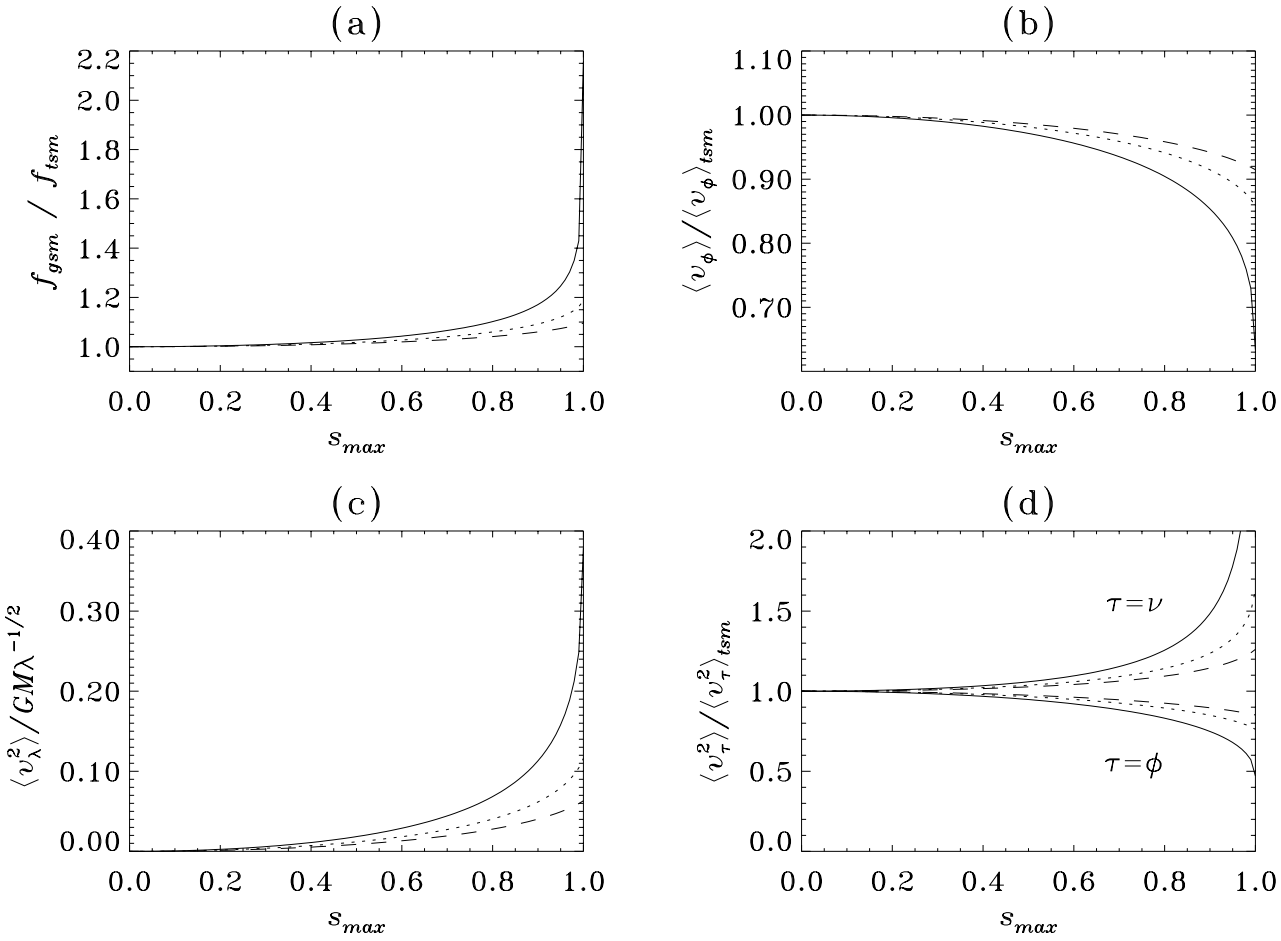

Figure 8. Limiting behaviour at large radii of various properties of models with a density fall-off $\rho_m \propto 1/\lambda^2$, and functions $g_{\rm sm}$ with $q = 0$ (solid), 1 (dotted), and 2 (dashed), and values of $s_{\rm max}$ between 0 and 1. Here $\lambda \sim r^2$, and $f_{\rm gsm}$ becomes a constant factor $C_g/L_g(2)$ times the thin-orbit distribution function $f_{\rm tsm}$ (see eq. [4.9]). Shown are, as a function of $s_{\rm max}$: a) the factor $C_g/L_g(2)$, b) the intrinsic mean streaming motion $\langle v_\phi \rangle$ in units of the maximum possible streaming $\langle v_\phi \rangle_{\rm tsm}$, assuming all stars have the same sense of rotation around the symmetry axis, c) the second moment $\langle v_\lambda^2 \rangle$ of the 'radial' velocity, in units of $GM/\sqrt{\lambda}$, and d) the second moments $\langle v_\phi^2 \rangle$ and $\langle v_\nu^2 \rangle$ in units of their values in the thin-orbit model. These results are valid for $\lambda_m(1 - s_{\rm max}) \gg -\alpha$.

where we have defined

$$L_g(p) = \frac{1}{\pi} \int_0^{s_{\rm max}^2} ds^2 g_{\rm sm}(s) \int_{-s}^{s} \frac{dt\, L(s,t)}{(1+t)^{\frac{3}{2}-p} \sqrt{s^2 - t^2}}. \tag{4.7}$$

The u-integration in equation (4.6) can be carried out, and equals $\pi\rho_i^\nu(\nu)$. Since $L_g(p)$ is a constant, it follows that the triple integration over $f_{\rm tsm}\{\rho_i\}$ is proportional to $\rho_i^\nu(\nu)/\lambda^p$, i.e., it is proportional to ρ_i itself:

$$\rho_{i+1} \simeq \rho_i \Big[1 - \frac{L_g(p)}{C_g}\Big]. \tag{4.8}$$

Thus, the residual density at large radii becomes smaller by a constant factor $[1 - L_g(p)/C_g]$ at each iteration step,

In the thin orbit limit $g_{\rm sm} = \delta(s^2)$, and we have $C_g = L_g(p) = 1$, so that $\rho_{i+1} = 0$ for all i. This is as it should be, since $f_{\rm gsm}$ equals $f_{\rm tsm}\{\rho_m\}$ exactly in this case. Equation (4.8) implies that for broadened functions $g_{\rm sm}$ the distribution function $f_{\rm gsm}$ at large values of λ_m is given by

$$f_{\rm gsm}(\nu_0,\lambda_m) \simeq \frac{C_g}{L_g(p)} f_{\rm tsm}\{\rho_m\}, \qquad (\lambda_m \gg -\alpha), \tag{4.9}$$

so that we can find it without iteration.

The values of the constants C_g and $L_g(p)$ can be found by numerical evaluation of the integrals (B10) and (4.7). For sharply peaked $g_{\rm sm}$ they can be approximated by expanding the integrands in powers of s^2, and evaluating term by term. This gives

$$\begin{aligned} C_g &\simeq 1 + \langle s^2 g_{\rm sm}\rangle + \tfrac{501}{256}\langle s^4 g_{\rm sm}\rangle + O(\langle s^6 g_{\rm sm}\rangle), \\ L_g(p) &\simeq 1 + (\tfrac{25}{16} - \tfrac{7}{8}p + \tfrac{1}{4}p^2)\langle s^2 g_{\rm sm}\rangle + (\tfrac{1005}{128} - \tfrac{471}{128}p + \tfrac{227}{128}p^2 - \tfrac{11}{32}p^3 + \tfrac{1}{32}p^4)\langle s^4 g_{\rm sm}\rangle \\ &\qquad + O(\langle s^6 g_{\rm sm}\rangle), \end{aligned} \tag{4.10}$$

so that

$$\rho_{i+1} \simeq \rho_i[(\tfrac{9}{16} - \tfrac{7}{8}p + \tfrac{1}{4}p^2)\langle s^2 g_{\rm sm}\rangle + (\tfrac{45}{32} - \tfrac{359}{128}p + \tfrac{195}{128}p^2 - \tfrac{11}{32}p^3 + \tfrac{1}{32}p^4)\langle s^4 g_{\rm sm}\rangle + \ldots]. \tag{4.11}$$

This shows again that for sharply peaked $g_{\rm sm}$ its first moment is mostly responsible for the convergence of the iterative scheme.

In a similar fashion it is possible to derive approximations for the intrinsic velocity moments. Substituting approximations (B1) in (3.18), we find that the velocities can be written as a

$$\nu_\tau^2 = \frac{GM}{\sqrt{\lambda}} \ell_\tau(u) L_\nu^\tau(s,t), \qquad (\tau = \lambda,\nu,\phi), \tag{4.12}$$

where L_ν^τ is given in (B12), and $\ell_\tau = 1,(1-u),u$ for $\tau = \lambda,\nu,\phi$, respectively. Substitution of (4.12) and (4.9) in (3.17) yields

$$\rho_{\rm m}\langle \nu_\tau^n\rangle = \frac{L_{g\nu}^{\tau n}}{L_g(p)} \frac{1}{\pi\lambda^p} \Big(\frac{GM}{\sqrt{\lambda}}\Big)^{n/2} \int_0^1 \frac{du\, f_{\rm tsm}^\nu(u)\ell_\tau(u)}{\sqrt{u(1-u)}}, \tag{4.13}$$

where we have introduced

$$L_{g\nu}^{\tau n}(p) == \frac{1}{\pi} \int_0^{s_{\rm max}^2} ds^2 g_{\rm sm}(s) \int_{-s}^{s} \frac{dt\, L_\nu^\tau(s,t) \frac{n}{2} L(s,t)}{(1+t)^{\frac{3}{2}-p}\sqrt{s^2-t^2}}. \tag{4.14}$$

Again, the u-integration can be carried out. Since $L^{\tau}_{\nu}(0,0) = 1$ for $\tau = \nu,\phi$, the u-integral equals $\rho_{\rm m}\langle v^n_\nu\rangle_{\rm tsm}$ and $\rho_{\rm m}\langle v^n_\phi\rangle_{\rm tsm}$, respectively, which are the velocity moments of the thin-orbit model. For $\tau = \lambda$ the u-integral equals $\rho_{\rm m}$, hence

$$\begin{aligned}\langle v^n_\tau\rangle &= \langle v^n_\tau\rangle_{\rm tsm}\frac{L^{\tau n}_{gv}(p)}{L_g(p)}, \qquad (\tau = \nu,\phi),\\ \langle v^n_\lambda\rangle &= \Big(\frac{GM}{\sqrt{\lambda}}\Big)^{n/2}\frac{L^{\lambda n}_{gv}(p)}{L_g(p)}.\end{aligned} \tag{4.15}$$

For sharply peaked $g_{\rm sm}$ functions the dispersions and rotation velocity can therefore be approximated by

$$\begin{aligned}\langle v_\phi\rangle &\simeq \langle v_\phi\rangle_{\rm tsm}[1 + (\tfrac{3}{64} - \tfrac{1}{8}p)\langle s^2 g_{\rm sm}\rangle(\tfrac{993}{8192} - \tfrac{175}{512}p + \tfrac{7}{128}p^2)\langle s^4 g_{\rm sm}\rangle + \ldots];\\ \langle v^2_\lambda\rangle &\simeq \tfrac{GM}{\sqrt{\lambda}}[\tfrac{1}{8}\langle s^2 g_{\rm sm}\rangle + (\tfrac{67}{128} - \tfrac{1}{8}p)\langle s^4 g_{\rm sm}\rangle + \ldots];\\ \langle v^2_\nu\rangle &\simeq \langle v^2_\nu\rangle_{\rm tsm}[1 + (-\tfrac{9}{8} + \tfrac{3}{4}p)\langle s^2 g_{\rm sm}\rangle(-\tfrac{531}{128} - \tfrac{215}{64}p - \tfrac{3}{8}p^2)\langle s^4 g_{\rm sm}\rangle + \ldots];\\ \langle v^2_\phi\rangle &\simeq \langle v^2_\phi\rangle_{\rm tsm}[1 + (\tfrac{1}{8} - \tfrac{1}{4}p)\langle s^2 g_{\rm sm}\rangle + (\tfrac{41}{128} - \tfrac{45}{64}p + \tfrac{1}{8}p^2)\langle s^4 g_{\rm sm}\rangle + \ldots].\end{aligned} \tag{4.16}$$

Figure 8 illustrates the behaviour of $C_g/L_g(p)$ for our choice of $g_{\rm sm}$, for $p = 2$. It also shows intrinsic velocity dispersions and rotational velocity in terms of the thin-orbit values. The above results show that for a given density distribution $\rho_{\rm m}(\lambda,\nu)$, and with $g_{\rm sm}$ a function of s only, the kinematic properties at large radii do depend on λ and ν, but they follow from those in the thin orbit model by multiplication with a factor wich depends on $g_{\rm sm}$ and p only.

Equation (4.8) shows that our iterative scheme will converge for any $g_{\rm sm}$ for which $0 \le L_g(p)/C_g < 2$. A useful upper limit for $L_g(p)/C_g$ can be obtained by evaluating

$$\max_{0\le s\le s_{\rm max}}\frac{1}{\pi h(s)}\int_{-s}^{s}\frac{dt\,L(s,t)}{(1+t)^{\frac{3}{2}-p}\sqrt{s^2-t^2}}. \tag{4.17}$$

It is easily verified by numerical integration of (4.17) that $L_g/C_g < 2$ as long as $p < 9/2$. This includes all physically relevant cases, so our iterative scheme will always converge at large radii for all $g_{\rm sm}$ functions.

4.2 Behaviour near the foci

We now investigate the behaviour of the iterative scheme near the foci of the spheroidal coordinates, where $\lambda = \nu = -\alpha$. The variables s,t,u and x that appear in the basic relation (3.10) for the density residuals take their full range of values near the foci, but the triple integration over s,t and u can nevertheless be simplified, because the factors $f_{\rm tsm}\{\rho_i\}(t,u)$, $U^*(s,t,u)$, and $c_g(t,u)$ which appear in the integrand, all simplify.

The only orbits that contribute density at the foci in the thin-orbit model are those with $\lambda_m = \nu_0 = -\alpha$. Orbits with $\lambda_m > -\alpha$ lie on spheroidal shells which intersect the z-axis above the foci, while orbits with $\lambda_m = -\alpha$ and $\nu_0 < -\alpha$ are z-axis oscillations that do not reach the foci. It follows that $\rho_m(-\alpha, -\alpha)$ is determined exclusively by $f_{\rm tsm}\{\rho_m\}(-\alpha, -\alpha)$. The relation is (see ZH, eq. [2.44])

$$f_{\rm tsm}\{\rho_m\}(-\alpha, -\alpha) = \frac{\rho_m(-\alpha, -\alpha)\,[1 + x_0]}{8\pi^2\sqrt{\gamma - \alpha}\,U[-\alpha, -\alpha, -\alpha, -\alpha]}, \tag{4.18}$$

where

$$x_0 = \frac{-\alpha - \nu_0}{\lambda_m - \nu_0} = \frac{xu(1 + t)}{1 - x + xu(1 + t)}. \tag{4.19}$$

and $U[-\alpha, -\alpha, -\alpha, -\alpha] = U'''(-\alpha) > 0$. In the limit where $\lambda_m = \nu_0 = -\alpha$, the value of x_0 can still lie anywhere between 0 and 1, so that the factor in square brackets in equation (4.18) can take any value between 1 and 2, depending on the direction along which the *focal corner* in the (λ_m,ν_0)-plane is approached. ZH refer to this property of $f_{\rm tsm}$ by saying that it has *radial behaviour* in the focal corner (Figure 3, and ZH Figure 2). Without this behaviour of $f_{\rm tsm}$ it would not reproduce the correct density $\rho_m(-\alpha, -\alpha)$.

Since the thin-orbit distribution function $f_{\rm tsm}\{\rho_i\}$ is proportional to $\rho_m(-\alpha, -\alpha)$, the residual density ρ_1 depends only on the local behaviour of the distribution function near the focal corner. This means that we can approximate U^* in equation (3.10) by the constant value $[U'''(-\alpha)]^{3/2}$, so that it can be taken outside the triple integration.

We show in Appendix C that near the focal corner the function c_g can be approximated as

$$c_g(\nu_0,\lambda_m) \simeq \frac{\sqrt{2(\gamma - \alpha)}}{\sqrt{U'''(-\alpha)}}\,\frac{1}{J_g(x_0)}, \tag{4.20}$$

where $J_g(x_0)$ is a weighted integral of the function $g_{\rm sm}$, defined in equation (C7). As a result, c_g also has radial behaviour near the focal corner, except in the thin-orbit limit when $J_g(x_0) \equiv 1$.

Upon substitution of these approximations in relation (3.10), we find

$$\rho_1(-\alpha, -\alpha) \simeq \rho_m(-\alpha, -\alpha)[1 - F_g(x)], \tag{4.21}$$

where

$$F_g(x) = \frac{1}{\pi^2}\int_0^1 \frac{du}{\sqrt{u(1-u)(1-x+xu)}} \int_0^{s^2_{\rm max}} \frac{ds^2}{\sqrt{1-s^2}} \int_{-s}^{s} \frac{dt}{(1+t)^{3/2}} \frac{g_{\rm sm}(s)}{\sqrt{s^2 - t^2}} \frac{(1 + x_0)}{J_g(x_0)} \times \frac{[[1-x + xu(1 + t)]^2 - (1 - x)^2 s^2]}{\sqrt{(1+tx)^2 - (1-x)^2 s^2}\sqrt{1-x + xu(1+t)}}, \tag{4.22}$$

and we still have to substitute relation (4.19) for $x_0 = x_0(x,u,t)$. When $g_{sm}(s) = \delta(s^2)$ the integration over t and s gives π since then $J_g(x_0) \equiv 1$, and so does the remaining integral over u, so that then $F_g(x) \equiv 1$ and the residual $\rho_1 \equiv 0$, as it should be for the thin-orbit model. However, when g_{sm} is not infinitely sharply peaked, the value of ρ_1 at the foci ($\lambda = \nu = -\alpha$) depends on the direction of approach, i.e., on the value of x. Thus, the residual density has *radial behaviour* near the foci.

The triple integral (4.22) requires numerical evaluation for $0 < x < 1$ and general g_{sm}. We have found it to be a slowly varying monotonic function of x for our choice (3.6) of functions $g_{sm}(s)$ (see Figure 9). It is bounded by the values $F_g(0)$ and $F_g(1)$. We show in Appendix D that the triple integration reduces to a single integral for $x = 0$ and $x = 1$, and that the remaining integrals can be found explicitly for our set of functions (3.6). By combining equations (C9) and (D6) we find, for $q > 0$:

$$\begin{aligned} F_g(0) &= \frac{{}_2F_1(\tfrac{3}{4},\tfrac{5}{4};2+q;s_{\max}^2)}{{}_2F_1(\tfrac{1}{4},\tfrac{3}{4};2+q;s_{\max}^2)}, \\ F_g(1) &= \frac{{}_2F_1(1,1;2+q;s_{\max}^2)}{{}_2F_1(\tfrac{1}{2},1;2+q;s_{\max}^2)}, \end{aligned} \tag{4.23}$$

while for $q = 0$ we have (cf. eqs [C10] and [D8])

$$\begin{aligned} F_g(0) &= \frac{3[K(k) - ((1+s_{\max})E(k)]}{(1+s_{\max})[E(k) - (1-s_{\max})K(k)]}, \\ F_g(1) &= -\frac{(1+\sqrt{1-s_{\max}^2})}{2s_{\max}^2}\,\ln(1-s_{\max}^2), \end{aligned} \tag{4.24}$$

where K and E are the complete elliptic integrals of the first and second kinds, and $k^2 = 2s_{\max}/(1+s_{\max})$. For each $q \geq 0$ these functions increase monotonically with increasing $s_{\max}$. In the limit $s_{\max} \to 1$ each function reaches a finite value,

$$F_g(0) = \frac{q+\frac{3}{4}}{q}, \qquad F_g(1) = \frac{q+\frac{1}{2}}{q}, \tag{4.25}$$

provided $q > 0$. However, $F_g(0)$ and $F_g(1)$ diverge logarithmically when $q = 0$ and $s_{\max} \to 1$, although their ratio approaches 3/2, in agreement with the result $F_g(0)/F_g(1) \to (q+\frac{3}{4})/(q+\frac{1}{2})$ which follows from equation (4.25). For given q and $s_{\max}$ the total relative variation of $F_g(x)$ between $x = 0$ and $x = 1$ is therefore never larger than 1.5. Figure 9 illustrates the behaviour of $F_g(0)$ and $F_g(1)$ as a function of $s_{\max}$ for $q = 0$,1 and 2.

The radial behaviour of the residual density ρ_1 at the foci of the spheroidal coordinates, and the fact that the distribution function $f_{sm} = f_{gsm}\tilde{g}_{sm}$ is determined by the local density distribution when $s_{\max} < 1$, means that $f_{gsm}(\nu_0,\lambda_m)$ must have radial behaviour near the focal corner $\nu_0 = \lambda_m = -\alpha$, so that it must be of the form

$$\begin{aligned} f_{gsm}\{\rho_m\}(-\alpha,-\alpha) &= f_{tsm}\{\rho_m\}(-\alpha,-\alpha)K_g(x_0) \\ &= \frac{\rho_m(-\alpha,-\alpha)(1+x_0)K_g(x_0)}{8\pi^2\sqrt{\gamma-\alpha}\,U'''(-\alpha)}, \end{aligned} \tag{4.26}$$

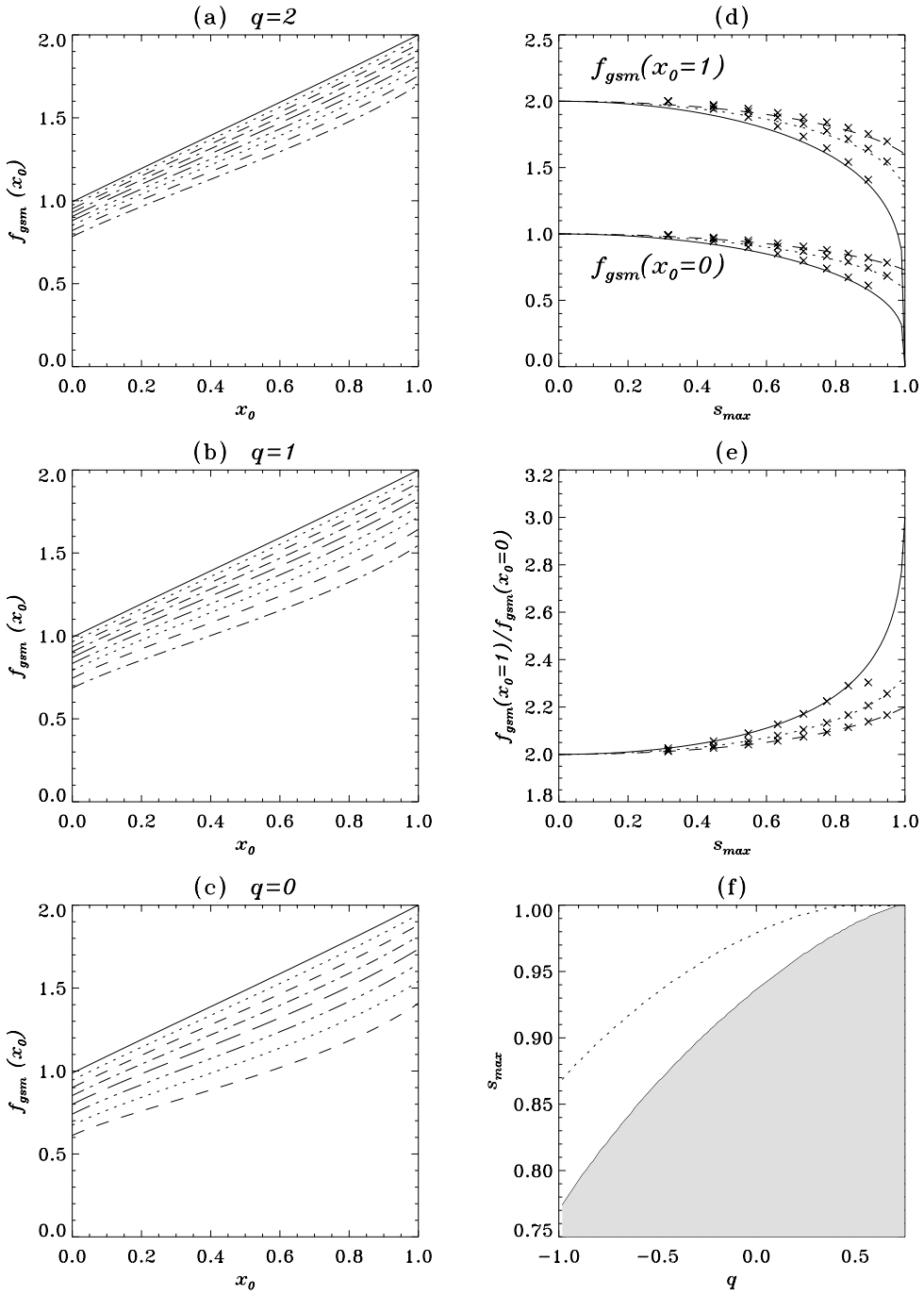

Figure 9. The behaviour of $(1 + x_0)/F_g(x_0)$ for (a) $q = 2$, (b) $q = 1$ and (c) $q = 0$, as calculated with our iterative scheme, for $s^2_{\rm max} = 0, \ldots, 0.9$ in steps of 0.1. The factor $1/F_g(x_0)$ decreases monotonically with $s_{\rm max}$. At most 10 iterations were computed for each model, regardless of the achieved accuracy. The scheme did not converge for the ($q = 0, s^2_{\rm max} = 0.9$) model. In (d) and (e) the results (crosses) from (a)-(c) are compared to the analytical value for $q = 0$ (solid), 1 (dotted) and 2 (dashed) as a function of $s_{\rm max}$. In (f) the lines $F_g(1) = 2$ (dotted) and $F_g(0) = 2$ (solid), which are in effect a relation between q and $s_{\rm max}$, are plotted for our $g_{\rm sm}$ functions. In the shaded area both $F_g(0) < 2$ and $F_g(1) < 2$, which is an indicator for convergence of the iterative scheme.

with K_g a function of the variable x_0 defined in equation (4.19). Since $x = 0$ corresponds to $x_0 = 0$, and since similarly $x = 1$ corresponds to $x_0 = 1$, it follows that

$$K_g(0) = \frac{1}{F_g(0)}, \qquad K_g(1) = \frac{1}{F_g(1)}. \tag{4.27}$$

This suggests — but does not prove — that $K_g(x_0)$ has a modest variation with x_0. It can be computed as follows, at least in principle. We insert $K_g(x_0)$ as a factor in the triple integral on the right-hand side of equation (4.22), and put the left-hand side equal to 1 for $0 \leq x \leq 1$. Transformation of the variables (u,t) to (x_0,t) then allows one to carry out the t and s-integrals. This leaves a one-dimensional integral equation for the function $K_g(x_0)$. In practice this must be solved numerically, and it is in fact easier to simply use our iterative scheme. We have applied it to compute $K_g(x_0)$ for our functions $g_{\rm sm}$ with $q = 0{,}1$ and $s_{\rm max} = 0{,}0.3{,}0.5{,}0.7$ and 0.9. The resulting functions are shown in Figure 9a,b,c. They are very nearly linear up to values of $s_{\rm max}$ as large as 0.7. This means that to good approximation we can take

$$K_g(x_0) \simeq \frac{1 - x_0}{F_g(0)} + \frac{x_0}{F_g(1)}, \tag{4.28}$$

so that we can find the local behaviour of the distribution function near the focal corner without iteration.

The results presented in Figure 9d,e also show that the jump in the value of $f_{\rm gsm}$ at the focal corner is a function of $s_{\rm max}$. The magnitude of the jump going from $x_0 = 0$ to $x_0 = 1$ is $2K_g(1)/K_g(0) = 2F_g(0)/F_g(1)$, and hence varies from 2 when $s_{\rm max} = 0$ in the thin-orbit model to $(2q + \frac{3}{2})/(q + \frac{1}{2})$ when $s_{\rm max} \to 1$.

The convergence of the iterative scheme near the foci of the model can not be derived by investigation of only the residual density ρ_1, as we have done in the above. However, equation (4.21) suggests that in cases where $0 \leq F_g(x) \leq 2$ also the higher order residuals $|\rho_i|$ with $i > 1$ will decrease in size, so that the scheme very likely will converge. This condition on $F_g(x)$ is met for all our functions $g_{\rm sm}$ when $q \geq 3/4$, and is also met for a large range of $s_{\rm max}$ when $-1 < q < 3/4$ (see Figure 9f).

The above results also hold when $s_{\rm max} = 1$ as long as $q > 0$. In this case there are orbits with arbitrarily large outer turning point λ_2 but low angular momentum that still provide density at the foci, but their contribution is vanishingly small. However, when $q = 0$ and $s_{\rm max} = 1$ this is no longer so, and our derivation of the approximate relation (4.21) is invalid. The density close to the foci depends on the details of the distribution of non-local orbits.

We remark that all self-consistent oblate models with density ρ_m in a potential V of the form (2.2) have distribution functions with radial behaviour in the focal corner, unless $q \leq 0$ and $s_{\rm max} = 0$. From our analysis it is not clear whether the radial behaviour is still present in the latter case. However, the two-integral distribution function $f_{\rm sm}(E,L_z)$ is generally well-behaved at the focal corner (Figure 4). When written in the form (2.16), it leads to a function $g_{\rm sm}$ which does not depend on s

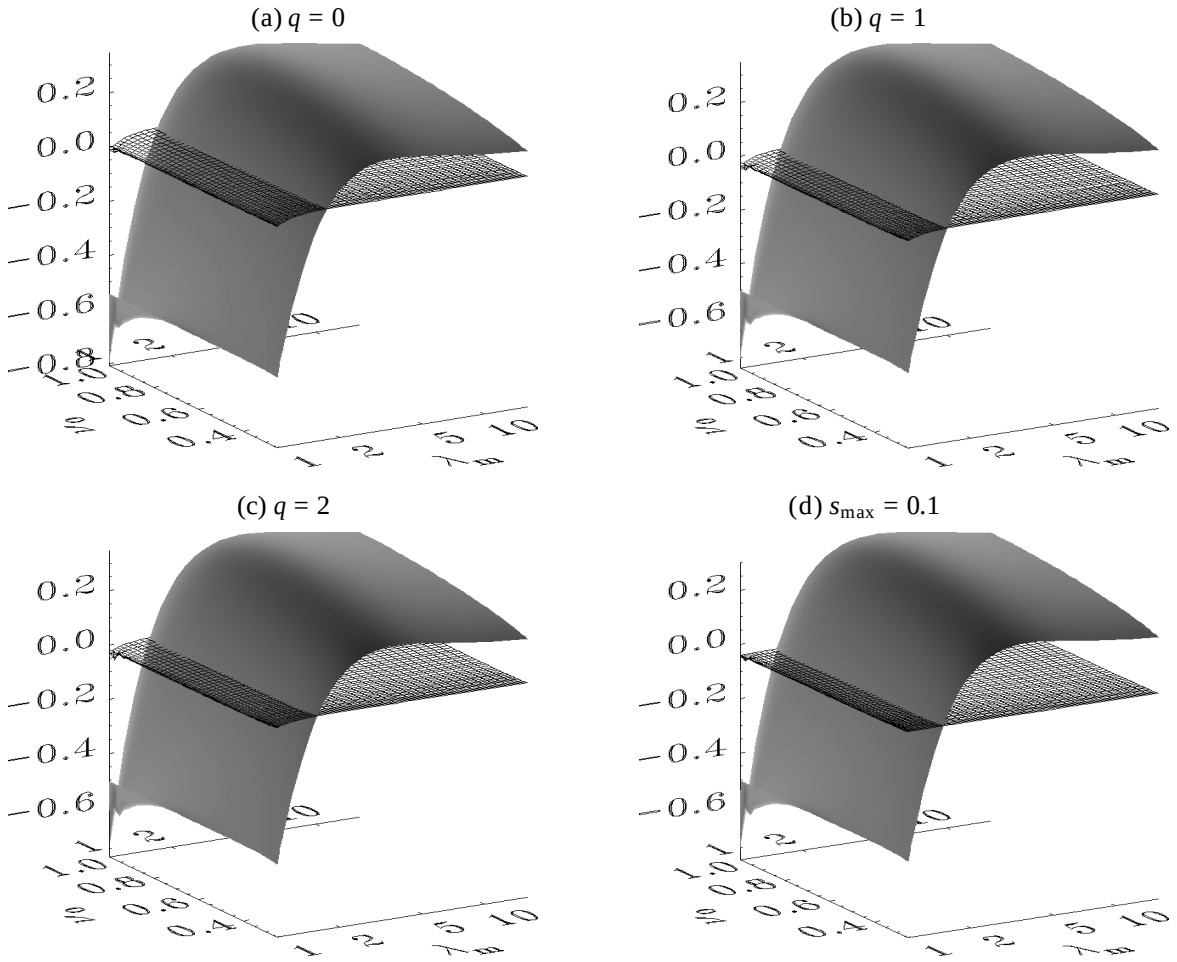

Figure 10. The function $\delta f/f_{\rm tsm}$ for an E5 Kuzmin-Kutuzov model as obtained from a model with $s_{\rm max} = 0.1$ and (a) $q = 0$, (b) $q = 1$ and (c),(d) $q = 2$ (shaded surfaces). The difference of $\delta f/f_{\rm tsm}$ obtained from (a)-(c) $s_{\rm max} = \sqrt{0.1}$ and $s_{\rm max} = 0.1$ and (d) $q = 0$ and $q = 2$ models are shown as wireframe surfaces.

alone. At the focal corner it is identical to our $q = 0$, $s_{\rm max} = 1$ function, and along $\nu_0 = -\alpha$ it has $q < 0$ behaviour. Our iterative scheme with $f_{\rm tsm}$ as initial guess for $f_{\rm gsm}$ fails to converge in this case.

4.3 Models with peaked $g_{\rm sm}$ functions

We have seen that the convergence of the iterative scheme is determined by the moments of the $g_{\rm sm}$ function. For models with sharply peaked $g_{\rm sm}$ functions only the first moment is significant; higher moments can be neglected. In this case only a single iteration is required to approximate $f_{\rm gsm}$ to high accuracy.

The expression for the residual density ρ_1 simplifies considerably. Since $|t| \leq s \leq s_{\rm max}$ and $s_{\rm max}$ is small, the $w_2(s,t,u)$ function in (3.10) can be expanded in a Taylor

series in t and s^2:

$$w_2(s,t,u) \simeq w_2 + \frac{\partial w_2}{\partial s^2}s^2 + \frac{\partial w_2}{\partial t}t + \tfrac{1}{2}\frac{\partial^2 w_2}{\partial t^2}t^2 + \ldots, \tag{4.29}$$

where the derivatives are evaluated at $s = t = 0$. Similarly, $f_{\rm tsm}(t,u)$ can be written as a Taylor series in t. The s- and t-integrations can be carried out. The $w_2(0,0,u)f_{\rm tsm}(0,0)$ term yields the model density ρ_0, hence the residual density ρ_1 is

$$\rho_1 = \langle s^2 g_{\rm sm}\rangle \delta\rho \tag{4.30}$$

with

$$\delta\rho = -\pi \int_0^1 du\, w_1(u) \left[\left(\frac{\partial w_2}{\partial s^2} + \frac{\partial^2 w_2}{4\partial t^2} \right) f_{\rm tsm} + w_2 \frac{\partial^2 f_{\rm tsm}}{4\partial t^2} \right], \tag{4.31}$$

with w_2 and $f_{\rm tsm}$ evaluated at $s = t = 0$. Hence $\delta\rho$ is independent of the shape of $g_{\rm sm}$. This relation even holds if $g_{\rm sm}$ also depends on λ_m and ν_0. The resulting $f_{\rm gsm}$ can be approximated by

$$f_{\rm gsm} \simeq f_{\rm tsm} + \langle s^2 g_{\rm sm}\rangle \delta f \tag{4.32}$$

where $\delta f = f_{\rm tsm}\{\delta\rho\}$ is also independent of $g_{\rm sm}$. Thus, all models with sharply peaked $g_{\rm sm}$ functions can effectively be described by the one-parameter family (4.32).

We have computed δf for an E5 Kuzmin-Kutuzov model with q = 0,1,2 and $s^2_{\rm max}$ = 0.01 and 0.1. The results are displayed in Figure 10 as shaded surfaces. To verify that δf is indeed independent of $g_{\rm sm}$, i.e. of q and $s_{\rm max}$, we compare the difference of two δf-functions obtained for a different set of $(q,s_{\rm max})$ with δf itself. It is clear from Figure 10 that the differences are indeed much smaller, so that (4.32) holds to high accuracy.

4.4 Spherical limit

When $\gamma \to \alpha$, the prolate spheroidal coordinates (λ,ϕ,ν) reduce to spherical coordinates (r,θ,ϕ) with $r^2 = \lambda + \alpha$ (e.g., dZ). The potential (2.2) now is spherical, and equals $V(r) = -G(\lambda)$. The thin-orbit model reduces to the spherical model built exclusively with circular orbits (ZH, §IIg). Our iterative scheme will produce spherical models with a pre-assigned distribution of relative orbital thickness. We summarize briefly how the algorithm simplifies in this case.

In the limit $\gamma = \alpha$, we must have $\nu = \nu_0 = -\alpha$, so that $x = 0$. This reduces the expressions for w_1 and w_2 that appear in the basic relation (3.10) to the forms already given in equation (4.1). Furthermore, the thin-orbit function $f_{\rm tsm}$ becomes a function of λ_m only. It can be evaluated without the need for integration since the density at radius r_m, say, is provided only by the circular orbits with radius r_m. We write $f_{\rm tsm}$ as (cf. ZH, corrected for a typographical error of a factor of 3)

$$f_{\rm tsm}\{\rho_i\}(r_m) = \frac{\rho_i(r_m)}{\pi^2 r_m \kappa_0^2(r_m)}, \tag{4.33}$$

where κ_0^2 is the epicyclic frequency, given by $r\kappa_0^2(r) = 3V'(r) + rV''(r)$, and r_m is defined by $r_m^2 = \lambda_m + \alpha$. Also,

$$c_g = \frac{r_m^3}{S_g(r_m)}, \tag{4.34}$$

where S_g is the integral in the denominator of the definition (3.4). It contains the factor $|\partial J_\lambda/\partial s^2|$ which is given in equation (A3), and must be evaluated with $-\gamma = \nu_0 = -\alpha$. Finally, the function U^* defined in equation (2.15) reduces to

$$U^* = \frac{U[-\alpha,\lambda_1,\lambda_1,\lambda_2]U[-\alpha,\lambda_1,\lambda_2,\lambda_2]}{\sqrt{U[-\alpha,\lambda_1,\lambda,\lambda_2]}}. \tag{4.35}$$

We write $r_1^2 = \lambda_1 + \alpha$ and $r_2^2 = \lambda_2 + \alpha$, so that r_1 and r_2 are the inner- and outer radius reached by an orbit, and $r_m^2 = \frac{1}{2}(r_1^2 + r_2^2)$. Since $U(\lambda) = -(\lambda + \alpha)^2 G(\lambda) = r^4 V(r)$, it follows from the definition (2.9) of the divided differences that the function U^* is a combination of $V(r)$ and its derivative $V'(r)$ evaluated at r, r_1 and r_2. These are related to the variables s and t by

$$s = \frac{2(r_2^2 - r_1^2)}{r_m^2}, \qquad t = \frac{r^2 - r_m^2}{r_m^2}. \tag{4.36}$$

so that $U^* = U^*(r,s,t)$, $c_g = c_g(r,t)$ and $f_{\rm tsm} = f_{\rm tsm}(r,t)$. This means that we can carry out the u-integration in equation (3.10) to give π.

Substitution of the above results and exchange of the order of the s- and t-integrations, then reduces the basic relation (3.10) for the residuals ρ_i to

$$\rho_{i+1}(r) = \rho_i(r) - \frac{4\sqrt{2}}{\pi} \int_{-s_{\max}}^{s_{\max}} dt\, \frac{H_g(r,t)}{(1+t)^{3/2}} \frac{r_m^2 \rho_i(r_m)}{S_g(r_m)\kappa_0^2(r_m)}, \tag{4.37}$$

where $r_m = r(1+t)^{-1/2}$, and we have defined

$$H_g(r,t) = \int_{t^2}^{s_{\max}^2} \frac{ds^2}{\sqrt{s^2 - t^2}}\, g_{\rm sm}(s) U^*(r,s,t). \tag{4.38}$$

Hence, we can choose a function $g_{\rm sm}$, evaluate $H_g(r,t)$ once, and then compute ρ_{i+1} at each radius r as a single weighted integral over $\rho_i(r)$. In practice it is convenient to use r_m rather than t as the integration variable in equation (4.37). No further work is needed to find the entire distribution function $f_{\rm sm} = f_{\rm gsm}\tilde{g}_{\rm sm}$ of the model, because it is given by

$$f_{\rm sm}(r_m,s) = \frac{g_{\rm sm}(s)}{\pi^2 r_m S_g(r_m)\kappa_0^2(r_m)} \sum_{i=0}^{\infty} \rho_i(r_m). \tag{4.39}$$

Calculation of the distribution function is thus considerably faster than in the flattened case, where computation of each ρ_i requires a double integration over a distribution function $f_{\rm tsm}$ which itself is evaluated as a quadrature.

We remark that the arguments r_m and s of the above spherical distribution function each depend on the classical integrals of motion E and L^2. The relations follows from

$$\begin{aligned} E &= \frac{r_2^2 V(r_2) - r_1^2 V(r_1)}{r_2^2 - r_1^2}, \\ L^2 &= 2r_1^2 r_2^2 \frac{V(r_2) - V(r_1)}{r_2^2 - r_1^2}. \end{aligned} \tag{4.40}$$

with $r_1^2 = r_m^2(1 - s)$ and $r_2^2 = r_m^2(1 + s)$. For given r_m and s these relations must generally be inverted numerically to give the associated E and L^2.

4.5 Disks

The iterative scheme (2.22)–(2.23) can also be applied in the limit where the density flattens to a circular disk with surface density $\Sigma_m(\lambda) = \int \rho_m\, dz$, where $\lambda + \alpha = R^2$. The only orbits that can now be populated are those in the equatorial plane $z = 0$, so that we must have $\nu = \nu_0 = -\gamma$ and hence $u = 1$ in our fundamental relation (3.10). This leads to a number of simplifications.

When $u \uparrow 1$, the thin-orbit function $f_{\rm tsm}$, defined in equation (2.19) can be approximated as

$$f_{\rm tsm}\{\rho_i\} = \frac{1}{8\pi^2\sqrt{\lambda_m + \gamma}} \frac{1}{U[-\gamma\lambda_m\lambda_m\lambda_m]} \frac{\sqrt{U[-\gamma,-\alpha\lambda_m\lambda_m]}}{\sqrt{U[-\gamma,-\gamma\lambda_m\lambda_m]}} \lim_{u\uparrow 1}\Big\{\frac{\partial}{\partial u}\int_0^u \frac{\rho_i(\lambda_m,u')\,du'}{\sqrt{u-u'}}\Big\}, \tag{4.41}$$

where $\rho_i(\lambda_m,u') = \Sigma_i(\lambda_m)\delta(u' - 1)$. The function c_g now is

$$c_g = \frac{(\lambda_m + \alpha)\sqrt{\lambda_m + \gamma}}{D_g(\lambda_m)}, \tag{4.42}$$

with D_g the integral in the denominator of equation (3.4), evaluated at $\nu = \nu_0 = -\gamma$. The function U^* reduces slightly, and becomes

$$U^* = U[-\gamma,\lambda_1,\lambda_1,\lambda_2]\, U[-\gamma,\lambda_1,\lambda_2,\lambda_2]\sqrt{\frac{U[-\gamma,-\gamma,\lambda_1,\lambda_2]}{U[-\gamma,\lambda_1,\lambda,\lambda_2]\, U[-\gamma,-\alpha,\lambda_1,\lambda_2]}}. \tag{4.43}$$

If we write $R_1^2 = \lambda_1 + \alpha$, $R_2^2 = \lambda_2 + \alpha$, $R_m^2 = \lambda_m + \alpha$, and use $U(\lambda) = -(\lambda + \alpha)(\lambda + \gamma)G(\lambda) = R^2(R^2 + \gamma - \alpha)V(R)$, with $V(R)$ the potential in the equatorial plane, then we can express all the above third-order divided differences in terms of V and its derivatives. In particular, we have

$$\begin{aligned} U[-\gamma,-\alpha,\lambda,\lambda] &= \tfrac{1}{2}\Omega_0^2(R), \\ U[-\gamma,\lambda,\lambda,\lambda] &= \tfrac{1}{8}\kappa_0^2(R), \end{aligned} \tag{4.44}$$

with κ_0 the epicyclic frequency defined in Section 4.3, and Ω_0 the circular frequency, given by $R\Omega_0^2(R) = V'(R)$. The cylindrical radius R coincides with the spherical radius r in the equatorial plane, so equation (4.36) can be used to find $U^* = U^*(R,s,t)$, $c_g = c_g(R,t)$ and $f_{\rm tsm} = f_{\rm tsm}(R,t)$.

We substitute the above approximations in equation (3.10), and integrate if over z in order to obtain the basic relation for the residuals in the surface density. The u-integration can be carried out, and we are left with

$$\Sigma_{i+1}(R) = \Sigma_i(R) - \frac{4}{\pi} \int_{-s_{\max}}^{s_{\max}} \frac{dt\, \tilde{H}_g(R,t) R_m^2 \Omega_0(R_m) \Sigma_i(R_m)}{(1+t)^{3/2}(1+xt)^{1/2} D_g(R_m) \kappa_0^2(R_m)}, \tag{4.45}$$

where $R_m = R(1+t)^{-1/2}$, $x = (\gamma - \alpha)/(R_m^2 + \gamma - \alpha)$, and we have defined

$$\tilde{H}_g = \int_{t^2}^{s_{\max}^2} ds^2 g_{\rm sm}(s) U^*(R,s,t) \frac{\sqrt{(1+xt)^2 - (1-x)^2 s^2}}{\sqrt{s^2 - t^2}\sqrt{1-s^2}}. \tag{4.46}$$

Just as in the spherical limit, the iterative scheme (2.22)–(2.23) simplifies considerably. We can choose a function $g_{\rm sm}(s)$, integrate it to get $\tilde{H}_g(R,t)$, and then evaluate Σ_{i+1} at radius R by a single quadrature. We have written $g_{\rm sm}$ here as a function of s alone, but a dependence on R_m can be included easily.

The three-dimensional distribution function of an infinitesimally thin disk can be written as

$$f_{\rm sm}(J_\lambda, J_\phi, J_\nu) = f_{\rm disk}(J_\lambda, J_\phi) \frac{\delta(J_\nu)}{2\pi}, \tag{4.47}$$

where the division by 2π ensures that $f_{\rm disk}(J_\lambda, J_\phi)$ is the proper distribution function for the disk considered as a two-dimensional system. It follows from equations (2.22) and (4.45) that our scheme gives $f_{\rm disk}$ as

$$f_{\rm disk}(R_m, s) = \frac{\Omega_0(R_m)}{\pi \kappa_0^2(R_m)} \frac{g_{\rm sm}(s)}{D_g(R_m)} \sum_{i=0}^{\infty} \Sigma_i(R_m). \tag{4.48}$$

The distribution function (4.48) can be written as a function of E and $J_\phi = L_z$ by use of equation (4.40), with r replaced by R, and L^2 by L_z^2.

We conclude that our iterative scheme provides a swift way to construct distribution functions for spheres and disks with a chosen distribution of the relative weights of orbits with different 'thickness' $r_2^2 - r_1^2$ and mean radial extent r_m^2. Based on our results in Sections 4.1 and 4.2, we expect the scheme to converge quickly, except for choices of $g_{\rm sm}$ that put a lot of weight on radial orbits, i.e., that have $g_{\rm sm}(1) > 0$.

5 Concluding remarks

We have presented a simple numerical scheme for the construction of three-integral distribution functions for self-consistent and non-consistent oblate galaxy models

with a potential of Stäckel form. The intrinsic velocity moments can be computed simultaneously. The algorithm allows one to choose in advance the distribution of the inner and outer turning points of the short-axis tube orbits that are populated. It then derives the entire distribution function from the density distribution by means of an iterative process that starts from the explicitly known distribution function of the thin-orbit (maximum streaming) model, in which only the tubes with equal inner and outer turning points are occupied. We have shown that this scheme works well, and is capable of producing tangentially anisotropic models with a substantial radial velocity dispersion within a few iteration steps. The algorithm simplifies considerably in the spherical and disk limits.

Dehnen & Gerhard (1993) have shown that three-integral flattened models display a large variety of observable kinematic properties, which include the line-of-sight mean velocity and velocity dispersion, as well as the entire distribution of the line-of-sight velocity (the velocity profile), all as a function of projected position on the sky. The observable kinematics of the tangentially anisotropic models constructed here can be computed in a straightforward way by numerical integration of the velocity moments and the distribution function, all of which are given with high accuracy by the algorithm.

We have investigated three special cases where three-integral distribution functions can be found without iteration.

First, models that have modest radial dispersions can be approximated adequately by a one-parameter family of distribution functions, which is insensitive to the detailed shape of the assigned function $g_{\rm sm}$, but depends only on its first moment. We will use this family in Chapter 4 to investigate the stability of cold oblate models.

Second, the structure of the model near the foci of the prolate spheroidal coordinate system in which the equations of motion separate provides information on the convergence of the algorithm. When the function $g_{\rm sm}$ is chosen such that only a vanishingly small number of orbits with $L_z = 0$ and a large outer turning point are occupied, the density near the foci is determined locally, i.e., by stars on orbits that are very close to the z–axis oscillations that just reach the foci. We have derived the local behaviour of the distribution function in all such models, and we have shown by analysis of the first residual density that the algorithm is very likely to converge in these cases, as indeed found numerically. However, when $L_z = 0$ orbits with large outer turning points contribute significantly to the density at the foci — which occurs in the $f(E,L_z)$ model, and in strongly radially anisotropic models — our algorithm appears to have problems, at least when we take $f_{\rm tsm}$ as initial guess for $f_{\rm gsm}$. In view of Bishop's (1986) work, we expect that a similar iterative scheme can be used for such models, but with $f(E,L_z)$ as zeroth order distribution function.

Third, the distribution functions of the models also simplify at large radii. There they reduce to a known factor times the distribution function of the thin-orbit model, which can be calculated easily. The internal velocity moments similarly simplify at large radii. This is useful, as it allows a straightforward calculation of the observable

kinematic properties in the outer regions of these anisotropic flattened models. We intend to do so in a future paper. Absorption line kinematic measurements of elliptical galaxies now reach beyond two effective radii, and a comparison of these data with anisotropic models of the kind produced by our algorithm should provide further constraints on the presence and shape of a massive dark halo and the dynamics of the outer luminous regions of these systems (e.g., Carollo et al. 1995).

Finally, we remark that the iterative scheme is not restricted to oblate galaxy models. Prolate Stäckel models have two families of tube orbits, and the thin-orbit solutions have been described by Hunter et al. (1990). By applying our algorithm separately to the two tube orbit families, we can construct models with thick tubes. Triaxial Stäckel models contain three families of tube orbits as well as box orbits. The thin-orbit distribution functions for all three tube families can be found by simple quadratures (Hunter & de Zeeuw 1992; Arnold, de Zeeuw & Hunter 1994), and these can again be thickened by our algorithm. The tube orbits account for part of the density; the remainder must be reproduced by the box orbits. Their distribution function can be found by (numerically) solving a set of linear equations after the tube orbits have been populated. This last construction step is the same in thin and thick orbit models. Work on these triaxial models is in progress.

It is a pleasure to thank Richard Arnold and Marijn Franx for useful discussions and for comments on the manuscript.

References

Arnold, R., de Zeeuw, P.T., Hunter, C., 1994, Mon. Not. R. Astr. Soc. **271**, 924
Batsleer P., Dejonghe H.B., 1993, Astron. Astroph. **271**, 104
Binney J.J., 1976, Mon. Not. R. Astr. Soc. **177**, 19
Binney J.J., 1978, Comments on Astrophysics **8**, 27
Bishop J.L., 1986, Astroph. J. **305**, 14
Bishop J.L., 1987, Astroph. J. **322**, 618
Byrd P.F., Friedman M.D., 1971, *Handbook of Elliptic Integrals for Engineers and Scientists*. Springer Verlag, Berlin
Carollo C.M., de Zeeuw P.T., van der Marel R.P., Danziger I.J., Qian, E.E., 1995, Astroph. J. Lett. **441**, L25
Dehnen W., Gerhard O.E., 1993, Mon. Not. R. Astr. Soc. **261**, 311
Dehnen W., Gerhard O.E., 1994, Mon. Not. R. Astr. Soc. **268**, 1019
Franx M., Illingworth G.D., de Zeeuw P.T., 1991, Astroph. J. **383**, 112
Fridman A.M., Polyachenko V.L., 1984, *Physics of Gravitating Systems*. Springer, New York
Gerhard O.E., 1991, Mon. Not. R. Astr. Soc. **250**, 812
Gerhard O.E., 1993, Mon. Not. R. Astr. Soc. **265**, 213
Gerhard O.E., Saha P., 1991, Mon. Not. R. Astr. Soc. **251**, 449
Gradshteyn I.S., Ryzhik I.M., 1980, *Table of Integrals, Series, and Products*, 4th edition. Academic Press
Dejonghe H.B., de Zeeuw P.T., 1988, Astroph. J. **333**, 90 (DZ)
de Zeeuw P.T., 1985, Mon. Not. R. Astr. Soc. **216**, 273 (dZ)
de Zeeuw P.T., Hunter, C., 1990, Astroph. J. **356**, 365 (ZH)

de Zeeuw P.T., Peletier R.F., Franx M., 1986, Mon. Not. R. Astr. Soc. **221**, 1001
Hénon, M., 1959, Ann. d'Astrophys. **22**, 126
Hunter C., de Zeeuw P.T., Park Ch., Schwarzschild M., 1990, Astroph. J. **363**, 367
Hunter C., de Zeeuw P.T., 1992, Astroph. J. **389**, 79
Hunter C., Qian E.E., 1993, Mon. Not. R. Astr. Soc. **262**, 401
Innanen K.P., Papp K.A., 1977, Astron. J. **82**, 322
Kalnajs A., 1977, Astroph. J. **212**, 637
Kuijken K., 1995, Astroph. J., in press
Kuzmin G.G., 1953, Tartu Astr. Obs Teated, **1**
Kuzmin G.G., 1956, Astr. Zh. **33**, 27
Levison H.F., Richstone D.O., 1985a, Astroph. J. **295**, 340
Levison H.F., Richstone D.O., 1985b, Astroph. J. **295**, 349
Magorrian J., 1995, Mon. Not. R. Astr. Soc., submitted
Merritt D.R., 1987, in de Zeeuw P.T., ed., Proc. IAU Symp. 127, *Structure and Dynamics of Elliptical Galaxies*. Reidel, Dordrecht, p. 315
Merritt D.R., Stiavelli M., 1990, Astroph. J. **358**, 399
Palmer P.L., Papaloizou J., 1987, Mon. Not. R. Astr. Soc. **224**, 1043
Petrou M., 1983a, Mon. Not. R. Astr. Soc. **202**, 1195
Petrou M., 1983b, Mon. Not. R. Astr. Soc. **202**, 1209
Polyachenko V.L., Shukhman I.G., 1981, Sov. Astr. **25**, 533
Qian E.E., de Zeeuw P.T., van der Marel R.P., Hunter C., 1995, Mon. Not. R. Astr. Soc., in press
Richstone D.O., 1980, Astroph. J. **238**, 103
Richstone D.O., 1982, Astroph. J. **252**, 496
Richstone D.O., 1984, Astroph. J. **281**, 100
Saaf A., 1968, Astroph. J. **154**, 483
Saha P., 1991, Mon. Not. R. Astr. Soc. **248**, 494
Saha P., 1992, Mon. Not. R. Astr. Soc. **254**, 132
Shu F.H., 1969, Astroph. J. **158**, 505
Weinberg M.D., 1989, Mon. Not. R. Astr. Soc. **239**, 549
Weinberg M.D., 1991, Astroph. J. **368**, 66

Appendix A. The function $\partial J_\lambda/\partial s^2$

In order to evaluate c_g defined in equation (3.4), we need to calculate $|\partial J_\lambda/\partial s^2|$ at fixed ν_0 and λ_m. The action J_λ as a function of the turning points $(\nu_0,\lambda_1,\lambda_2)$ is defined in equation (2.11) as a single quadrature. Upon transformation to $(\nu_0,\lambda_m,\varepsilon)$ we have

$$J_\lambda = \frac{\sqrt{2}}{\pi}\int_{\lambda_m-\varepsilon}^{\lambda_m+\varepsilon} d\lambda\,\frac{\sqrt{(\lambda-\lambda_m+\varepsilon)(\lambda_m-\lambda+\varepsilon)}}{(\lambda+\alpha)\sqrt{\lambda+\gamma}}\sqrt{(\lambda-\nu_0)U[\nu_0,\lambda_m-\varepsilon,\lambda,\lambda_m+\varepsilon]}. \quad \text{(A1)}$$

Since $s = \varepsilon/(\lambda_m+\alpha)$, we have, at fixed λ_m,

$$\frac{\partial J_\lambda}{\partial s^2} = \frac{(\lambda_m+\alpha)^2}{2\varepsilon}\frac{\partial J_\lambda}{\partial \varepsilon}. \quad \text{(A2)}$$

The integrand in equation (A1) vanishes at the lower and upper limits of integration, so we can simply carry out the differentiation with respect to ε inside the

integral. This is straightforward upon repeated use of the definition (2.9) of divided differences. The result can be written compactly as:

$$\frac{\partial J_\lambda}{\partial s^2} = \frac{(\lambda_m+\alpha)^2}{\pi\sqrt{2}} \int_{\lambda_1}^{\lambda_2} \frac{d\lambda}{(\lambda+\alpha)} \sqrt{\frac{\lambda-\nu_0}{\lambda+\gamma}} \sqrt{\frac{U[\nu_0,\lambda_1,\lambda,\lambda_2]}{(\lambda_2-\lambda)(\lambda-\lambda_1)}} \times \left\{1+\frac{(\lambda_2-\lambda)(\lambda-\lambda_1)U[\nu_0,\lambda_1,\lambda_1,\lambda,\lambda_2,\lambda_2]}{U[\nu_0,\lambda_1,\lambda,\lambda_2]}\right\}. \tag{A3}$$

This is a function of ν_0, λ_1 and λ_2, and hence depends on ν_0, λ_m and ε, or s. We remark that the expressions for J_λ and $\partial J_\lambda/\partial s^2$ are invariant under the exchange $\lambda_1 \leftrightarrow \lambda_2$. This means that both these functions are even in s, and hence are functions of s^2.

We found it convenient to evaluate $J_\lambda(\nu_0,\lambda_m,s)$ and $\partial J_\lambda/\partial s^2(\nu_0,\lambda_m,s)$ by transformation to the integration variable w, defined as

$$w = \frac{2\lambda-\lambda_1-\lambda_2}{\lambda_1+\lambda_2} = \frac{\lambda-\lambda_m}{\varepsilon} = \frac{t}{s}. \tag{A4}$$

Then $d\lambda = s(\lambda_m+\alpha)dw$, and the integration limits are $w(\lambda_1) = -1$ and $w(\lambda_2) = 1$. As a result

$$\begin{aligned} J_\lambda &= \frac{\sqrt{2}}{\pi} s^2(\lambda_m+\alpha)\sqrt{\lambda-\nu_0} \int_{-1}^{1} dw\, \sqrt{1-w^2}\, \frac{\sqrt{1+(1-x_0)sw}}{1+sw} \sqrt{\frac{U[\nu_0,\lambda_1,\lambda,\lambda_2]}{\lambda+\gamma}}, \\ \frac{\partial J_\lambda}{\partial s^2} &= \frac{(\lambda_m+\alpha)\sqrt{\lambda_m-\nu_0}}{\pi\sqrt{2}} \int_{-1}^{1} \frac{dw}{\sqrt{1-w^2}} \frac{\sqrt{1+(1-x_0)sw}}{1+sw} \sqrt{\frac{U[\nu_0,\lambda_1,\lambda,\lambda_2]}{\lambda+\gamma}} \\ &\quad \times \left\{1+\frac{s^2(\lambda_m+\alpha)^2(1-w^2)U[\nu_0,\lambda_1,\lambda_1,\lambda,\lambda_2,\lambda_2]}{U[\nu_0,\lambda_1,\lambda,\lambda_2]}\right\}, \end{aligned} \tag{A5}$$

where we still have to substitute $\lambda = \lambda_m + sw(\lambda_m+\alpha)$, $\lambda_1 = \lambda_m - s(\lambda_m+\alpha)$, and $\lambda_2 = \lambda_m + s(\lambda_m+\alpha)$. The quantity x_0 is defined in equation (4.19):

$$x_0 = \frac{-\alpha-\nu_0}{\lambda_m-\nu_0}, \tag{A6}$$

so that $0 \le x_0 \le 1$. It is a constant as far as the integration over w is concerned.

In the thin-orbit limit we have $\lambda_1 = \lambda_m = \lambda_2$, i.e., $s = 0$, and hence

$$\begin{aligned} J_\lambda &= 0, \\ \frac{\partial J_\lambda}{\partial s^2} &= (\lambda_m+\alpha)\sqrt{\frac{(\lambda_m-\nu_0)U[\nu_0,\lambda_m,\lambda_m,\lambda_m]}{2(\lambda_m+\gamma)}}. \end{aligned} \tag{A7}$$

Substitution in equation (3.4) for c_g now immediately gives (3.5).

Appendix B. Approximations at large radii

The various third-order divided differences $U[\tau_0,\tau_1,\tau_2,\tau_3]$ that occur in the fundamental integral equation simplify when the potential V becomes Keplerian $\propto -GM/\lambda^{-1/2}$ when $\lambda \to \infty$ (ZH, Hunter & de Zeeuw 1992). Here we need the case $\tau_0 \leq -\alpha$ and $-\alpha \ll \tau_1,\tau_2,\tau_3$. Upon substitution of the asymptotic behaviour $U(\lambda) \simeq -GM\lambda^{3/2}$ in the definition (2.9) we obtain

$$\begin{aligned} U[\nu,\lambda_1,\lambda_2,\lambda_3] &\simeq \frac{GM}{(\sqrt{\lambda_1}+\sqrt{\lambda_2})(\sqrt{\lambda_1}+\sqrt{\lambda_3})(\sqrt{\lambda_2}+\sqrt{\lambda_3})}, \\ U[\sigma,\nu,\lambda_1,\lambda_2] &\simeq \frac{GM}{\sqrt{\lambda_1\lambda_2}(\sqrt{\lambda_1}+\sqrt{\lambda_2})}. \end{aligned} \tag{B1}$$

The function $U^*(\lambda,\nu;\nu_0,\lambda_1,\lambda_2)$ defined in equation (2.15) can therefore be approximated by

$$U^* \simeq \frac{(GM)^{3/2}}{4}\frac{(\sqrt{\lambda_1}+\sqrt{\lambda})^{1/2}(\sqrt{\lambda}+\sqrt{\lambda_2})^{1/2}}{\sqrt{\lambda_1\lambda_2}(\sqrt{\lambda_1}+\sqrt{\lambda_2})^{7/2}}. \tag{B2}$$

In terms of the variables s and t this can be written as:

$$U^* \simeq \frac{(GM)^{3/2}}{2^{9/2}}\frac{(1+t)^{9/4}}{\lambda^{9/4}}L(s,t), \tag{B3}$$

where

$$L(s,t) = 2^{5/2}\frac{[\sqrt{1+t}+\sqrt{1-s}]^{1/2}[\sqrt{1+t}+\sqrt{1+s}]^{1/2}}{\sqrt{1-s^2}[\sqrt{1-s}+\sqrt{1+s}]^{7/2}}, \tag{B4}$$

so that $L(0,0) = 1$ and $L(s,t)$ is even in s.

When $-\alpha \ll \lambda_1 \leq \lambda_2$, the integral (2.11) for the action J_λ is elementary and independent of ν_0. It is given by

$$J_\lambda \simeq \sqrt{2GM}\frac{(\lambda_2^{1/4}-\lambda_1^{1/4})^2}{(\sqrt{\lambda_1}+\sqrt{\lambda_2})^{1/2}}. \tag{B5}$$

Transformation to the variables s and t results in

$$J_\lambda \simeq \sqrt{2GM}\frac{\lambda^{1/4}}{(1+t)^{1/4}}\frac{[(1+s)^{1/4}-(1-s)^{1/4}]^2}{[\sqrt{1+s}+\sqrt{1-s}]^{1/2}}. \tag{B6}$$

Straightforward differentiation with respect to s now gives

$$\frac{\partial J_\lambda}{\partial s^2} \simeq \frac{\sqrt{GM}}{4}\frac{\lambda^{1/4}}{(1+t)^{1/4}}h(s), \tag{B7}$$

where

$$h(s) = \frac{\sqrt{2}[4+2\sqrt{1-s^2}-(1-s^2)^{1/4}(\sqrt{1-s}+\sqrt{1+s})]}{(1-s^2)^{3/4}[\sqrt{1-s}+\sqrt{1+s}]^{5/2}}, \tag{B8}$$

so that h is even in s. It is not difficult to show that $h(0) = 1$ and $h(s) > 1$ for $0 < s \leq 1$.

The normalization function $c_g(\nu_0,\lambda_m)$ can now be evaluated by substituting the above approximations in the definition (3.4). It becomes independent of ν_0, and can be written as

$$c_g \simeq \frac{4}{C_g\sqrt{GM}}\frac{\lambda^{5/4}}{(1+t)^{5/4}}, \tag{B9}$$

where the constant C_g is given by

$$C_g = \int_0^1 ds^2\, g_{\rm sm}(s)h(s). \tag{B10}$$

Since $h(s) \geq 1$, it follows that $C_g \geq 1$ for normalized $g_{\rm sm}$.

The intrinsic velocity moments are computed by inserting (3.18) as weight functions in the fundamental equation (3.17). With the help of equation (B1) we can approximate the velocities (3.18):

$$\begin{aligned} v_\lambda^2 &= \frac{GM}{\sqrt{\lambda}}L_\nu^\lambda(s,t), \\ v_\nu^2 &= \frac{GM}{\sqrt{\lambda}}L_\nu^\nu(s,t)(1-u), \\ v_\phi^2 &= \frac{GM}{\sqrt{\lambda}}L_\nu^\phi(s,t)u, \end{aligned} \tag{B11}$$

where the (s,t)-dependent part has been separated:

$$\begin{aligned} L_\nu^\lambda &= \frac{2(s^2-t^2)}{(1+t)^{\frac{3}{2}}(\sqrt{1-s}+\sqrt{1+s})(\sqrt{1+t}+\sqrt{1-s})(\sqrt{1+t}+\sqrt{1+s})}, \\ L_\nu^\nu &= \frac{2((1+t)^2-s^2)}{\sqrt{1-s^2}(\sqrt{1-s}+\sqrt{1+s})\sqrt{1+t}}, \\ L_\nu^\phi &= \frac{2\sqrt{1-s^2}}{(\sqrt{1-s}+\sqrt{1+s})\sqrt{1+t}}, \end{aligned} \tag{B12}$$

so that $L_\nu^\phi(0,0) = L_\nu^\nu(0,0) = 1$ and $L_\nu^\lambda(0,0) = 0$.

Appendix C. Approximations near the focal corner

Near the focal corner in the (ν_0,λ_m)–plane, where $\lambda_m = \nu_0 = -\alpha$, the function $U[\nu_0,\lambda_1,\lambda,\lambda_2]$ can be approximated by $U[-\alpha,-\alpha,-\alpha,-\alpha] = U'''(-\alpha) > 0$, so that it can be taken out of the integral for J_λ. It then follows that

$$\frac{\partial J_\lambda}{\partial s^2} \simeq \frac{(\lambda_m+\alpha)\sqrt{\lambda_m-\nu_0}}{\sqrt{2(\gamma-\alpha)}}\sqrt{U'''(-\alpha)}\,j(x_0,s), \tag{6.1}$$

where

$$j(x_0,s) = \frac{1}{\pi}\int_{-1}^{1} \frac{dw}{\sqrt{1-w^2}} \frac{\sqrt{1+(1-x_0)sw}}{1+sw}. \tag{6.2}$$

The trigonometric substitution $w = \cos t$, followed by use of the integral tables of Byrd & Friedman (1971), shows that

$$j(x_0,s) = \frac{2}{\pi\sqrt{1+(1-x_0)s}}\left[(1-x_0)K(k) + \frac{x_0}{1+s}\Pi(\alpha^2,k)\right], \tag{6.3}$$

where K and Π are the complete elliptic integrals of the first and third kind, respectively, with arguments given by

$$\alpha^2 = \frac{2s}{1+s}, \qquad k^2 = \frac{2(1-x_0)s}{1+(1-x_0)s}. \tag{6.4}$$

in the thin-orbit limit $j(0,0) = 1$, so that expression (6.1) reduces to (A7) evaluated at $\lambda_m = \nu_0 = -\alpha$. Two special cases of interest are

$$\begin{aligned} j(0,s) &= \frac{2}{\pi\sqrt{1+s}}K(k) = {}_2F_1(\tfrac{1}{4},\tfrac{3}{4};1;s^2), \\ j(1,s) &= \frac{1}{\sqrt{1-s^2}}. \end{aligned} \tag{6.5}$$

Here we have used formulae 8.114 and 9.134.1 of Gradshteyn & Ryzhik (1980, hereafter GR), to write $j(0,s)$ explicitly as a (hypergeometric) function of s^2.

The function c_g can now be approximated as

$$c_g(\nu_0,\lambda_m) \simeq \frac{\sqrt{2(\gamma-\alpha}}{\sqrt{U'''(-\alpha)}}\frac{1}{J_g(x_0)}, \tag{6.6}$$

with

$$J_g(x_0) = \int_0^1 ds^2\, g_{\rm sm}(s) j(x_0,s). \tag{6.7}$$

This shows that $c_g(\nu_0,\lambda_m)$ has radial behaviour

Chapter III

Potential-density pairs in axisymmetric coordinates

We present a general scheme for constructing potential-density basis sets in axisymmetric coordinates. A number of examples are given, starting from simple functions. The basis sets constructed are useful for galaxy modelling, N-body simulations and three-dimensional stability analyses of dynamical equilibria. Symbolic manipulation software implementing the technique is available.

Preliminary version of a paper co-authored by David J.D. Earn.

1 Introduction

Potential-density (PD) pairs are the basic building blocks of galaxy models (e.g., Binney & Tremaine 1987, chapter 2). Due to the linearity of Poisson's equation, $\nabla^2\Phi = 4\pi G\rho$, complicated models can be constructed as linear combinations of simple PD pairs. More to the point, the potential and density of any reasonable mass configuration can be approximated arbitrarily well by sufficiently many terms of an expansion in a complete basis of PD pairs. Such expansions are exceedingly useful, for modelling of real objects, N-body simulations and stability analyses of dynamical equilibria.

Much effort has been devoted to finding PD basis sets where both the potential and density are simple expressions in elementary or special functions (e.g., Clutton-Brock 1972, 1973; Kalnajs 1976; Qian 1992, 1993; Hernquist & Ostriker 1992; Earn 1995). Discovering convenient and biorthogonal basis sets suited to particular problems is usually very difficult, and attempts can easily lead to intractable integrals or unmanageable expressions. Fortunately, modern computers running symbolic manipulation programs can overcome the requirement of simplicity of the expressions. Only the computability is important. Once computable basis functions are available they can be tabulated and accurately interpolated for efficiency.

In this paper we describe several ways to generate PD basis sets starting from simple functions. The starting functions can be tailored to the problem at hand, which makes this approach very powerful. These methods are in principle applicable to all coordinate systems, but in this paper we concentrate on (orthogonal) axisymmetric coordinates. In the case of spherical coordinates this type of basis construction has already been explored (Saha 1993) and applied to practical problems (Saha 1991). In many cases spheroidal or cylindrical coordinates are more appropriate. In particular, some of the basis sets described below have been used in stability studies of oblate galaxy models (Chapter 4).

Many PD sets in spherical coordinates are based on spherical harmonics. In Section 3 we generalize this and show how to build basis sets from spheroidal and cylindrical harmonics. Section 4 examines the use of these harmonic PD sets to model finite systems. The harmonic functions are not very well suited for flattened coordinate systems ; Section 5 describes alternative PD sets.

2 Coordinate systems

The coordinates used in this paper are spherical (S), oblate spheroidal (OS), prolate spheroidal (PS) and cylindrical. All systems are denoted (u,v,ϕ), where u is the 'radial', v the 'angular' coordinate and $\phi \in [0,2\pi)$ the azimuth. In the case of cylindrical coordinates, u and v are Cartesian coordinates in the planes of fixed ϕ. If we follow the deformation of the coordinates from spherical via spheroidal to cylindrical, we see that the lines of constant angular variable in prolate coordinates become lines of constant z in the cylindrical limit; when viewed as the limiting case

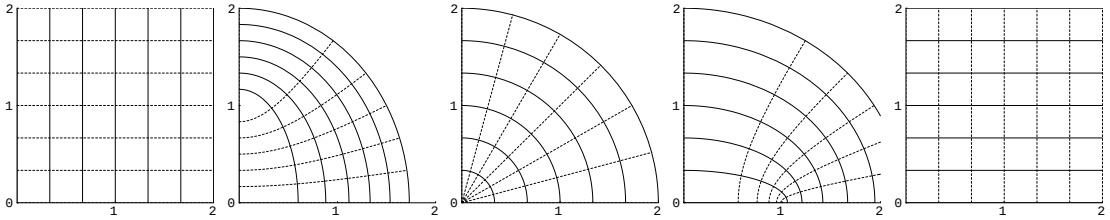

	CC Cylindrical	**PS** Prolate Spheroidal	**S** Spherical	**OS** Oblate Spheroidal	**CP** Cylindrical
(u,v)	(R,z) $0 \le u < \infty$ $-\infty < v < \infty$	(ξ,η) $1 \le u < \infty$ $-1 \le v \le 1$	$(r,\cos\theta)$ $0 \le u < \infty$ $-1 \le v \le 1$	(ξ,η) $0 \le u < \infty$ $-1 \le v \le 1$	(z,R) $-\infty < u < \infty$ $0 \le v < \infty$
h_u	1	$e\sqrt{\frac{u^2-v^2}{u^2-1}}$	1	$e\sqrt{\frac{u^2+v^2}{u^2+1}}$	1
h_v	1	$e\sqrt{\frac{u^2-v^2}{1-v^2}}$	u	$e\sqrt{\frac{u^2+v^2}{1-v^2}}$	1
h_ϕ	u	$e\sqrt{(u^2-v^2)(1-v^2)}$	u	$e\sqrt{(u^2-v^2)(1-v^2)}$	v
R	u	$e\sqrt{(u^2-1)(1-v^2)}$	$u\sqrt{1-v^2}$	$e\sqrt{(u^2+1)(1-v^2)}$	v
z	v	euv	uv	euv	u

Table 1. The axisymmetric coordinate systems used in this paper. The plots show the coordinate systems in the (Cartesian) xz-plane, where z is the symmetry axis. The cylindrical system is present twice: surfaces of constant 'radial' coordinate u are cylinders (CC) or planes (CP). The scaling parameter e is determined by the position of the focal point $z = e$ at $\xi = \eta = 1$ in PS and focal 'circle' $R = e$ at $\xi = 0, \eta = 0$ in the OS system (see also Abramowitz & Stegun (1972) §21. For the plots $e = 1$ is used.

of an oblate spheroidal system, the 'angular' coordinate is R. The structure of the harmonic functions (§3) is different in each of these two limits so we give them distinct labels in Table 1: CC is the *c*ylindrical system where surfaces of constant 'radial' coordinate are *c*ylinders, while in CP these surfaces are *p*lanes.

The metric coefficients h_τ ($\tau = u,v,\phi$) are defined as

$$h_\tau^2 = \left(\frac{\partial x}{\partial \tau}\right)^2 + \left(\frac{\partial y}{\partial \tau}\right)^2 + \left(\frac{\partial z}{\partial \tau}\right)^2, \tag{2.1}$$

with (x,y,z) the standard Cartesian coordinates. The gradient and Laplacian operators are given by

$$\begin{aligned} \nabla &= \left(\frac{1}{h_u}\frac{\partial}{\partial u}, \frac{1}{h_v}\frac{\partial}{\partial v}, \frac{1}{h_\phi}\frac{\partial}{\partial \phi}\right), \\ \nabla^2 &= \frac{1}{h_u h_v h_\phi} \sum_{i=1}^{3} \frac{\partial}{\partial \tau_i}\left(\frac{h_{\tau_j} h_{\tau_k}}{h_{\tau_i}} \frac{\partial}{\partial \tau_i}\right), \end{aligned} \tag{2.2}$$

where (i,j,k) in the last equation is a cyclic permutation of (1,2,3) and $(\tau_1,\tau_2,\tau_3) = (u,v,\phi)$.

	CC $u = R;\quad v = z$	PS $u = \xi,\quad v = \eta$	S $u = r;\quad v = \cos\theta$	OS $u = \xi;\quad v = \eta$	CP $u = z;\quad v = R$
$\nabla^2_{v,m}$	$\frac{d^2}{dv^2}$	$\frac{d}{dv}(1-v^2)\frac{d}{dv} - \frac{m^2}{1-v^2}$	$\frac{d}{dv}(1-v^2)\frac{d}{dv} - \frac{m^2}{1-v^2}$	$\frac{d}{dv}(1-v^2)\frac{d}{dv} - \frac{m^2}{1-v^2}$	$\frac{1}{v}\frac{d}{dv}v\frac{d}{dv} - \frac{m^2}{v^2}$
$\nabla^2_{u,l,m}$	$\frac{1}{u}\frac{d}{du}u\frac{d}{du} - l^2 - \frac{m^2}{u^2}$	$\frac{d}{du}(u^2-1)\frac{d}{du} - l(l+1) - \frac{m^2}{u^2-1}$	$\frac{d}{du}u^2\frac{d}{du} - l(l+1)$	$\frac{d}{du}(u^2+1)\frac{d}{du} - l(l+1) - \frac{m^2}{u^2+1}$	$\frac{d^2}{du^2} - l^2$
$c(u,v)$	1	$e^2(u^2-v^2)$	u^2	$e^2(u^2+v^2)$	1
$\Phi^{lm}_v(v)$	$\frac{1}{2\pi}\,\mathrm{e}^{ilv}$	$n^{lm}P^m_l(v)$	$n^{lm}P^m_l(v)$	$n^{lm}P^m_l(v)$	$\sqrt{\frac{l}{2\pi}}J_m(lv)$
$H^{lm}_i(u)$	$I_m(lu)$	$P^m_l(u)$	u^l	$(-i)^{l+m}P^m_l(iu)$	e^{lu}
$H^{lm}_o(u)$	$K_m(lu)$	$Q^m_l(u)$	u^{-l-1}	$i^{l+m}Q^m_l(iu)$	e^{-lu}

Table 2. The separated Laplace operator and the solutions of the homogeneous Laplace equation for the coordinate systems of Table 1. The norm $n^{lm} = \sqrt{\frac{2l+1}{4\pi}\frac{(l-|m|)!}{(l+|m|)!}}(-1)^{\max(0,m)}$. The prefactors for H^{lm}_i and H^{lm}_o in the OS system have been chosen to make the functions real-valued.

3 PD pairs based on harmonics

The potential Φ that corresponds to a given density ρ is the unique solution of Poisson's equation, $\nabla^2\Phi = 4\pi G\rho$ with appropriate boundary conditions. For galaxies, ρ must be non-negative and it is customary to insist that Φ be negative and continuously differentiable. Satisfactory boundary conditions are that the spherical average of Φ vanishes at infinity (e.g., Pfenniger 1984).

For the axisymmetric coordinate systems given in Table 1, the homogeneous Poisson equation (Laplace's equation) separates into three ordinary differential equations (ODEs) when the potential is of the form $\Phi_u(u)\Phi_v(v)\Phi_\phi(\phi)$. In the S, OS and PS systems, the angular parts $\Phi_v(v)\Phi_\phi(\phi)$ of the separated solutions are called spherical or spheroidal harmonics. Similarly, we group the v and ϕ factors of the separated Laplace solutions together and call them 'cylindrical harmonics' in the CC and CP cases. The (v,ϕ)-harmonics form a complete orthonormal basis set for functions of v and ϕ in all systems.

If a potential is separable with harmonic (v,ϕ) factors then the associated density is also of this form, and the radial functions for the PD pair are related through an ODE. Rather than try to find special solutions, we simply choose a set of radial basis functions for the potential and differentiate to find the corresponding density functions. Because the harmonics appear in both the potential and density, the inner product of two basis functions reduces to a 1D integral, which can be evaluated rapidly numerically if not analytically.

The choice of radial basis set must be made with some care, since the boundary conditions must always be satisfied. Before formulating a useful condition for the radial functions alone, we take a closer look at Poisson's equation.

3.1 Separating Poisson's equation

The separation of Poisson's equation is treated in the literature (e.g., Morse & Feshbach 1953). In this subsection, we review the results to introduce our notation.

A separable solution of Poisson's equation, $\nabla^2\Phi = 4\pi G\rho$, is of the form

$$\Phi(u,v,\phi) = \Phi_u(u)\Phi_v(v)\,\mathrm{e}^{im\phi}\,. \tag{3.1}$$

The Laplacian operator can be split into u- and v-dependent parts (see Table 2) so the left hand side of Poisson's equation can be written as

$$\nabla^2\Phi = \frac{1}{c(u,v)}\left[\nabla^2_{u,\alpha,m} + \nabla^2_{v,m} + \alpha^2\right]\Phi_u(u)\Phi_v(v)\,\mathrm{e}^{im\phi}\,, \tag{3.2}$$

where $c(u,v)$ is a metric factor and α is a separation constant that arises from solving the equation

$$\nabla^2_{v,m}\Phi_v(v) + \alpha^2\Phi_v(v) = 0. \tag{3.3}$$

We choose the constant α^2 to be positive in keeping with the convention for spherical coordinates. Choosing a negative constant does not yield additional independent solutions. For the S, OS and PS coordinates $\alpha^2 = l(l+1)$ where $l \geq 0$ is an integer; for CC and CP $\alpha = l \geq 0$ is a real number.

The differential operator for u, $\nabla^2_{u,\alpha,m}$, depends on both separation constants m and α. There are two solutions $H_i^{lm}(u)$ and $H_o^{lm}(u)$ of the homogeneous equation

$$\nabla^2_{u,\alpha,m}\Phi_u(u) = 0, \tag{3.4}$$

of which $H_i^{lm}(u)$ is regular for $u = u_{min}$ (the lowest value of the u-coordinate: 1 for PS and 0 for the others) and $H_o^{lm}(u)$ is regular as $u \to \infty$.

Table 2 summarizes the solutions Φ_v^{lm}, H_i^{lm} and H_o^{lm} for the five coordinate systems. The Φ_v^{lm} functions have been normalized so that an arbitrary function $f(v,\phi)$ can be written

$$f(v,\phi) = \sum_{l,m} c_{lm}\Phi_v^{lm}(v)\,\mathrm{e}^{im\phi}\,, \tag{3.5}$$

with

$$c_{lm} = \int\int w_v(v)\Phi_v^{lm}(v)^*\,\mathrm{e}^{-im\phi}\,f(v,\phi)\,dvd\phi\,, \tag{3.6}$$

where the weight function $w_v(v) = v$ for CP and $w_v(v) = 1$ for all the other coordinate systems.

3.2 Orthonormal basis of potential functions

The harmonics $\Phi_v^{lm}(v)\,\mathrm{e}^{im\phi}$ form a complete, orthonormal set on the 'sphere' u = constant (Hobson 1965, Morse & Feshbach 1953). They can be extended to a basis for all space by appending a complete set of radial factors $\left\{F_u^{lmn}(u) : n = 0,1,2,\ldots\right\}$ to each (l,m)-harmonic. It is most convenient to start with a basis of potential functions and derive the corresponding density functions $\left\{D_u^{lmn}(u)\right\}$ by differentiation:

$$D_u^{lmn} = \nabla^2_{u,l,m}F_u^{lmn}. \tag{3.7}$$

Any potential can be written as a sum of the basis functions:

$$\Phi = 4\pi G \sum_{l,m,n} d^{lmn} F_u^{lmn}(u) \Phi_v^{lm}(v)\, \mathrm{e}^{im\phi}\,, \tag{3.8a}$$

and the corresponding density is

$$\rho = \frac{1}{c(u,v)} \sum_{l,m,n} d^{lmn} D_u^{lmn}(u) \Phi_v^{lm}(v)\, \mathrm{e}^{im\phi}\,, \tag{3.8b}$$

and $c(u,v)$ is given in Table 2 for the different coordinate systems.

There is considerable freedom in choosing the radial basis $\left\{F_u^{lmn}(u)\right\}$. To be formally complete, the basis must be able to represent any 'reasonable' function of u on the (infinite) u-domain. A useful *ansatz* is the form

$$F_u^{lmn}(u) = W^{lm}(u) f^{lmn}(u), \tag{3.9}$$

where $W^{lm}(u)$ is a fixed function that is suggested by the nature of the physical problem, and f^{lmn} are polynomials of degree n in a finite variable derived from u. In this paper we shall use the functions

$$F_u^{lmn}(u) = \frac{1}{(u+h)^p} \cdot \frac{u^n}{(u+h)^n}, \tag{3.10}$$

for $n \geq 0$, where $h > 0$ and $p \geq 1$ are free parameters. It is then possible to represent any analytic, integrable function of u. The function $W^{00}(u) = (u+h)^{-p}$ with $p \geq 1$ ensures that the total mass associated with a basis function is finite in the S, OS and PS systems. We choose the f^{lmn} functions to be polynomials in $t_u = u/(u+h)$, which increases monotonically with u, ranging from 0 to 1.

Ideally, the basis set should be orthonormal with respect to the inner product

$$\langle \Phi_1, \Phi_2 \rangle = -\frac{1}{4\pi G} \iiint \Phi_1 \nabla^2 \Phi_2 h_u h_v h_\phi \, du dv d\phi, \tag{3.11}$$

for two potential functions. The inner product of two harmonic basis functions reduces to

$$\langle F_u^{lmk}, F_u^{lmn} \rangle_u = -\int w_u(u) F_u^{lmk}(u)^* D_u^{lmn}(u)\, du\,, \tag{3.12}$$

with $w_u(u) = u$ for the CC system, e for OS and PS and 1 for S and CP.

It is not immediately clear that (3.12) is indeed an inner product. Three conditions have to be satisfied for all potential functions F_1, F_2, F_3:

(i) $\langle \alpha F_1 + \beta F_2, F_3 \rangle_u = \alpha \langle F_1, F_3 \rangle_u + \beta \langle F_2, F_3 \rangle_u$,
(ii) $\langle F_1, F_2 \rangle_u = \langle F_2, F_1 \rangle_u^*$, and
(iii) $\langle F_1, F_1 \rangle_u \geq 0$.

Condition (i) is manifest, but (ii) and (iii) are non-trivial. For the OS coordinates, we can integrate (3.12) by parts to obtain

$$\begin{aligned}\langle F_1,F_2\rangle_u &= \frac{1}{4\pi G}\left[-F_1^*(0)\frac{dF_2(0)}{du} + \int_0^\infty (u^2+1)\frac{dF_1^*}{du}\frac{dF_2}{du} + \left(l(l+1)+\frac{m}{1+u^2}\right)F_1^*F_2\,du\right] \\ &= \frac{1}{4\pi G}\left[\frac{dF_1^*(0)}{du}F_2(0) - F_1^*(0)\frac{dF_2(0)}{du}\right] + \langle F_2,F_1\rangle_u^*.\end{aligned} \tag{3.13}$$

Condition (ii) holds only for radial functions F that satisfy vanishing conditions, $F'(0) = 0$ and / or $F(0) = 0$. The same is true for CP coordinates. For the three other coordinate systems it is sufficient that the radial functions are bounded: the equivalent of the first term in (3.13) is proportional to

$$\lim_{u\downarrow u_{min}} (u-u_{min})F_1^*(u)\frac{dF_2(u)}{du}, \tag{3.14}$$

where $F_1^*(u)$ is bounded, hence $F_2'(u)/(u-u_{min}) \to 0$ for $u \downarrow u_{min}$ and the term vanishes. From (3.13) it is evident that condition (iii) is then satisfied as well. The $n = 0,1$-functions (3.10) do not satisfy the vanishing conditions: for $n = 0$ both $F_u^{lm0}(0)$ and $\frac{d}{du}F_u^{lm0}(0)$ are non-zero, while for $n = 1$ the derivative does not vanish. In physical terms, a non-zero $F'(0)$ means that the $u = \xi$-component of the force field corresponding to the potential F is not continuous for all points in the equatorial plane within the 'focal circle' ($\xi = 0, \eta = 0$). For physically relevant potentials, the coefficients of F_u^{lm0} and F_u^{lm1} are related to produce a zero derivative at $\xi = 0$. Hence we modify (3.10) slightly:

$$\begin{aligned}\tilde{F}_u^{lm0} &= F_u^{lm0} + \tfrac{p}{h}F_u^{lm1}, \\ \tilde{F}_u^{lmn} &= F_u^{lm,n+1} \qquad \text{for } n > 0.\end{aligned} \tag{3.15}$$

Even if a basis is not orthogonal, the Gram-Schmidt algorithm can be applied to make it orthonormal. An arbitrary potential component $\Phi_u^{lm}(u)$ can then be written as

$$\Phi_u^{lm}(u) = \sum_n \langle \Phi_u^{lm}, F_u^{lmn}\rangle_u F_u^{lmn}(u). \tag{3.16}$$

Since $\langle \Phi_1,\Phi_2\rangle = \langle \Phi_2,\Phi_1\rangle^*$, (3.16) allows us to compute the expansion coefficients from a given mass density to obtain the potential, as well as from a given potential using the density basis functions.

Saha (1991) used this technique to construct a basis set for perturbations of spherical galaxies. Saha (1993) points out that it is not necessary for the basis to be orthogonalized; the coefficients of an expansion (3.16) can be found by solving of a set of linear equations, which is equivalent to orthonormalization. In practice, the difference is whether to solve the linear equations before (Gram-Schmidt) or after (Saha 1993) the expansion coefficients have been found.

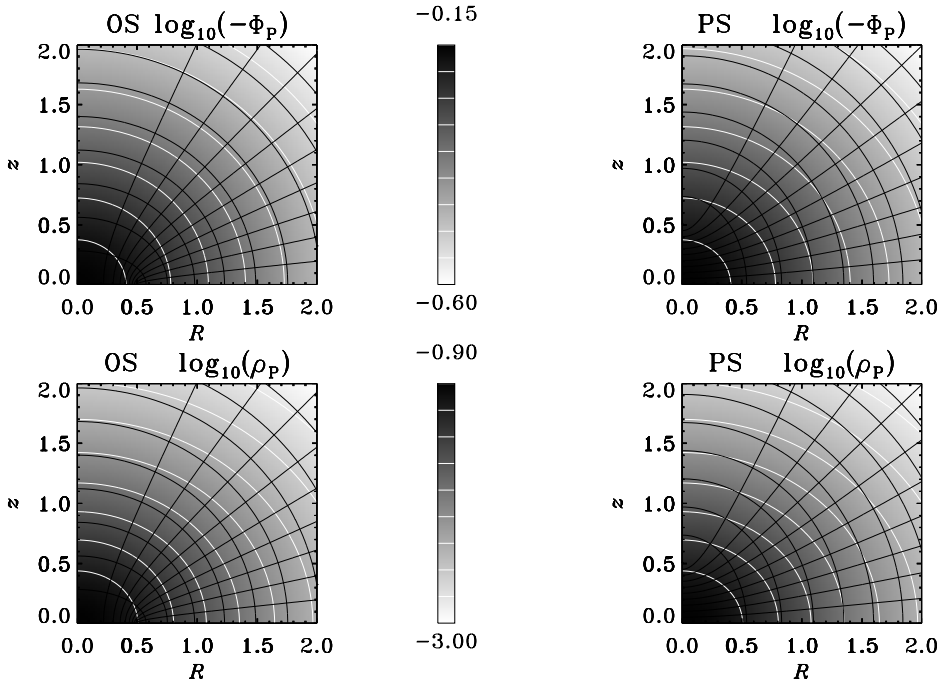

Figure 1. The potential (top) and density (bottom) of the perfect oblate spheroid for $e = 0.5$, an E3 galaxy, as logarithmic gray scale and (white) contour plot. The black contours show the OS (left) and PS (right) coordinate system. The OS system matches the equipotential and equidensity contours of the model more closely.

3.3 Example: an oblate galaxy model

One of the applications of PD basis sets used in many N-body calculations is to compute the gravitational force $-\nabla\Phi$ when a density is known. The potential itself is also used to check the conservation of energy in the system. As an example, consider the perfect oblate spheroid (de Zeeuw 1985) with density

$$\rho_P(R,z) = \frac{M}{\pi^2\sqrt{1-e^2}}\left(1 + R^2 + \frac{z^2}{1-e^2}\right)^{-2} \tag{3.17a}$$

and potential

$$\Phi_P = -\frac{2GM}{\pi}\,\frac{\Phi_\tau(\xi) - \Phi_\tau(\eta)}{\xi^2 - \eta^2}, \tag{3.17b}$$

where

$$\Phi_\tau(\tau) = \frac{\tau}{e}\arctan\frac{e\tau}{\sqrt{1-e^2}}, \tag{3.17c}$$

and (ξ,η) are PS coordinates. The flattening varies from $e = 0$ (sphere) to $e = 1$ (disk). Figure 1 shows the density and potential of this model for $e = 0.5$. Throughout this paper we use $G = 1$ and $M = 1$ when plotting functions.

We use the global basis functions (3.15) in OS coordinates to reproduce the density and potential of the model. The OS system is used because it matches the

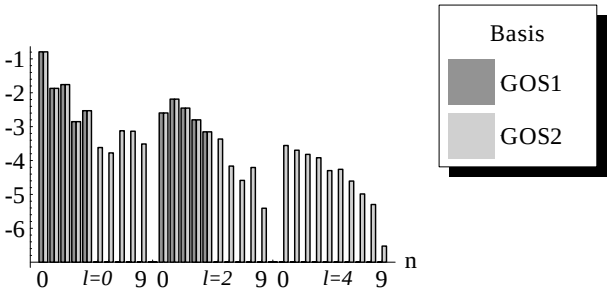

Figure 2. The coefficients c_i for the expansion of the E3 perfect oblate model in basis sets GOS1 and GOS2. Plotted is $\log|c_i|$ as function of the values of (l,n) for the starting basis function (before Gram-Schmidt).

contours of the model density and potential more closely than the PS system, as can be seen in Figure 1. In fact, the density contour of $\rho = \rho_{centre}/4$ coincides with the $\xi = 1/e^2 - 1$ contour. We construct two basis subsets, GOS1 and GOS2, of 10 and 30 elements, respectively. Each basis element consists of a single function (3.15):

$$\begin{aligned}
\text{GOS1}: \quad & (l,m) = (0,0) \quad n = 0\ldots5 \quad \text{and} \\
& (l,m) = (2,0) \quad n = 0\ldots5. \\
\text{GOS2}: \quad & (l,m) = (0,0) \quad n = 0\ldots9, \\
& (l,m) = (2,0) \quad n = 0\ldots9 \quad \text{and} \\
& (l,m) = (4,0) \quad n = 0\ldots9.
\end{aligned}$$

The parameter h is set to the arbitrary value 1. Figure 2 shows the expansion coefficients of the orthogonalized basis functions, which generally consist of several elementary functions (3.15) with the same l-value. The errors in the density and potential of the fits are displayed in Figure 3. The potential is fitted within 0.3% by GOS1 and within 0.07% by GOS2. Deviation of the fitted potential from the model potential introduces an additional acceleration, which is also shown in Figure 3. Away from the origin $R = z = 0$, where the acceleration vanishes, the mean error in the acceleration is 1% for GOS1 and 0.2% for GOS2.

Unfortunately the density is not fitted very accurately, especially near the focal 'circle' of the coordinate system. The problem is that a spheroidal harmonic times a single elementary radial function (3.10) for low n is not a valid potential: it is not twice differentiable at the focal circle, causing the corresponding density to diverge. If all l and n values are used in the expansion the singularities of the elementary functions cancel out. Truncating the basis set, as in GOS 1 and 2, leaves out functions to compensate for the singularity. It is clear from Figure 3 that the density is fitted much better away from the focal circle. The singularity is due to the factor $c(u,v)$ in the Laplace operator being a function of both u and v. If c does not depend on v, the singularity can be avoided by choosing the radial functions carefully. Hence this problem is unique to the OS and PS systems.

3.4 Behaviour at large radii

The potential and density can be represented very accurately out to a finite radius using functions of the form (3.9), but at sufficiently large radii the deviations may

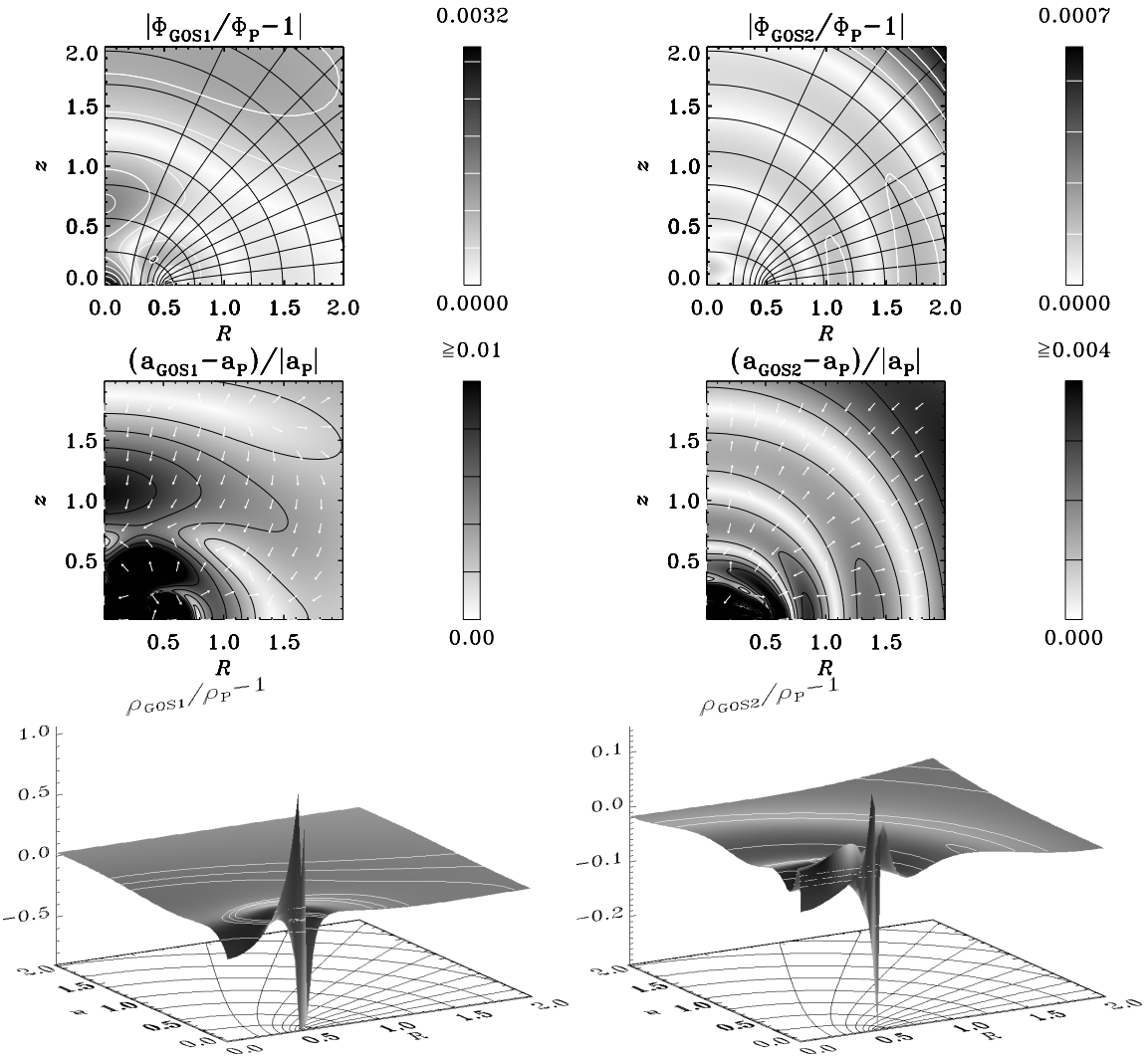

Figure 3. The errors in the potential (top, linear gray scale plots) and density (bottom) of the expansion of the model density from Figure 1 in the GOS1 (left) and GOS2 (right) bases. The white contours in the density plots are at 0.01,0.1,1. Note that the vertical scales are different in the left and right hand panels. The error in the accelerations is depicted in the middle left (GOS1) and right (GOS2) panel: the linear gray scale plot and black contours give its magnitude, the arrows its direction. Near the origin the ratio diverges because a_P vanishes.

be significant. The asymptotic form of W^{lm} for large u contributes little to the inner product of a model density and a basis potential function: the largest contribution comes from the region where the density is large, i.e., the centre. Hence the coefficient of a basis function in an expansion of the density does not change much when the form of W^{lm} is changed at large radii. The W^{lm} function should match the large scale behaviour of the radial potential components Φ_u^{lm} whenever that is known.

It is tempting to let W^{lm} have the same behaviour at large radii as the homogeneous solution H_o^{lm} of the Laplace equation, but that will not work in general. As can

CC	$u = R$	$\sigma_{lm}(R) = \int_{-\infty}^{\infty} dz \int_0^{2\pi} d\phi\, \frac{1}{2\pi}\, \mathrm{e}^{-ilz}\, \mathrm{e}^{-im\phi}\, \rho(R,z,\phi)$
	$v = z$	$\Phi_u^{lm}(R) = 4\pi G \left[K_m(lR) \int_0^R uI_m(lu)\sigma_{lm}(u)\, du + I_m(lR) \int_R^{\infty} uK_m(lu)\sigma_{lm}(u)\, du \right]$
PS	$u = \xi$	$\sigma_{lm}(\xi) = \int_{-1}^{1} d\eta \int_0^{2\pi} d\phi\, n^{lm} P_l^m(\eta)\, \mathrm{e}^{-im\phi} (\xi^2 - \eta^2) \rho(\xi,\eta,\phi)$
	$v = \eta$	$\Phi_u^{lm}(\xi) = \frac{4\pi G}{g_{lm}} \left[Q_l^m(\xi) \int_1^{\xi} P_l^m(u)\sigma_{lm}(u)\, du + P_l^m(\xi) \int_{\xi}^{\infty} Q_l^m(u)\sigma_{lm}(u)\, du \right]$
S	$u = r$	$\sigma_{lm}(r) = \int_{-1}^{1} dv \int_0^{2\pi} d\phi\, n^{lm} P_l^m(v)\, \mathrm{e}^{-im\phi}\, \rho(r,v,\phi)$
	$v = \cos\theta$	$\Phi_u^{lm}(r) = \frac{4\pi G}{2l+1} \left[r^{-l-1} \int_0^r u^{l+2}\sigma_{lm}(u)\, du + r^l \int_r^{\infty} u^{1-l}\sigma_{lm}(u)\, du \right]$
OS	$u = \xi$	$\sigma_{lm}(\xi) = \int_{-1}^{1} d\eta \int_0^{2\pi} d\phi\, n^{lm} P_l^m(\eta)\, \mathrm{e}^{-im\phi} (\xi^2 + \eta^2) \rho(\xi,\eta,\phi)$
	$v = \eta$	$\Phi_u^{lm}(\xi) = \frac{4\pi G}{ig_{lm}} \left[Q_l^m(i\xi) \int_0^{\xi} P_l^m(iu)\sigma_{lm}(u)\, du + P_l^m(i\xi) \int_{\xi}^{\infty} Q_l^m(iu)\sigma_{lm}(u)\, du \right]$
CP	$u = z$	$\sigma_{lm}(z) = \int_0^{\infty} dR \int_0^{2\pi} d\phi\, R \sqrt{\frac{l}{2\pi}} J_m(lR)\, \mathrm{e}^{-im\phi}\, \rho(R,z,\phi)$
	$v = R$	$\Phi_u^{lm}(z) = \frac{2\pi G}{l} \left[\mathrm{e}^{-lz} \int_{-\infty}^{z} \mathrm{e}^{lu}\, \sigma_{lm}(u)\, du + \mathrm{e}^{lz} \int_z^{\infty} \mathrm{e}^{-lu}\, \sigma_{lm}(u)\, du \right]$

Table 3. The components Φ_u^{lm} in equation (A1) as obtained by the multipole expansion (Appendix A) are listed in this table. These expressions can be used to find the behaviour of the potential on the boundary of the u-domain.

be seen from the multipole expansion (which is derived in Appendix A; the results are listed in Table 3), it will be meaningful only when the integrals in the expression for Φ_u^{lm} are bounded on the u-domain. This can fail to occur, even in common physical situations. As an example, consider a spheroidal mass distribution

$$\rho(r,\theta) = \rho_v(\theta)(1+r)^{-4}, \tag{3.18}$$

in spherical (S) coordinates. Because of the symmetry, only the functions $\sigma_{lm}(r)$ with $m = 0$ are non-zero. Furthermore it is clear that

$$\sigma_{l0}(r) = \sigma_{l0}^0 (1+r)^{-4}, \tag{3.19}$$

where σ_{l0}^0 depends on ρ_v. The potential components can readily be computed. To lowest order in $1/r$ they read:

$$\begin{aligned} \Phi_u^{00}(r) &\simeq 4\pi G \sigma_{00}^0 r^{-1}, \\ \Phi_u^{10}(r) &\simeq \tfrac{4}{3}\pi G \sigma_{10}^0 r^{-2} \log r, \\ \Phi_u^{l0}(r) &\propto 4\pi G \sigma_{l0}^0 r^{-2} \qquad (l \geq 2). \end{aligned} \tag{3.20}$$

In this case the basis set should consist of functions (3.10) with $W^{l0} \simeq (u+h)^{-2}$ for every $l \geq 2$, and $W^{l0} \simeq (u+h)^{-2} \log(u+h)$ for $l = 1$. Logarithmic large-radii behaviour is quite common in expansion procedures (see Qian 1992).

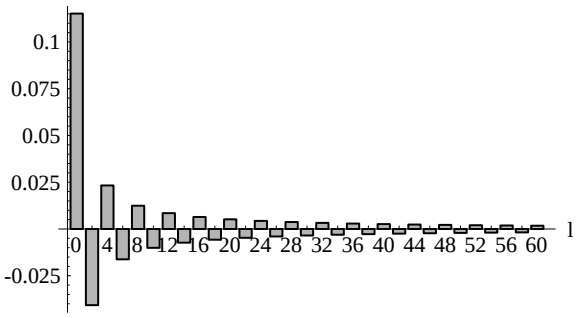

Figure 4. The coefficient d^{l00} for the lowest order basis function in an expansion of the Kuzmin disk model for $l = 0,2,\ldots,60$. The basis is a harmonic PD set in PS coordinates.

3.5 Flattened models in prolate coordinates

Although OS coordinates are the most obvious choice for describing an oblate galaxy model, there are situations where one is forced to use a different system. For example, the Kuzmin-Kutuzov model (Kuzmin 1956, Kuzmin & Kutuzov 1962, for density and potential see eq. (2.24) and (2.25) in Chapter 2) is a Stäckel model: the equations of motion separate in PS coordinates. In dynamical studies it is therefore preferable to use PS coordinates.

In principle, expansion of the model in PS coordinates is identical to the example presented in the previous section. Again, we need bounded density functions to avoid a singularity of the expansion of the density at the focal points. Because the shape of the coordinate system does not match the shape of the model as close as OS, more spheroidal harmonics are needed to reach a similar accuracy. As the model becomes more flattened, the density is more concentrated towards the equatorial plane. The angular functions become sharply peaked near $\nu = 0$ and the number of spheroidal harmonics needed increases dramatically.

In the limiting case of a disk galaxy it is possible to do part of the expansion analytically, and indicate the severity of the problem in the nearly flat limit. As an example, consider the disk limit $e = 1$ of the Kuzmin-Kutuzov model, which is the Kuzmin (1956) disk:

$$\begin{aligned} \Phi_K(\xi,\eta) &= -\frac{GM}{\xi + |\eta|} \\ \sigma_K(\xi) &= \frac{M}{2\pi\xi^3}, \end{aligned} \tag{3.21}$$

with σ_K the surface density of the disk. The form of the potential suggests a lowest order radial function

$$F_u^{l00} = \frac{\sqrt{3}}{\sqrt{2 + 3l(l+1)}} u^{-1}, \tag{3.22}$$

which has already been normalized. It is straightforward to compute the expansion coefficients of the set $\{F_u^{l00}\Phi_\nu^{l0}\}_l$ (for even $l \geq 0$) by computing the inner product of the potential basis functions and the model density:

$$\begin{aligned} d^{l00} &= \langle 4\pi G F_u^{l00}\Phi_\nu^{l0}, \Phi_K \rangle \\ &= (-1)^{\frac{l}{2}} \frac{\sqrt{3}\sqrt{2l+1}(l-1)!!}{6\sqrt{\pi}\, l!!\sqrt{2 + 3l(l+1)}}, \end{aligned} \tag{3.23}$$

which has a limiting behaviour of l^{-1} for large values of l. The d^{l00} coefficient is plotted in Figure 4. Because the convergence is so slow, it is clear that any practical use of the *radial function* $\times$ *spheroidal harmonic* series is excluded in this limiting case.

4 Harmonic PD sets for finite systems

There are many examples where the region of interest is limited in the u-coordinate: finite models for galaxies, localized perturbations etc. The advantage of the *radial basis* $\times$ *angular harmonic* approach is that we are free to choose a basis that has a local support, i.e., is zero outside a finite volume. To illustrate this point, assume that we are studying a shell or ring-like perturbation that is concentrated within $u_1 + \varepsilon < u < u_2 - \varepsilon$ for some small $\varepsilon > 0$. We introduce a radial basis set

$$F_u^{lmn}(u) = \begin{cases} (1-y^2)^3 y^n, & y \in (-1,1), \\ 0, & |y| > 1, \end{cases} \tag{4.1}$$

for $n \geq 0$, with

$$y = \frac{u - \frac{1}{2}(u_1 + u_2)}{u_2 - u_1}. \tag{4.2}$$

The potential functions are twice differentiable and form a complete basis for functions with support in (u_1,u_2). Any combination of these functions yields a potential that is zero at infinity. One would be inclined to accept the set (4.1) as a suitable basis.

However, the set (4.1) cannot represent the potential of a general ring-like perturbation, so it is not complete. From the multipole expansion (derived in Appendix A, summarized in Table 3) it is clear that a ring-like density has a potential proportional to $H_i^{lm}(u)$ for $u < u_1$ and $H_o^{lm}(u)$ for $u > u_2$. The set (4.1) cannot represent the non-zero potential of the perturbation outside the domain (u_1,u_2).

There seems to be a paradox here. It is a well-known fact that the potential of a given density is uniquely determined (e.g., Jackson 1975). Since the multipole expansion disagrees with a potential expansion in the basis (4.1), the latter must be wrong. On the other hand, the $H_\bullet^{lm}$ functions, as solutions of the homogeneous Laplace equation, correspond to zero density. Hence adding $H_\bullet^{lm}$ to the basis does not improve the ability of the basis to represent the density. What is the status of these extra functions?

There are two answers to this problem. First, when solving for the potential of a given density, we are in fact solving a second order partial differential equation. The general solution includes the two $H_\bullet^{lm}$ functions with free coefficients that are determined by the boundary conditions. The coefficients have a physical meaning: e.g., the coefficient of H_o^{00} is connected to the total mass. An expansion (3.16) of a given density using the basis (4.1) still solves the differential equation, but does not satisfy the appropriate boundary conditions: it is a solution to a different problem.

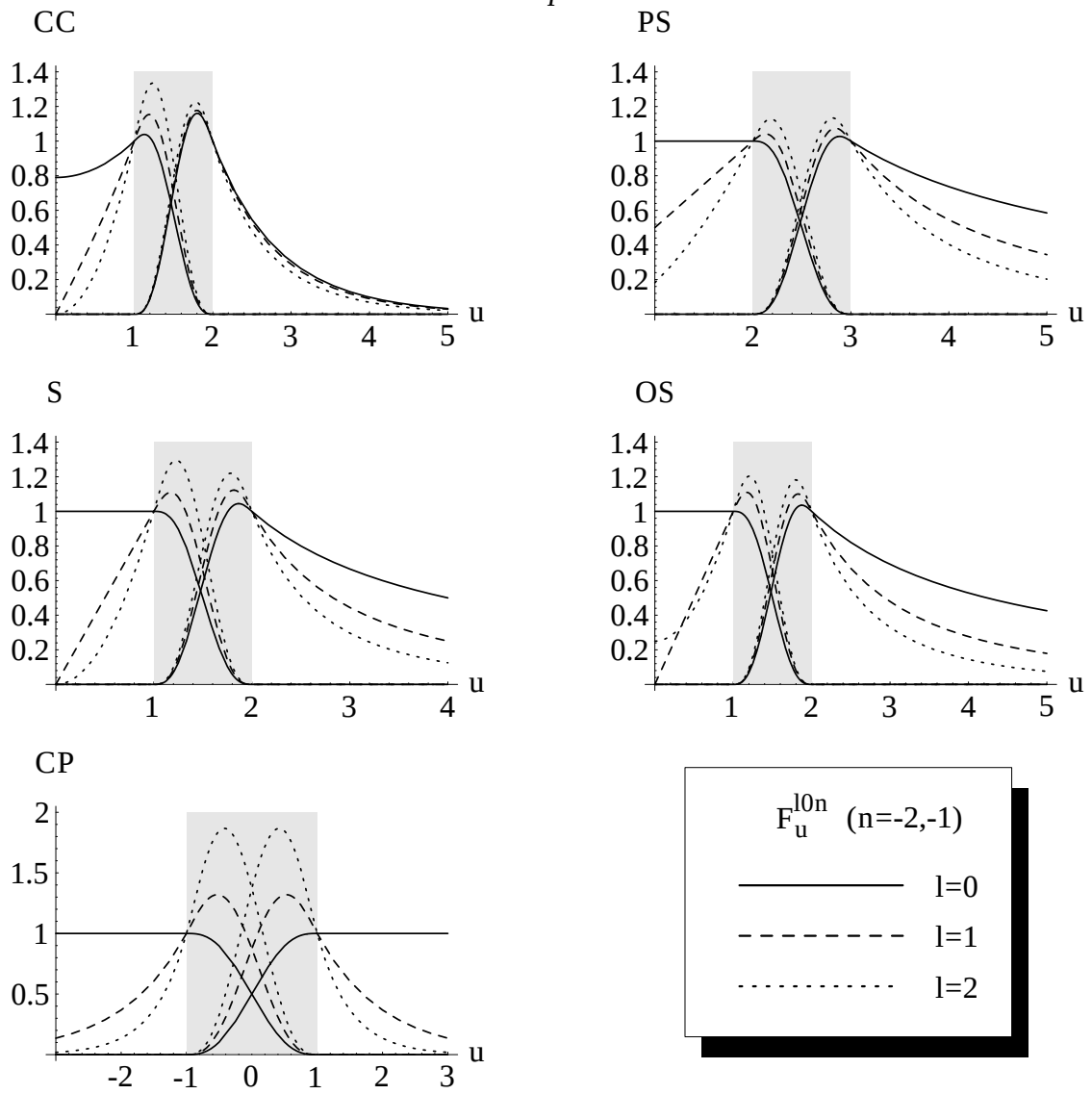

Figure 5. The functions $F_u^{lm,-2}$ and $F_u^{lm,-1}$ for the five coordinate systems, with $m = 0$ and $l = 0$ (solid), $l = 1$ (dashed) and $l = 2$ (dotted). The functions are normalized by $F_u^{lm,-2}(u_1) = F_u^{lm,-1}(u_2) = 1$. The gray area indicates the domain where the basis functions F_u^{lmn} with $n \geq 0$, as given in (4.1), are non-zero.

Although the $H_\bullet^{lm}$ functions are solutions of the homogeneous Laplace equation, they do not correspond to zero density on the infinite u-domain: $H_i^{lm}(u)$ is not bounded for $u \to \infty$ and $H_o^{lm}(u)$ for $u \downarrow u_{min}$. Hence they are not proper potential functions. Any valid potential function that has a limiting behaviour of H_i^{lm} for $u < u_1$ and H_o^{lm} for $u < u_2$ must deviate from either function in the domain (u_1,u_2), and hence contribute to the density.

The boundary conditions can be incorporated in the set (4.1) by adding two

functions

$$\begin{aligned} F_u^{lm,-2}(u) &= \left[\sum_{j=0}^{2} a_{-2,j}^{lm}(1+y)^j\right](1-y)^3 && u \in D, \\ &= H_i^{lm}(u) && u \le u_1, \\ &= 0 && u \ge u_2; \\ F_u^{lm,-1}(u) &= \left[\sum_{j=0}^{2} a_{-1,j}^{lm}(1-y)^j\right](1+y)^3 && u \in D, \\ &= 0 && u \le u_1, \\ &= H_o^{lm}(u) && u \ge u_2, \end{aligned} \tag{4.3}$$

with

$$\begin{aligned} a_{-2,0}^{lm} &= \tfrac{1}{8}H_i^{lm}(u_1), \\ a_{-2,1}^{lm} &= \tfrac{3}{16}H_i^{lm}(u_1) + \tfrac{u_2-u_1}{16}\tfrac{d}{du}H_i^{lm}(u_1), \\ a_{-2,2}^{lm} &= \tfrac{3}{16}H_i^{lm}(u_1) + \tfrac{3(u_2-u_1)}{32}\tfrac{d}{du}H_i^{lm}(u_1) + \tfrac{(u_2-u_1)^2}{64}\tfrac{d^2}{du^2}H_i^{lm}(u_1); \\ a_{-1,0}^{lm} &= \tfrac{1}{8}H_o^{lm}(u_2), \\ a_{-1,1}^{lm} &= \tfrac{3}{16}H_o^{lm}(u_2) - \tfrac{u_2-u_1}{16}\tfrac{d}{du}H_o^{lm}(u_2), \\ a_{-1,2}^{lm} &= \tfrac{3}{16}H_o^{lm}(u_2) - \tfrac{3(u_2-u_1)}{32}\tfrac{d}{du}H_o^{lm}(u_2) + \tfrac{(u_2-u_1)^2}{64}\tfrac{d^2}{du^2}H_o^{lm}(u_2). \end{aligned} \tag{4.4}$$

The coefficients for the $n < 0$ basis functions are not determined in the usual way (3.16), but by the multipole expansion (Table 3). If there is no inner boundary for the u-domain (e.g., in the case of a finite galaxy model) the $n = -2$ function can be omitted. Examples of F_u^{lmn} functions with $n < 0$ are given in Figure 5. The set (4.1), completed with (4.3), has been used in the stability analysis of oblate galaxy models, which is presented in Chapter 4.

There is a minor issue concerning the application of Gram-Schmidt when the set (4.1) and (4.3) is used. In all numerical applications the basis set is truncated to include N elements. It is favourable to have a basis set for which the expansion coefficients do not depend strongly on N, i.e., when $N + 1$ elements are present, the coefficients of the first N elements should not change much. This will not occur if we use the $n < 0$ functions above as our lowest order elements. The Gram-Schmidt procedure then yields a basis set where all elements are non-zero outside the finite u-domain. It follows that by adding an extra element to the basis, the total change in the first N coefficients must be equal to the $N + 1$-th.

A better approach is to consider the $n < 0$ functions as the highest order elements of the basis. Then adding another element to the basis does not change the first N coefficients at all: the $n \ge 0$ elements are unchanged in shape. The coefficients for $n < 0$ are determined by the density or potential being expanded and do not depend on the other basis functions, but the *shape* of the $n < 0$ functions within the u-domain does change in this case.

5 Non-harmonic PD pairs

The method described thus far is not useful if many 'angular' functions have to be included in typical expansions. Apart from the disk limit in the PS system (§3.5) lengthy expansions may be required in the CC and CP systems. Unfortunately, if we do not use harmonic (v,ϕ)-functions the Laplace equation (3.2) does not separate into three ODEs anymore.

However, we can use a different set of orthonormal v-functions that is better suited to the problem at hand, and still profit from the separability of the Laplace operator. Each function of the new set $\{F_v^{km}(v)\}_{km}$ can be expanded in harmonics:

$$F_v^{km}(v) = \sum_l S_{km}(l)\Phi_v^{lm}(v), \tag{5.1}$$

where the summation is an integration in case of CC and CP. The inner product of two v-functions reduces to

$$\langle F_v^{jm}, F_v^{km}\rangle_v = \sum_l S_{jm}(l)S_{km}(l) = \delta_{jk}. \tag{5.2}$$

The new basis functions can be specified directly by prescribing F_v^{km}, or by assuming a basis for the S_{jm} transforms. If a v-basis is not orthonormal by itself it can be modified by Gram-Schmidt. We can proceed as in Section 3 by appending a complete set of radial factors $\left\{F_u^{kmn}(u,l) : n = 0,1,2,\ldots\right\}$ to each (k,m) angular function. The inner product of two radial functions, the equivalent of (3.12), becomes

$$\langle F_u^{kmj}, F_u^{kmn}\rangle_u = -\sum_l S_{km}(l)^2 \int w_u(u) F_u^{kmj}(u,l)^* \nabla^2_{u,\alpha,m} F_u^{kmn}(u,l)\, du\,, \tag{5.3}$$

where $\alpha = \alpha(l)$ is the separation constant given in Section 2.

As an example, consider a flat disk in CP coordinates. The 'radial' coordinate is $u = z$ and the density is proportional to $\delta(u)$. A basis of a single 'radial' function is sufficient:

$$\begin{aligned} F_u^{km0}(z,l) &= -\,\mathrm{e}^{-l|z|}/\sqrt{2l}, \\ D_u^{km0}(z,l) &= \delta(z)\sqrt{2l}, \end{aligned}$$

which has already been normalized. In the equatorial plane $z = 0$ the potential and surface density σ are given by

$$\begin{aligned} \Phi(R,\phi) &= -2\sqrt{\pi}G\sum_{k,m} d^{km0}\,\mathrm{e}^{im\phi}\int_0^\infty S_k(l)J_m(lR)\,dl, \\ \sigma(R,\phi) &= \tfrac{1}{\sqrt{\pi}}\sum_{k,m} d^{km0}\,\mathrm{e}^{im\phi}\int_0^\infty l S_k(l)J_m(lR)\,dl, \end{aligned} \tag{5.4}$$

in analogy with (3.8). The l-integrals are recognized as Hankel transforms. This result was first used to construct galaxy models by Toomre (1963); for a construction of a discrete basis for the $S_k(l)$ functions see Clutton-Brock (1972).

The expansion (5.1) is needed only in the process of making the set orthonormal by means of (5.3). The alternative is to compute the inner products directly by evaluating a two-dimensional (u,v)-integral. The inner product (5.3) of radial functions is also a two-dimensional integral (for CC and CP) or an integral and an infinite sum. Hence the detour (5.1) is advantageous only if either the u-integral in (5.3) or the l-summations can be done analytically. In a future paper we intend to examine non-harmonic PD pairs where the inner products are evaluated by the two-dimensional (u,v)-integral directly.

6 Summary and discussion

We have presented several methods for constructing an orthonormal basis of PD pairs in five types of axisymmetric coordinate systems. The basis is initialized using simple functions. The considerable freedom in the choice of the starting functions is one of the key features of the methods and makes it possible to adapt the basis to the application. We have demonstrated that gravitational systems with an infinite extent can be fitted accurately. The same methods can be used to set up a basis to describe the density in a constrained region. Some simple conditions, formulated in Section 4, have to be satisfied to ensure that the potential and density are physical.

We have intentionally avoided the delicate question of completeness. In numerical applications, completeness is not crucial because we shall never use more than a few functions and the precise space that is spanned by the full set will not be important. We are always just producing a reasonably smooth approximation to the function being expanded.

DE gratefully acknowledges the hospitality of the Sterrewacht Leiden, where the initial part of the work was done. It is a pleasure to thank Tim de Zeeuw for careful reading of the manuscript.

References

Abramowitz M., Stegun I.A., 1972, *Handbook of Mathematical Functions.* Dover, New York
Binney J., Tremaine S., 1987, *Galactic Dynamics.* Princeton University Press, Princeton NJ
Clutton-Brock M., 1972, Astroph. and Space Sc. **16**, 101
Clutton-Brock M., 1973, Astroph. and Space Sc. **23**, 55
de Zeeuw P.T., 1985, Mon. Not. R. Astr. Soc. **216**, 273
Earn D.J.D., 1995, in Blitz, L., ed., Proc. IAU Symp. 169, *Unsolved problems of the Milky Way*. (to appear)
Gradshteyn I.S., Ryzhik I.M., 1994, *Table of Integrals, Series and Products,* 5th edition. Academic Press (GR)

Hernquist L., Ostriker J.P., 1992, Astroph. J. **386**, 375
Hobson E.W., 1965, *The theory of spherical and ellipsoidal harmonics.* Chelsea publishing company, New York
Jackson J.D., 1975, *Classical Electrodynamics.* New York, Wiley
Kalnajs A.J., 1976, Astroph. J. **205**, 745
Kuzmin G.G., 1956, Astr. Zh. **33**, 27
Kuzmin G.G., Kutuzov S.A., 1962, Bull. Abastumani Ap. Obs. **27**, 82
Morse P.M., Feshbach H., 1953, *Methods of theoretical physics.* McGraw-Hill, New York
Pfenniger D., 1984, Astron. Astroph. **141**, 171
Qian E.E., 1992, Mon. Not. R. Astr. Soc. **257**, 581
Qian E.E., 1993, Mon. Not. R. Astr. Soc. **263**, 394
Saha P., 1991, Mon. Not. R. Astr. Soc. **248**, 494
Saha P., 1993, Mon. Not. R. Astr. Soc. **262**, 1062
Toomre A., 1963, Astroph. J. **166**, 275

Appendix A. Multipole expansion

For reference we derive the multipole expansion for axisymmetric coordinate systems, following the derivation given by Binney & Tremaine (1987, §2.4) for spherical systems.

The principle of the multipole expansion is that the potential Φ corresponding to a general mass distribution $\rho(u,v,\phi)$ is expanded in harmonics $\Phi_v^{lm}(v)\,\mathrm{e}^{im\phi}$:

$$\Phi(u,v,\phi) = \sum_{l,m} \Phi_u^{lm}(u)\Phi_v^{lm}(v)\,\mathrm{e}^{im\phi}\,. \tag{A1}$$

Note that for CC and CP the summation over l is actually an integration. We want to find an expression relating the coefficients Φ_u^{lm} to ρ.

Formally, we can describe the mass distribution as a collection of 'shells' $u = u_0$ (a cylinder in CC and a plane in CP):

$$\rho(u,v,\phi) = \int \rho(u_0,v,\phi)\delta(u_0 - u)\,du_0. \tag{A2}$$

For each of the shells with density $\rho_s(u,v,\phi) = \delta(u - u_0)\sigma(v,\phi)$, the corresponding potential Φ_s satisfies the homogeneous Laplace equation outside the shell, hence it must be a linear combination of the H_i^{lm} and H_o^{lm} functions:

$$\Phi_s(u,v,\phi) = \begin{cases} \displaystyle\sum_{l,m} c_{lm}H_i^{lm}(u)\Phi_v^{lm}(v)\,\mathrm{e}^{im\phi} & u < u_0, \\ \displaystyle\sum_{l,m} d_{lm}H_o^{lm}(u)\Phi_v^{lm}(v)\,\mathrm{e}^{im\phi} & u > u_0. \end{cases} \tag{A3}$$

At $u = u_0$ the potential is continuous, but not differentiable. The jump in the first derivative can be computed by applying the Gauss theorem:

$$\begin{aligned} \int_{\partial V} \nabla\Phi_s(u,v,\phi)\cdot dS &= \int \nabla^2\Phi_s\,dV \\ &= 4\pi G \int_V \rho_s(u,v,\phi)\,dV, \end{aligned} \tag{A4}$$

where dS is the normal to the surface ∂V of the volume V and dV is the volume element. If we apply this to a small volume V which contains the point (u,v,ϕ) and is infinitely thin in the u-direction, we find that

$$\int \frac{1}{h_u}\left[\frac{\partial\Phi_s(u^+,v,\phi)}{\partial u} - \frac{\partial\Phi_s(u^-,v,\phi)}{\partial u}\right] h_v h_\phi \, dvd\phi = 4\pi G \int \sigma(v,\phi) h_u h_v h_\phi \, dvd\phi, \qquad \text{(A5)}$$

where $f(u^+) = \lim_{u'\downarrow u} f(u')$ and $f(u^-) = \lim_{u'\uparrow u} f(u')$. For an infinitesimally small volume V this simplifies to

$$\frac{\partial\Phi_s(u^+,v,\phi)}{\partial u} - \frac{\partial\Phi_s(u^-,v,\phi)}{\partial u} = 4\pi G\sigma(v,\phi)h_u^2(u,v). \qquad \text{(A6)}$$

Substitute equation (A3) into (A6), multiply by $w_v(v)\Phi_v^{lm}(v)^* \, \mathrm{e}^{-im\phi}$ and integrate over v and ϕ to arrive at

$$c_{lm}\frac{dH_o^{lm}(u)}{du} - d_{lm}\frac{dH_i^{lm}(u)}{du} = 4\pi G h_{uu}(u)\sigma_{lm}(u), \qquad \text{(A7)}$$

where the scale factor $h_u(u,v) = h_{uu}(u)h_{uv}(u,v)$ has been split and

$$\sigma_{lm}(u) = \int\int h_{uv}(u,v)\Phi_v^{lm}(v)^* \, \mathrm{e}^{-im\phi} \, \sigma(v,\phi) \, dvd\phi. \qquad \text{(A8)}$$

The factors h_{uu} and h_{uv} depend on the coordinate system:

$$\begin{aligned} CC,S,CP: &\quad h_{uu}^2 = 1, && h_{uv}^2 = 1; \\ PS: &\quad h_{uu}^2 = (u^2-1)^{-1}, && h_{uv}^2 = u^2 - v^2; \\ OS: &\quad h_{uu}^2 = (u^2+1)^{-1}, && h_{uv}^2 = u^2 + v^2. \end{aligned} \qquad \text{(A9)}$$

The constants c_{lm} and d_{lm} have been determined from (A7) using the properties of the special functions $H_\bullet^{lm}$:

$$H_i^{lm}(u)\frac{d}{du}H_o^{lm}(u) - H_o^{lm}(u)\frac{d}{du}H_i^{lm}(u) = \begin{cases} -u^{-1} & \text{CC} \quad \text{(GR 8.486.4, 8.486.13, 8.477.2)} \\ -\dfrac{g_{lm}}{u^2-1} & \text{PS} \quad \text{(GR 8.741.2)} \\ -\dfrac{2l+1}{u^2} & \text{S} \\ -i\dfrac{g_{lm}}{u^2+1} & \text{OS} \quad \text{(GR 8.741.2)} \\ -2l & \text{CP} \end{cases} \qquad \text{(A10)}$$

where the GR numbers refer to Gradshteyn & Ryzhik (1980) and

$$g_{lm} = 4^m \frac{\Gamma\left(\frac{l+m+1}{2}\right)\Gamma\left(\frac{l+m+2}{2}\right)}{\Gamma\left(\frac{l-m+1}{2}\right)\Gamma\left(\frac{l-m+2}{2}\right)}. \qquad \text{(A11)}$$

As a last step, the contributions Φ_s of the shells to the potential Φ can be integrated; the resulting expressions for Φ_u^{lm} are given in Table 3.